AD-A261 359

ION PAGE

Form Approved
OMB No. 0704-0188

1. AGENCY USE ONLY (Leave blank)	2. REPORT DATE	3. REPORT TYPE AND DATES COVERED
	11-15-92	Final Report 9/15/91-9/14/92

4. TITLE AND SUBTITLE
Investigation of Coupled Analysis Techniques for Adaptive Material Structural Systems

5. FUNDING NUMBERS
AFOSR-91-0416 DEF
2302/DS

6. AUTHOR(S)
Prof. Craig A. Rogers

7. PERFORMING ORGANIZATION NAME(S) AND ADDRESS(ES)
Center for Intelligent Material Systems and Structures
Virginia Polytechnic Institute and State University
840 University City Blvd.
Blacksburg, Virginia 24061-0261

8. PERFORMING ORGANIZATION REPORT NUMBER
AFOSR-TR-

9. SPONSORING / MONITORING AGENCY NAME(S) AND ADDRESS(ES)
Air Force Office of Scientific Research

10. SPONSORING / MONITORING AGENCY REPORT NUMBER
AFOSR-91-0416

11. SUPPLEMENTARY NOTES

12a. DISTRIBUTION / AVAILABILITY STATEMENT
Approved for public release; distribution unlimited

12b. DISTRIBUTION CODE

13. ABSTRACT *(Maximum 200 words)*

The objective of this research program is to investigate coupled analysis techniques for adaptive material structural systems. There are two aspects of this research: one is to develop a nonlinear full-field constitutive model for ferroelectric materials, including piezoelectric and electrostrictive materials; the other is to develop an impedance-based analysis technique for adaptive material systems.

A coupled electro-thermal-mechanical nonlinear constitutive relation for piezoelectric materials has been developed and verified based on experimental data from the literature. This model uses the polarization fraction as a newly established internal variable. This internal variable is related to other parameters such as electric field, stress, frequency, etc., using a hyperbolic tangent function, which accurately describes the nonlinearity, including the hysteresis of ferroelectric materials. The same approach has also been utilized in the modeling of relaxor ferroelectric PMN-PT materials. An impedance methodology for the dynamic analysis of adaptive material systems has been developed. This approach can provide accurate theoretical prediction of the dynamic response of a structure driven by any type of actuator and yet reflect the physical essence of the actuator/structure interaction. This model has been experimentally verified.

14. SUBJECT TERMS	15. NUMBER OF PAGES
Nonlinear modeling, piezoelectric actuators, impedance, dynamics, adaptive materials	111
	16. PRICE CODE

17. SECURITY CLASSIFICATION OF REPORT	18. SECURITY CLASSIFICATION OF THIS PAGE	19. SECURITY CLASSIFICATION OF ABSTRACT	20. LIMITATION OF ABSTRACT
unclassified	unclassified	unclassified	unlimited

Approved for public release;

Final Technical Report

Investigation of Coupled Analysis Techniques for Adaptive Material Structural Systems
Grant No. AFOSR-91-0416 DEF

Principal Investigator: Prof. Craig A. Rogers
Center for Intelligent Material Systems and Structures
Virginia Polytechnic Institute and State University
Blacksburg, Virginia 24061-0261

Research Objectives

The objective of this research program is to investigate coupled analysis techniques for adaptive material structural systems. There are two aspects to this research objective: one is to develop a nonlinear full-field constitutive model for ferroelectric materials, including piezoelectric and electrostrictive materials; the other is to develop an impedance-based analysis technique for adaptive material systems.

Major Technical Achievements:

Nonlinear Modeling of Piezoelectric Ceramics

A coupled electro-thermal-mechanical nonlinear constitutive relation for piezoelectric materials has been developed and verified based on experimental data from the literature. This model uses the polarization fraction as a newly established internal variable. This internal variable is related to other parameters such as electric field, stress, frequency, etc., using a hyperbolic tangent function, which accurately describes the nonlinearity, including the hysteresis of ferroelectric materials.

Constitutive Modeling of Relaxor Ferroelectric PMN-PT Materials

The nonlinear constitutive relations for electrostrictive materials have also been investigated. The same polarization fraction function used in the modeling of piezoelectric materials has also been utilized here to describe the change in the dielectric and electrostrictive properties of the electrostricitve materials. The model has considered the influence of grain size, temperature, frequency, and bias electric field on the sensing and actuation behavior of electrostrictive materials. This model has been experimentally verified.

Impedance Modeling Technique for Dynamic Analysis of Adaptive Materials

Presently, there are two approaches to the dynamic analysis of adaptive material systems with

integrated actuators. One is to use a statically determined force which is determined based on the stiffness aspect ratio of actuator to structure as a forcing function. The other is the so-called thermal moment technique. The first approach, the static approach, is not correct at all because the dynamic force provided by an actuator depends on the structural impedance, not the stiffness, in the structural dynamics. Therefore, the force provided by an integrated actuator is not a constant force. The static approach also ignores the mass loading and stiffening of integrated actuators, which in some cases can have a significant influence on the predicted dynamic response. The thermal moment approach may more accurately predict the dynamic response, but it does not represent the physical structural interaction between actuators and structures. The thermal moment approach does not consider the electric stiffening effect, which may also cause some error.

Based on the above consideration, an impedance methodology for dynamic analysis of adaptive material systems has been developed. This approach can provide accurate theoretical prediction of the dynamic response of a structure driven by any type of actuator and yet reflect the physical essence of actuator/structure interaction. This model has been experimentally verified.

This final technical report consists of three sections which are papers published or to be published, as follows:

- Zhang, X. D. and Rogers, C. A., 1992. "A Macroscopic Phenomenological Formulation for Coupled Electromechanical Effects in Piezoelectricity," Proceedings, Conference on Recent Advances in Adaptive and Sensory Materials and Their Applications, Blacksburg, VA, 27-29 April 1992, Technomic Publishing Co., Inc., Lancaster, PA, pp. 183-203.

- Namboodri, C. G. and Rogers C. A., "Experimental Investigation of the Electrostrictive Relaxor Ferroelectric Lead Magnesium Noibate - Lead Titinate," Proceedings, 34th SDM Conference, LaJolla, CA, April 19-21, 1993; in press.

- Namboodri, C. G. and Rogers C. A., "Constitutive Modeling of the Electrostrictive Relaxor Ferroelectric Lead Magnesium Noibate - Lead Titinate," Proceedings, 34th SDM Conference, LaJolla, CA, April 19-21, 1993; in press.

- Liang, C., Sun, F. P., and Rogers C. A., "An Impedance Method for Dynamic Analysis of Adaptive Material Systems," to be submitted to ASME *Journal of Vibration and Acoustics*.

The first paper deals with the nonlinear modeling of piezoelectric materials, the second and third paper is about the characterization and constitutive modeling of PMN-PT electrostrictive materials, and the forth one describes the development of an impedance modeling technique for the dynamic analysis of adaptive materials.

Nonlinear Modeling of Piezoelectric Ceramics

A MACROSCOPIC PHENOMENOLOGICAL FORMULATION FOR COUPLED ELECTROMECHANICAL EFFECTS IN PIEZOELECTRICITY

X. D. Zhang, C. A. Rogers

ABSTRACT

A phenomenological formulation of polarization reversal of piezoelectric materials is proposed based on the dynamics of domain switching. This formulation provides a method to describe the hysteresis in piezoelectricity as well as in electromagnetics. It is shown that a good approach to describe the nonlinear induced strain-field behavior and electromechanical hysteresis in piezoelectricity is by combining the macroscopic phenomenological aspects with the microscopic material properties. A one-dimensional thermo-electro-mechanical constitutive model for piezoceramics which undergo polarization reversal is presented using a continuum mechanics approach. This model is based on thermodynamic principles and reflects the essence of the electromechanical behavior of piezoceramics in a simple form. It is illustrated that this theory can describe the electromechanical behavior of piezoceramics simply and reasonably well.

NOMENCLATURE

A_0	Cross-sectional area of a thin ferroelectric surface
A_c	Actual area covered by domains at time t
A_{ex}	Extended area covered by domains at time t
C_σ, k_σ	Stress-state factors
C_T, k_T	Temperature factors
C_ω, k_ω	Frequency factors
C_h, k_h	Geometric factors
C_d, k_d	Grain-size factors
d	Diameter of grain size
D	Electric displacement
E	Applied electric field
E_0	Amplitude of sinusoidal field
E_c	Coercive field
E_L	Local electric field

Center for Intelligent Material Systems and Structures, Virginia Polytechnic Institute and State University, Blacksburg, VA 24061-0261

E_∞	Coefficient of coercive field
f	Deformation gradient
h	Thickness of specimen
h_0	Surface-layer thickness of specimen
i	Switching current
i_{max}	Maximum switching current
k	Newly introduced material parameter
k'	A parameter similar to k for piezoelectric cases
L	Deformation velocity
N	Number of aligned dipoles
N_1	Number of domain nucleation sites
P	Instantaneous polarization at time t
P_{cer}	Spontaneous polarization of ceramics
P^{int}	Introduced polarization as internal variable
P^r	Reversible polarization
P_s	Spontaneous polarization
P_{sc}	Spontaneous polarization of a single crystal in a certain direction
Q	Electrostriction constant
q	Internal heat source
q_{sur}	Heat flux from the surroundings
S	Entropy density
T	Temperature
t	Time
t_s	Domain switching time
t_{max}	Domain switching time corresponding to i_{max}
U	Internal energy density
v	Sideways wall velocity
v_∞	Coefficient of sideways wall velocity
X	Original coordinate system
x	Current coordinate system
Y	Young's modulus
α	Activation field for sideways wall motion
β	Correcting coefficient for calculating coercive field
ν	Rate constant
ϵ, $\boldsymbol{\epsilon}$	Engineering strain
ω	Angular frequency of a sinusoidal field
$\bar{\epsilon}$, $\bar{\boldsymbol{\epsilon}}$	Green strain
Γ	Electromechanical tensor
Θ	Thermoelastic tensor
ξ	Relative polarization
ρ	Mass density in current coordinate system
ρ_0	Mass density in original coordinate system
σ	Engineering stress
$\bar{\sigma}$, $\bar{\boldsymbol{\sigma}}$	The second Piola-Kirchhoff stress
Ω	Polarization reversal tensor

Φ	Helmholtz free energy

SUBSCRIPTS AND SUPERSCRIPTS

0	Initial condition
cer	Ceramics
d	Grain size
h	Geometric
int	Internal variable
r	Reversal
T	Temperature
σ	Stress
ω	Frequency

INTRODUCTION

The microstructural and electromechanical aspects of piezoelectric ceramics are currently being studied extensively. An increasing number of practical applications have been demonstrated and proposed in recent years for piezoelectric ceramics. With the technological trend for less driving power and miniaturization of devices, piezoelectric materials are playing a more and more important role in intelligent material systems and structures.

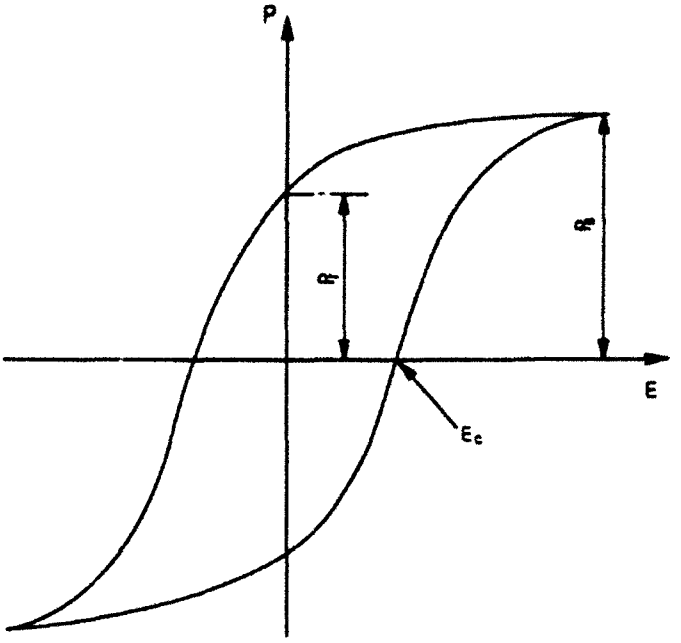

Figure 1: Schematic diagram of a typical hysteresis loop for piezoelectric ceramics

Ferroelectric ceramics are composed of many crystallites with randomly-distributed polar axis orientations. When a piece of ferroelectric ceramics is poled by applying a high electric field during processing, the ceramics become piezoelectric and are called piezoceramics. Lead zirconate titanate (PZT) type ceramics, which have numerous applications, are the most researched piezoceramics.

Piezoceramics exhibit a linear relationship between the components of the electric-field vector and the induced strain tensor components. But the linear relationship is only valid for a low field (usually less than 100 V/mm for commercial PZTs). For large fields, the nonlinearity and hysteresis appear during the increase and decrease of the field and influence the accuracy of large induced-strain actuation. The electric field-induced strain hysteresis may result in a multi-valued output problem, namely, for a given input value, the output strain can be one of the many values (Anderson and Crawley, 1989).

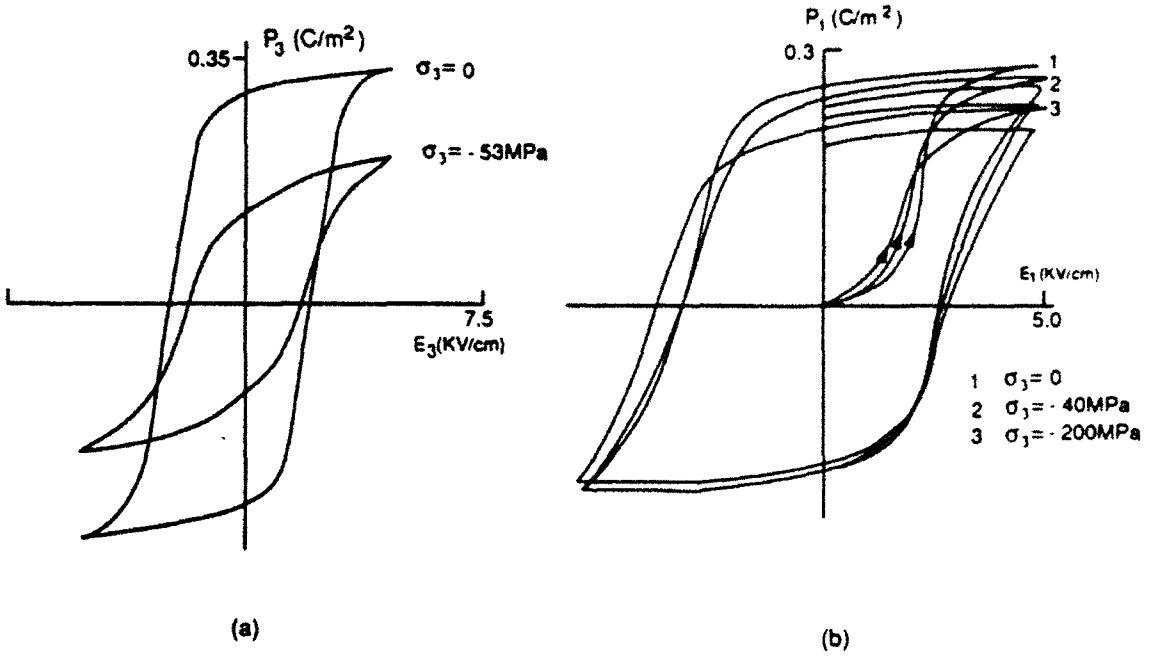

Figure 2: Dielectric hysteresis loop for different biasing compressive stresses (Arndt, Schmidt and Vogel, 1984) (a) parallel compressive stresses (b) compressive stresses perpendicular to the field.

In piezoceramics, the relationship between electric displacement D and applied field E forms a hysteresis loop. A typical hysteresis loop for electric displacement D and applied field E is shown in Fig. 1. The important parameters which determine the shape of the hysteresis loop are spontaneous polarization P_s, remanent polarization P_r, and coercive field E. There is general agreement that the hysteresis loop is a consequence of the delayed responses of polarization reversal and domain switching. The hysteresis

arises from the energy needed to switch the domain and polarization during each cycle of the field. Although the hysteresis loop appears to be independent of time, it is known that each point on the loop is a function of time because the polarization reversal and domain switching depend not only on material properties and temperatures but also on time rates and the magnitude of the applied field. More specifically, the polarization P is a function of applied field E and time of domain switching t: $P = f(E,t)$ (Pulvari and Kuebler, 1958).

The hysteretic behavior of the piezoceramics is a complex issue, sensitive to applied stresses and temperature. Figure 2 exhibits the influence of an applied stress field on the hysteresis loop (Armdt, Schmidt and Vogel, 1984). It is shown that a parallel compressive stress decreases the spontaneous and remanent polarization as well as the coercive field, but a compressive stress perpendicular to the field only slightly increases the coercive field. The temperature is also an important factor which influences the hysteresis loop. Figure 3 shows that the remanent polarization P_r and coercive field E_c are functions of temperature (Gerthsen and Krüger, 1976). It is shown that the whole hysteresis loop shrinks with increasing temperature. It is thus revealed that the hysteresis loop is a manifestation of the coupled electromechanical behavior of piezoceramics.

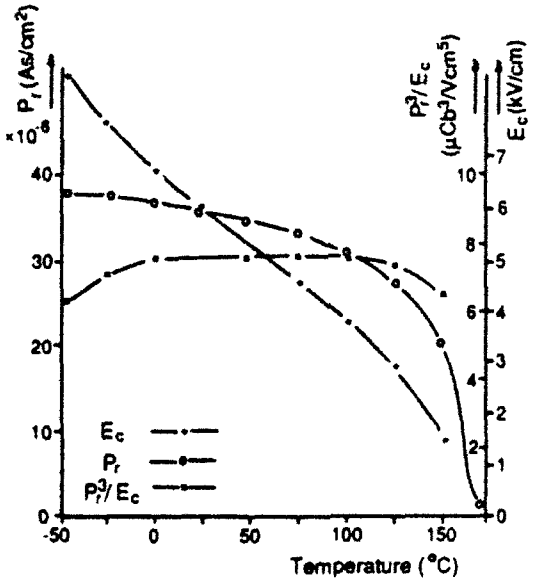

Figure 3: Remanent polarization P_r, coercive field E_c, and ratio P_r^3/E_c shown as functions of temperature for PLZT ceramics (Gerthsen and Krüger, 1976).

In order to exploit piezoceramics for engineering applications and describe the nonlinear behavior of the material, it is necessary to formulate a theoretical model which can predict the performance of piezoceramics under various conditions. In this paper, a general phenomenological formulation for polarization reversal dynamics will be proposed.

The factors which affect the electromechanical hysteresis will be analyzed. A procedure for formulating a mathematical model for piezoelectricity will be presented based on the detailed analyses of domain switching dynamics and on the material properties. A one-dimensional thermo-electro-mechanical constitutive model will be formulated using a continuum mechanics approach.

PRELIMINARY CONSIDERATIONS

Much work has been done on single crystals from a microscopic viewpoint. Among these investigations, the thermodynamic theory of single crystals has been intensively researched. Devonshire (1949) put forward a phenomenological theory of ferroelectricity which proposes an expression of the free energy in terms of polarization P, temperature T and stress σ, namely, $G = f(P, \sigma, T)$. The relationships between the parameters of electric field, polarization, and temperature can be inferred from this theory. Devonshire's work has been extended by numerous studies and is qualitatively in agreement with experimental results. Even in recent years, this theory has been used in thermodynamic studies of $PbTiO_3$ single crystals (Haun et al., 1987; Rossetti et al., 1990). This theory has also been extended to model the dielectric properties of $BaTiO_3$ polycrystals (Shaikh and Vest, 1989).

Another aspect of the microscopic studies of ferroelectricity is the domain switching process and polarization reversal (Pulvari and Kuebler, 1958). Through either the direct observation of domain wall motion during polarization reversal or measurement of the switching transient under pulsing conditions, the domain switching processes have been intensively studied in ferroelectric materials. It has been shown that nucleation of domains and domain wall motion are the responsible mechanisms for the domain switching process. The domain switching time can be expressed as a function of applied field and the associated material properties. But, the mechanism of the domain configuration and the switching process are still not well understood. On the other hand, most of the practical ferroelectric materials are in polycrystalline ceramic form and more parameters, such as grain boundary and intergranular stresses will complicate the microscopic formulation. In addition, the single crystal properties must be averaged over the crystalline orientations. Therefore, it is difficult at the present time to propose a satisfactory theory of ferroelectrics from a microscopic viewpoint.

It is significant that a macroscopic theory of ferroelectric materials can be formulated in terms of external parameters such as applied electric field, stress state, temperature, dielectric properties and geometric configurations. If such a macroscopic theory can be developed, it will be very easy to use in the prediction of piezoelectric behavior. It is noted that formulation of such a theory with acceptable precision would still be a tremendous task. From a physical viewpoint, Chen and co-workers (Chen and Peercy, 1979; Chen and Montgomery, 1980) proposed a semi-macroscopic phenomenological theory for the hysteresis and butterfly loops in ferroelectric materials based on the relationship between the domain switching under an external electric field and the number of dipoles aligned in the direction of the field. This theory suggested that the mechanical stress

σ and electric displacement D are functions of the mechanical strain ϵ, the absolute temperature T, the external electric field E, and the number of aligned dipoles N:

$$\begin{cases} \sigma = \hat{\sigma}(\epsilon, T, E, N) \\ D = \hat{D}(\epsilon, T, E, N). \end{cases} \tag{1}$$

It is noted that the N is the effective number of aligned dipoles and is determined by the projection of the dipole moments to E. The number of aligned dipoles N obeys the rate law:

$$\dot{N} = h(\epsilon, T, E, N). \tag{2}$$

This theory represents a new method to characterize the behavior of the ferroelectric materials. It is mentioned that the parameter N has only a pure physical sense and is microscopic. The parameter N cannot match the real polycrystal material where dipoles are arranged in randomly-distributed domains.

Based on the first and second law of thermodynamics, Bassiouny and co-workers (Bassiouny, Ghaleb and Maugin, 1988, 1989) developed a complete phenomenological theory for coupled electromechanical hysteresis effects. Two sets of state variables are used to describe the coupled electromechanical process. One set is the normal state variable such as temperature, the total strain ϵ and the total polarization. The second type of state variable refers to internal variables such as plastic strain and residual polarization by which actual state depends also on the past history. In Bassiouny's theory, an introduced electric polarization P^{int} is chosen as an internal variable. The free energy per unit volume can be expressed as a function of total strain ϵ, reversible polarization P^r, internal variable P^{int} and temperature T:

$$\Phi = \Phi(\epsilon, P^r, P^{int}, T), \tag{3}$$

where P^r is the difference between total electric polarization and residual polarization. T denotes the absolute temperature measured from a reference temperature, T_0. After using the Clausius-Duhem inequality and decomposition of the dissipation inequality, a phenomenological theory for coupled electromechanical hysteresis is proposed by analogy of Drucker's inequality in plasticity and the assumption of loading functions. This theory provides a very good method of treating electromechanical hysteresis in a continuous media. It seems that the theory is purely a mathematical issue because too many assumptions and approximations are used. For example, the coercive field is assumed to be a constant in the loading functions and the material coefficients are introduced by expanding the free energy function Φ in terms of the independent variables.

There are two approaches to modeling a constitutive relation for a material. One is the macroscopic phenomenological method in which a few state variables are used to describe the material behavior in an analogous sense. The other is the microscopic physical method which derives the constitutive relation from fundamental physical concepts. The phenomenological approach is often used in engineering practice, but can rarely provide the physical essence of the material behavior. The microscopic method can explain the experimental phenomena physically, but is far from quantitative. Therefore, a combination of the two approaches will perhaps give a better prediction of the material behavior.

In modeling the coupled electromechanical behavior in piezoelectricity, a macroscopic phenomenological approach based on thermodynamics will yield a reasonable macroscopic theory which can describe the material behavior both phenomenologically and physically. This approach will consider the characteristics of the material properties and the domain dynamics.

DOMAIN DYNAMICS

CONCEPTS OF DOMAINS AND DOMAIN DYNAMICS

In a single crystal or a crystallite, the dipoles are usually not polarized uniformly in one direction. Single crystals or crystallites are composed of numerous domains which contain large numbers of dipoles all aligned in the same direction. The domains are separated by domain walls which are the loci of the points where the dipole orientation suddenly changes (Fatuzzo and Merz, 1967). Two kinds of domain walls are formed in one crystallite: 90° and 180° in tetragonal symmetry or 71°/109° and 180° in rhombohedral symmetry. The walls which separate antiparallel domains are called 180° domain walls and those which separate dipoles at right angles to each other are called 90° walls. Figure 4 is a graphical representation of 180° and 90° domains in barium titanate.

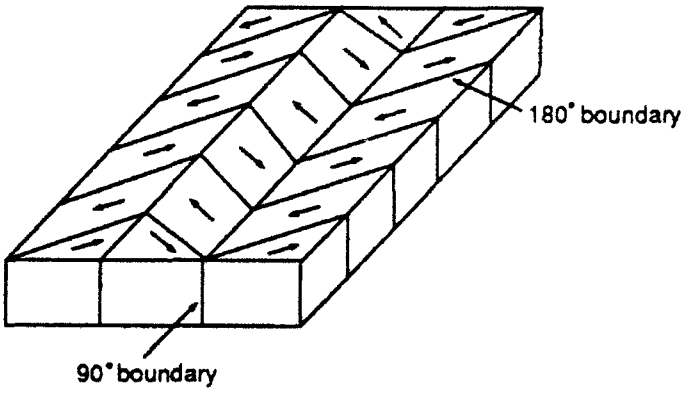

Figure 4: Schematic diagram of 180° and 90° domains in tetragonal symmetry.

The static configurations have been studied using several techniques such as induced strain, etching, powder, TEM and SEM. Domain reorientation can be caused by either an electric field or mechanical stress, but domain processes are influenced differently. In one crystallite, both 90° and 180° domain reorientations in tetragonal symmetry or both 71°/109° and 180° domain reorientations in rhombohedral symmetry can occur under a high d.c. electric field. Mechanical stress can only cause 90° domain reorientation in tetragonal symmetry or 71°/109° domain process in rhombohedral symmetry because only these non-180° domain processes incur the mechanical strain or dimensional change of the specimen.

The detailed dynamics of changes in domain configuration under an applied field or stress are complex. When a single crystal or a crystallite is under an applied electric field, the new domains are first nucleated and formed mainly at the surface. They grow forward through the thickness of the crystal, and then expand sideways and coalesce until all the region is occupied by the newly-formed domains. It has been shown that the sideways growth of domains plays an important role in the domain switching process. The sideways wall velocity at low electric field may be expressed as:

$$v = v_\infty \exp\left(-\frac{a}{E}\right), \tag{4}$$

where a is the activation field for sideways wall motion and v_∞ is a constant. a is a function of specimen thickness h and temperature, the value of a decreases linearly with increasing temperature. The relationship between activation field a and thickness h can be obtained as follows:

$$a = a_0\left(1 + \frac{h_0}{h}\right) \tag{5}$$

The above relations are valid for $h \geq h_0$, where h_0 is the surface-layer thickness where the domain switching behavior is independent of the thickness. The coercive field can be explained physically as a field where the reversed domains cover exactly one-half of the volume of the sample. The coercive field can also be expressed as a function of specimen thickness h in a similar way as activation field a.

$$E_c = E_\infty\left(1 + \frac{h_0}{h}\right), \tag{6}$$

where E_∞ is a constant.

BASIC THEORIES OF POLARIZATION REVERSAL DYNAMICS

Electrical techniques are widely used for studying the polarization reversal dynamics. The Miller-Sawage technique of analyzing the electric behavior of ferroelectric materials under square pulses is the most reliable and popular method used to study the domain wall motion and domain switching time t_s (Fatuzzo and Merz, 1967). The important parameters which can be measured experimentally are the switching time, the maximum switching current i_{max}, and the normalized shape of the pulse. The switching time t_s is basically defined as the time necessary to reverse a certain fraction (e.g., 95%) of the total polarization. In practice, t_s is usually defined as the time necessary for the switching current i to drop to a certain fraction of its maximum value i_{max}. The terms t_s and i_{max} are related to each other with spontaneous polarization, P_s, i.e., $2P_s = i_{max}t_s f$, where f is a shape factor which depends on the shape of the switching curve (generally ranges from 0.43 to 1.0). Merz (1954) found experimentally that both t_s and i_{max} in $BaTiO_3$ change with the electric field E following an exponential law at low electric field ($< 15KV/cm$):

$$\begin{aligned} i_{max} &= i_0 \exp\left(-\frac{a}{E}\right) \\ t_s &= t_0 \exp\left(\frac{a}{E}\right). \end{aligned} \tag{7}$$

where i_0 and t_0 are constants. Stadler (1958) extended Merz's measurements to the high-field range ($10 \sim 100KV/cm$) and found that the switching time t_s follows a power

law of the type: $t_s = aE^{-b}$, where a and b are constants. This coincides with the fact that for high electric field, only the first power term of the expanded exponential law of Eq. (7) remains significant.

Numerous theories for polarization reversal dynamics have been proposed either empirically or theoretically. Based on Merz's (1954) experimental results, Landauer, Young and Drougard (1956) proposed a polarization theory for $BaTiO_3$. The switching rate, dP/dt, varies with $\exp(-\frac{\alpha}{E(t)})$ as follows:

$$\frac{dp}{dt} = \nu(P_s - P)\exp(-\frac{\alpha}{E(t)}), \tag{8}$$

where $E(t)$ is the instantaneous field, ν is a rate constant which is independent of field and polarization, and, $(P_s - P)$ represents the fact that the probability of forming new domains is proportional to the residual volume of the original polarization. If the peak voltage value of the sine wave is twice the coercive voltage or larger, one can take $E(t)$ to be $\bar{E}t$ and integrate Eq. (8):

$$\frac{P}{P_s} = 1 - 2\exp[\frac{\nu\alpha}{\bar{E}}F(\alpha/E)] \tag{9}$$

where $F(u) = \frac{e^{-u}}{u} - \int_u^\infty \frac{e^{-x}}{x}dx$, and can be evaluated by mathematical series. The above equation exhibits the time dependence of the instantaneous polarization during the switching process and defines the shape of the hysteresis loop.

Pulvari and Kuebler (1958) developed a phenomenological theory of polarization reversal in $BaTiO_3$ single crystals based on the electric transient response under pulsed voltage. From the experimental results, it has been shown that the current transient can be expressed as $i = i_{max}f(\frac{t}{t_{max}})$ and $\int_0^\infty i\,dt$ =constant, where t_{max} is the domain switching time corresponding to i_{max}. It has also been demonstrated experimentally that t_{max} can be represented as a function of electric field: $\frac{1}{t_{max}} = \nu E\exp(-\alpha/E)$. α and ν have the same physical meaning as introduced above. A approximation function, f, which satisfies the physical principle of the transient response of the pulsed voltage is assumed as follows:

$$f(\frac{t}{t_{max}}) = e^{\frac{1}{2}}(\frac{t}{t_{max}})\exp[-\frac{1}{2}(\frac{t}{t_{max}})^2]. \tag{10}$$

According to the stated assumption and experimental evidence, one can obtain the polarization switching dynamics as follows:

$$\frac{P}{P_s} = 1 - 2\exp[-\frac{1}{2}(\nu tEe^{-\frac{\alpha}{E}})^2]. \tag{11}$$

It has been demonstrated that the dynamic expression of Eq. (11) is in agreement with some experimental results.

In addition to Landauer's theory and Pulvari's model, which are empirical and based on experimental results, theoretical models have also been proposed to account for the

polarization reversal dynamics. Avrami (1939, 1940, 1941) has demonstrated that the extended area $A_{ex}(t)$ of a thin ferroelectric material can be related to the actual area $A_c(t)$ which is covered by the domains at time t:

$$A_0 - A_c(t) = A_0 \exp\left[-\left(\frac{A_{ex}(t)}{A_0}\right)\right], \tag{12}$$

where A_0 represents the cross-sectional area of the thin ferroelectric surface. $A_{ex} = \sum_{i=1}^{n} a_i(t)$, and $a_i(t)$ is the area of the ith domain at time t while the influence of the other $(n-1)$ domains to the ith domain is neglected. For the sake of simplicity, a fixed number of nucleation sites N_1 and the same extended area a(t) for every domain are assumed for a unit surface area. In a thin layer of ferroelectric material, the total extended area per unit area of the electrode (in the same sense as $A_{ex}(t)$ in Eq. (12) if $A_0 = 1$ is assumed) for the positive half-period of a sinusoidal electric field can be expressed as (Janta, 1971):

$$A_{ex}(t) = N_1 a(t) = 2N_1\left[h_0 + \frac{v_\infty}{\omega} g(\omega t, \frac{E_0}{\alpha})\right], \tag{13}$$

where $g(\omega t, \frac{E_0}{\alpha}) = \int_0^{\omega t} \exp\left(-\frac{\alpha}{E_0 \sin x}\right) dx$. The velocity of the (apparent) sideways motion of the domain walls is assumed, as in Eq. (4). ω is the angular frequency of the electric field, v_∞ represents a constant which has the same meaning as in Eq. (4), h_0 denotes the initial domain half-width, and E_0 is the amplitude of the sinusoidal field. Setting $A_0 = 1$ in Eq. (4), one can obtain the expression for mutual overlap of growing domains per unit cross-sectional area as $A_c(t) = 1 - \exp\left[-A_{ex}(t)\right]$. The relative polarization can be expressed in terms of $A_{ex}(t)$ as:

$$\frac{P(t)}{P_s} = 2A_c(t) - 1 = 1 - 2\exp\left[-A_{ex}(t)\right]. \tag{14}$$

For steady-state hysteresis loops, one may use the symmetry condition $P(\pi) = -P(0)$ for a sinusoidal field to obtain the initial value h_0. Combination of Eq. (13) and Eq. (14) gives:

$$\frac{P(t)}{P_s} = 1 + \left[1 + \tanh\left(N_1 \frac{v_\infty}{\omega} g(\pi, \frac{E_0}{\alpha})\right)\right] \exp\left[-2N_1 \frac{v_\infty}{\omega} g(\omega t, \frac{E_0}{\alpha})\right]. \tag{15}$$

It should be noted that the above simplified theory is based on the sideways expansion of randomly-distributed 180° domains which are assumed to have the same size and form. Nucleation and forward wall motion are neglected. It has been shown that in the case of cylindrical domains, an expression similar to Eq. (15) may be obtained (Jnata, 1971). It should be noted that the above polarization reversal theories are only valid for single crystals. For polycrystals or ceramics, the situation may be quite different.

Polycrystalline ceramics are more important than single crystals because it is easier to maintain quality control with them and they are simple and inexpensive to produce. However, their domain dynamics and domain configuration are more complex than those for single crystals. The grain size and the grain boundary properties are very important

factors which influence the domain dynamics. Figure 5 represents spontaneous polarization of $BaTiO_3$ as a function of grain size (Shaikh and Vest, 1989). The spontaneous polarization increases with the increase in grain size because as grain size decreases, the grain boundary area (an amorphous state) increases where ferroelectricity does not exist. The spontaneous polarization of large-grain polycrystals of $BaTiO_3$ in an unpolarized state can be calculated from the single-crystal values as follows (Arlt and Sasko, 1980):

$$P_{cer} = \int_{-\frac{\pi}{2}}^{\frac{\pi}{2}} \int_{-\frac{\pi}{2}}^{\frac{\pi}{2}} \frac{P_a \cos\theta \cos\phi}{\pi^2} d\theta d\phi, \tag{16}$$

where $P_a = \frac{\sqrt{2}P_{sc}}{3}$, and P_{sc} is the spontaneous polarization of the single-crystal $BaTiO_3$ along the $< 001 >$ direction. Integrating the above equation yields $P_{cer} = 0.19P_{sc}$. For poled piezoceramics, the spontaneous polarization is larger than $0.19P_{sc}$.

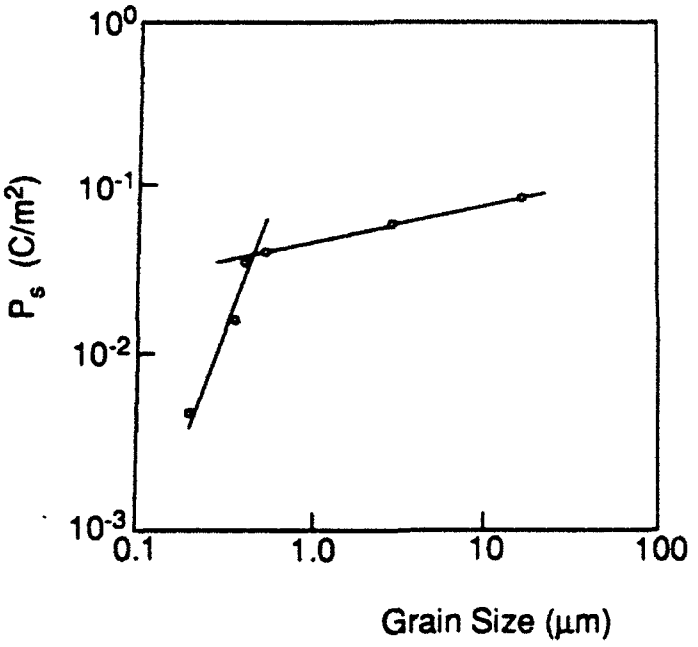

Figure 5: Variation of spontaneous polarization of $BaTiO_3$ ceramics at $70°C$ with grain size (Shaikh and Vest, 1989).

PHENOMENOLOGICAL FORMULATION OF THE POLARIZATION REVERSAL DYNAMICS FOR CERAMICS

As previously discussed, the mechanism and process of polarization reversal are still not well understood. The basic theories of polarization reversal introduced here are only approximate descriptions of the hysteresis loop. Therefore, it is very difficult to formulate a dynamic theory of polarization reversal by its mechanism or process. Phenomenological formulation may provide an alternative method to describe and predict the hysteresis loop in a simple form. As we know, the instantaneous polarization (P) or relative polarization (P/P_s) is an exponential function of the applied field. It is postulated that

an exponential function of electric field or a combination of exponential functions may provide a better formulation. If a typical hysteresis loop is represented as $\frac{P}{P_s} = f(E)$, where E may be a function of time, the basic characteristics of the hysteresis loop may be expressed as at $E = \pm E_c$, $\frac{\partial^2 f}{\partial E^2} = 0$, because two points $(\pm E_c, 0)$ are the points of inflection of the hysteresis loop, at $P > 0$, $\frac{\partial^2 f}{\partial E^2} < 0$ and at $P < 0$, $\frac{\partial^2 f}{\partial E^2} > 0$. It is fortunate that the hyperbolic tangent function $\frac{P}{P_s} = \tanh k(E \pm E_c)$ can match all the characteristics of the hysteresis loop. It is therefore logical that a phenomenological formulation for a steady-state loop may be proposed as follows:

$$\begin{cases} \frac{P}{P_s} = \tanh k(E - E_c) & \frac{dE}{dt} > 0 \\ \frac{P}{P_s} = \tanh k'(E + E_c) & \frac{dE}{dt} < 0, \end{cases} \tag{17}$$

where E_c represents the amplitude of the coercive field. k and k' are newly introduced material parameters. For the case of general ferroelectric ceramics in which the domains are randomly distributed, k is equal to k'. For piezoelectric ceramics, there is a difference between the polarization along the poling direction and the polarization antiparallel to the poling direction; different k and k' values are suitable for this case. It should be noted that the remanent polarization P_r can be obtained easily from Eq. (17) as $P_r = P_s \tanh k' E_c$. The virgin curve may be expressed as $P = P_s \tanh kE$.

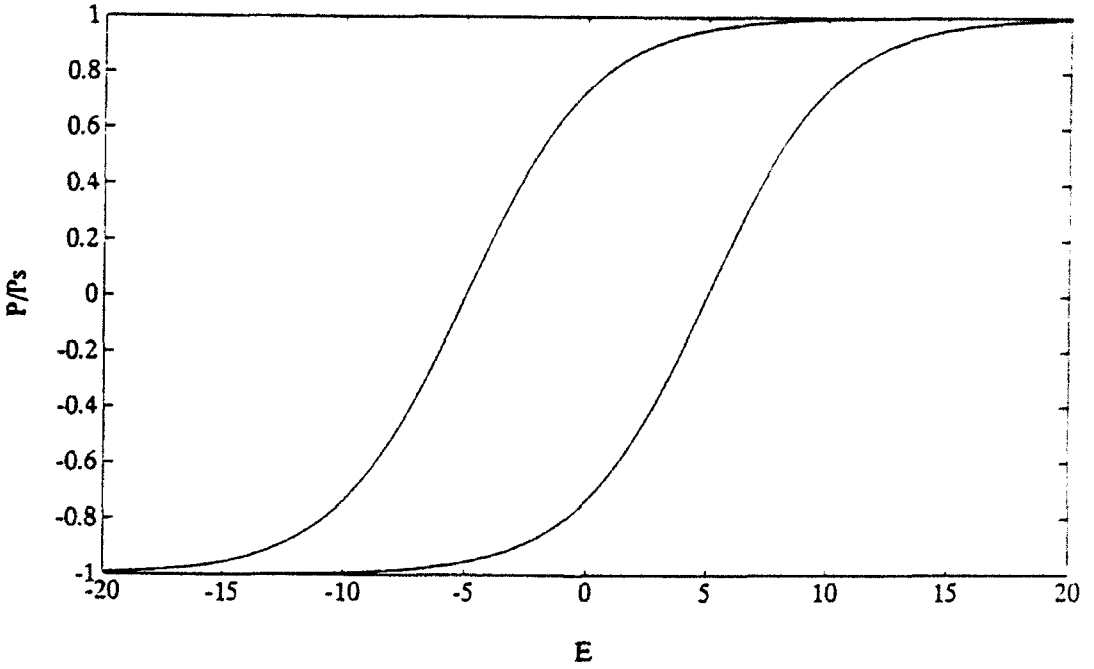

Figure 6: Typical hysteresis loops calculated from the proposed phenomenological polarization reversal model.

The shape of the steady-state hysteresis loop can be totally predicted and described by the two parameters k and E_c through Eq. (17). Figure 6 is an illustration of typical

hysteresis loops calculated from Eq. (17) for different k and E_c values. It is demonstrated that different k values give different curvatures and the amplitude of the coercive field, E_c, determines the horizontal size of the loop. It is necessary that the material parameter k and the coercive field E_c could be determined either theoretically or experimentally. As discussed above, the coercive field E_c is a function of stress state, temperature, frequency of the electric field, geometrical shape, and material properties such as grain size. Therefore the coercive field E_c can be represented mathematically in terms of external variables and material properties:

$$E_c = \hat{E}_c(\sigma, T, \omega, h, d), \tag{18}$$

where h represents the thickness of the specimen as in Eq. (6) and d denotes the diameter of the grain size. It seems very difficult at the current time to evaluate E_c theoretically. Gerthsen and Krüger (1976) calculated the coercive field assuming that polarization reversal is basically determined by 90° reorientation. This requires P_s^3/E_c to be constant (as is shown in Fig. 3 for P_r^3/E_c):

$$E_c = \beta Y Q^2 P_s^3, \tag{19}$$

where β is a correcting coefficient considering the different domain alignments in adjacent grains, Y is the elastic modulus, Q represents the electrostriction constant and P_s is the spontaneous polarization. Because P_s is also a complicated function of external variables and material properties, E_c still cannot be determined except when P_S is known. If it is assumed that the effect of external variable and material properties to the coercive field E_c are independent of each other, E_c may be obtained analogous to the determination of fatigue strength (Shigley and Mitchell, 1983):

$$E_c = C_\sigma C_T C_\omega C_h C_d E_{co}, \tag{20}$$

where C_σ, C_T, C_ω, C_h and C_d represent stress-state factor, temperature factor, frequency factor, geometric factor and grain size factor for coercive field, respectively. E_{co} denotes a coercive field at a reference state. By experimental parametric study, all the coefficients may be determined. The material parameter k may also be expressed as a function of external variables and material properties:

$$k = \hat{k}(\sigma, T, \omega, h, d), \tag{21}$$

and analogous to the arguments for the coercive field, the material parameter k may be obtained as:

$$k = k_\sigma k_T k_\omega k_h k_d k_0, \tag{22}$$

where k_σ, k_T, k_ω, k_h and k_d have similar meanings as the same coefficients of coercive field. k_0 denotes a specific k value at a reference state. All the coefficients of k may also be determined by experimental parametric study as in the determination of fatigue strength.

From an engineering viewpoint, the above polarization reversal phenomenology is significant due to its simplicity. This formulation does provide an approach to describe

the hysteresis loop in a sense similar to Paris's law predicting the crack-propagation behavior of fatigue. On one hand, there is no polarization reversal dynamic theory in existence which can describe the hysteresis loop in ceramics because of the complicated essence of the problem and because too many factors influence the hysteresis of ceramics. Although Chen's semi-microscopic theory and Bassiouny's thermodynamic theory may reveal some features of domain switching in ceramics, they are still in the mathematical stage and are too complicated to apply to engineering. On the other hand, the above phenomenological dynamic theory may be used directly in engineering with acceptable precision. With the development of ferroelectric memory appliances, k and E_c may be used as the criteria to evaluate whether or not the memory property of ferroelectric ceramics or thin films is sufficient. In these cases, the stress components are zero, and the frequency dependence of k and E_c at low-range frequencies is negligible (as shown in Fig. 7 for E_c). Therefore, k and E_c are material constants which depend only on material properties. In addition, the above polarization reversal phenomenology may be used to describe the electromagnetic hysteresis loops.

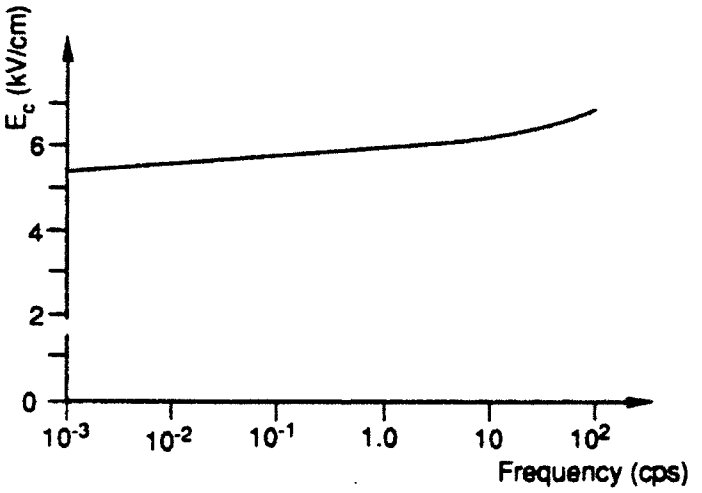

Figure 7: The frequency dependence of coercive field E_c for PLZT ceramics (Gerthsen and Krüger, 1976).

THERMODYNAMIC FORMULATION FOR COUPLED ELECTROMECHANICAL EFFECTS IN PIEZOELECTRICITY

As discussed above, formulation of a microscopic theory for piezoceramics is difficult due to the complexity of the problem. From a material viewpoint, the factors which influence the nonlinearity of piezoceramics are composition, ceramic structure, grain size,

internal defects and internal stress. From a mechanical aspect, applied stress, temperature and applied electric field may affect the nonlinear behavior of piezoceramics. In Chen's semi-microscopic theory, the number of aligned dipoles N cannot describe the polycrystal material in an engineering sense where dipoles are arranged in randomly-distributed domains. Bassiouny's theory does provide a reasonable approach to predict the electromechanical hysteresis in a continuous media. But this theory is still in a purely mathematical stage and is not easy to use in engineering applications. In this section, a one-dimensional macroscopic phenomenological formulation will be proposed based on the first and second laws of thermodynamics using a continuum mechanics approach. In this study, the material under consideration is polycrystal, and the polarization reversal and electromechanical processes may be considered as processes where both polarization inertia and gradients are neglected.

Analogous to Tanaka's model of SMA materials, which are subjected to thermoelastic martensitic transformation or its reverse transformation (Tanaka, 1986), a one-dimensional ceramic material is considered which is undergoing either polarization or reverse polarization. The energy balance equation and Clausius-Duhem inequality in the current x-coordinate may be expressed as:

$$\begin{aligned} &\rho\dot{U} - \sigma L + E_L\dot{D} + \tfrac{\partial q_{sur}}{\partial x} - \rho q = 0 \\ &\rho\dot{S} - \rho\tfrac{q}{T} + \tfrac{\partial}{\partial x}(\tfrac{q_{sur}}{T}) \geq 0, \end{aligned} \tag{23}$$

where ρ is the density in the current deformed configuration, L is the deformation velocity, and σ, U and q_{sur} denote the Cauchy stress, the internal energy density and the heat flux from the surroundings, respectively. E_L is the local electric field at a given point within the material and D is the electric displacement. The superposed dot denotes a material derivative. T, q and S represent the temperature, internal heat source, and entropy density, respectively. According to Tanaka's definition, the above energy balance equation and Clausius-Duhem inequality may be written in the original configuration state, X, as:

$$\begin{aligned} &\rho_0\dot{U} - \bar{\sigma}\dot{\bar{\epsilon}} + \tfrac{\rho_0}{\rho}E_L\dot{D} + f^{-1}\tfrac{\rho_0}{\rho}\tfrac{\partial q_{sur}}{\partial X} - \rho_0 q = 0 \\ &\rho_0\dot{S} - \rho_0\tfrac{q}{T} + f^{-1}\tfrac{\rho_0}{T\rho}\tfrac{\partial q_{sur}}{\partial X} - f^{-1}\tfrac{\rho_0 q_{sur}}{T^2\rho}\tfrac{\partial T}{\partial X} \geq 0, \end{aligned} \tag{24}$$

where ρ_0 is the mass density with reference to the original configuration, f is the deformation gradient, $\bar{\sigma} = \frac{\rho_0}{\rho}\frac{\sigma}{f^2}$ is defined as the second Piola-Kirchhoff stress, $\bar{\epsilon} = \frac{f^2-1}{2}$ is the Green strain.

The thermomechanical state of a ceramic material at a given point at time t is completely determined by a set of state variables. It is considered (Bassiouny, Ghaleb and Maugin, 1988) that the temperature T, the total strain ϵ and the instantaneous polarization P define the coupled electromechanical behavior for a reversible process. In order to use the proposed phenomenological polarization reversal formulation of Eq. (17), we assume that the set of state variables which describe the coupled electromechanical process of piezoceramics are total strain ϵ, temperature T, relative polarization $\frac{P}{P_s}$ (which will be

denoted by ξ), and external electric field E. It should be noted that except at the external surface of the specimen, the external electric field does not act on a given point within the material. It may be considered as a pseudo-state variable whose effect on a given point within the material is through a so-called local electric field E_L and relative polarization ξ which determines the polarization state of a given point. Such a state variable is assumed to reveal the implied relationship between the stress state and an applied electric field E in an explicit form. The assumed general state variable may be expressed as:

$$\Lambda \equiv (\bar{\epsilon}, T, \xi, E). \tag{25}$$

The Helmholtz free energy, which is the driving force of the electromechanical process, is a function of the state variable Λ and is given by:

$$\Phi(\Lambda) = U - TS. \tag{26}$$

Considering Eq. (25) and taking derivatives of Eq. (26) yields:

$$\dot{\Phi} = \frac{\partial \Phi}{\partial \bar{\epsilon}}\dot{\bar{\epsilon}} + \frac{\partial \Phi}{\partial T}\dot{T} + \frac{\partial \Phi}{\partial \xi}\dot{\xi} + \frac{\partial \Phi}{\partial E}\dot{E} = \dot{U} - \dot{T}S - \dot{S}T. \tag{27}$$

Substituting Eq. (27) and the energy balance equation (Eq. $(24)^1$) into the Clausius-Duhem inequality (Eq.$(24)^2$) and expressing every term in the original configuration X gives:

$$(\frac{\bar{\sigma}}{\rho_0} - \frac{\partial \Phi}{\partial \bar{\epsilon}})\dot{\bar{\epsilon}} - (S + \frac{\partial \Phi}{\partial T})\dot{T} - \frac{\partial \Phi}{\partial \xi}\dot{\xi} - \frac{\partial \Phi}{\partial E}\dot{E} - \frac{1}{\rho}E_L\dot{D} - \frac{1}{\rho T}f^{-1}q_{sur}\frac{\partial T}{\partial X} \geq 0. \tag{28}$$

From the thermodynamics of continuous media, the coefficients of $\dot{\bar{\epsilon}}$ and $\dot{T}$ should vanish. Therefore the inequality of Eq. (28) yields the electromechanical constitutive equation:

$$\bar{\sigma} = \rho_0 \frac{\partial \Phi}{\partial \bar{\epsilon}} = \hat{\sigma}(\bar{\epsilon}, T, \xi, E). \tag{29}$$

Taking the derivative of the above equation, the rate form of the electromechanical constitutive equation may be given as:

$$\dot{\bar{\sigma}} = Y\dot{\bar{\epsilon}} + \Theta\dot{T} + \Omega\dot{\xi} + \Gamma\dot{E}, \tag{30}$$

where Y, Θ, Ω and Γ represent Young's modulus, thermoelastic tensor, polarization reversal tensor and electromechanical tensor, respectively. These material properties so derived may be expressed in terms of Helmholtz free energy:

$$\begin{aligned} Y &= \rho_0 \tfrac{\partial^2 \Phi}{\partial \bar{\epsilon}^2} \\ \Theta &= \rho_0 \tfrac{\partial^2 \Phi}{\partial \bar{\epsilon} \partial T} \\ \Omega &= \rho_0 \tfrac{\partial^2 \Phi}{\partial \bar{\epsilon} \partial \xi} \\ \Gamma &= \rho_0 \tfrac{\partial^2 \Phi}{\partial \bar{\epsilon} \partial E}. \end{aligned} \tag{31}$$

Eq. (30) and (31) provide a simple coupled electromechanical model which describe the stress-strain relation in an explicit form. However, a detailed experimental procedure is needed to determine the material constants which are defined in Eq. (31). It should be noted that the 'one-dimensional' is only required for the induced strain and the external applied stress but not for the applied field.

A SPECIAL CASE

In an isothermal process, where there is no temperature change, the T term in Eq. (30) will vanish ($\dot{T} = 0$). Therefore, Eq. (30) may be rewritten as:

$$\dot{\bar{\sigma}} = Y\dot{\bar{\epsilon}} + \Omega\dot{\xi} + \Gamma\dot{E}. \tag{32}$$

For a low-frequency case where the stress-strain process may be considered as quasi-static, the stress $\bar{\sigma}$, strain $\bar{\epsilon}$ and relative polarization ξ can be envisioned as functionals of the electric field E where the independent variable is time t. The time derivatives may be given as: $\dot{\bar{\sigma}} = \frac{\partial \bar{\sigma}}{\partial E}\dot{E}$, $\dot{\bar{\epsilon}} = \frac{\partial \bar{\epsilon}}{\partial E}\dot{E}$, and $\dot{\xi} = \frac{\partial \xi}{\partial E}\dot{E}$. Substituting into Eq. (32) one may obtain:

$$\frac{\partial \bar{\sigma}}{\partial E} = Y\frac{\partial \bar{\epsilon}}{\partial E} + \Omega\frac{\partial \xi}{\partial E} + \Gamma. \tag{33}$$

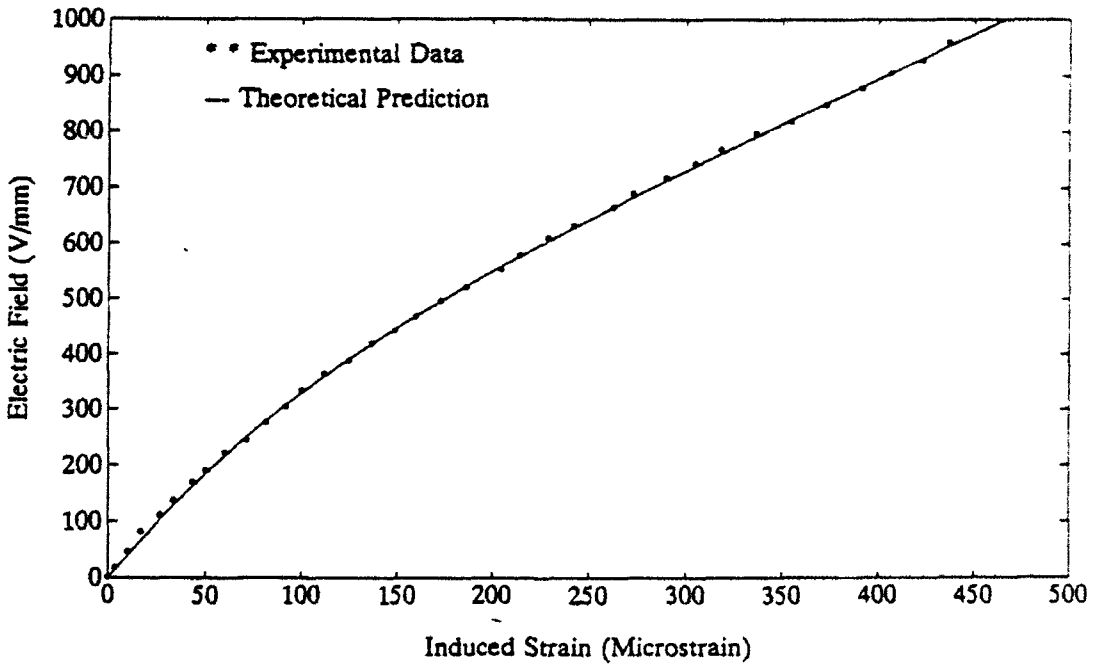

Figure 8: Comparison of experimental data (Anderson and Crawley, 1989) and theoretical prediction.

Integrating every term of the above equation over E gives:

$$\bar{\sigma} - \bar{\sigma}_0 = Y(\bar{\epsilon} - \bar{\epsilon}_0) + \Omega(\xi - \xi_0) + \Gamma(E - E_0) \tag{34}$$

where $\bar{\sigma}_0$, $\bar{\epsilon}_0$, ξ_0 and E_0 represent initial stress, strain, relative polarization and initial electric field, respectively. The physical meaning of the above equation is very clear. The first two terms represent a basic mechanical stress-strain relation. The third term denotes the contribution of the polarization reversal to the stress-strain relation of the material. The fourth term gives the linear reverse piezoelectric effect. For a stress-free case with zero initial conditions, if the proposed phenomenological formulation of polarization reversal for a virgin curve ($\xi = \tanh kE$) is used, the above equation may be simplified as:

$$\epsilon = -\frac{\Omega}{Y}\tanh kE - \frac{\Gamma}{Y}E. \tag{35}$$

The above equation may provide a nonlinear relationship between the induced strain and the applied field. Due to lack of experimental data, the material constants required by the model are still not available and we cannot verify the above model at the current time. However, the validation of our model may be illustrated indirectly. As shown in Figure 8, the nonlinear field-strain experimental data, E_3 vs. ϵ_1 (Anderson and Crawley, 1989), can be matched 'perfectly' with the above equation through curve-fit techniques. The expression for the theoretical curve in Fig. 8 is $\epsilon = 0.665E - 206\tanh 0.002E$ (E is in V/mm and ϵ is in microstrain). In principle, any experimental curve can be matched by regression analysis but may not match the physical principle. In our case, the theoretical expression matches both the experimental data and the physical principle of the nonlinearity.

CONCLUDING REMARKS

A general phenomenological formulation of polarization reversal is proposed in a simple form. This formulation provides a very good method to describe the hysteresis in piezoelectricity as well as in electromagnetics. With the development of ferroelectric memory devices, the material parameters k and E_c may be used as criteria to evaluate the memory quality of the materials. A good approach to describe the nonlinear induced strain-field behavior and electromechanical hysteresis in piezoelectricity is by combining a macroscopic phenomenological method with microscopic material properties. A one-dimensional thermo-electro-mechanical constitutive model for piezoceramics which undergo polarization reversal is presented using a continuum mechanics approach. This model is based on the basic laws of thermodynamics and reflects the essence of the electromechanical behavior of piezoceramics in a simple form. It is significant that the proposed model provides an explicit form of the stress-strain relation which may facilitate engineering design of piezoelectric actuators. It is illustrated that this theory can describe the electromechanical behavior of piezoceramics simply and reasonably well. It should be noted that material constants for the proposed model are not yet determined due to lack of experimental data at the present time.

ACKNOWLEDGMENT

The authors gratefully acknowledge the support of the Air Force Office of Scientific Research, Grant Number: AFOSR-91-0416 and Dr. Spencer Wu the Scientific Officer.

REFERENCES

Anderson, E.H. and Crawley, E.F., 1989, "Piezoceramic Actuation of One- and Two-Dimensional Structures" Report SSL #5-89, MIT, Cambridge, MA 02139.

Arlt, G. and Sasko, P., 1980, "Domain Configuration and Equilibrium Size of Domains in $BaTiO_3$ Ceramics", *Journal of Applied Physics*, Vol. 51, pp. 4956-4960.

Arndt, H., Schmidt, G. and Vogel, N., 1984, " Influence of Uniaxial Pressure On the Properties of PLZT Ceramics", Vol. 61, pp. 9-18.

Avrami, M., 1939, "Kinetics of Phase Change.I", *Journal of Chemical Physics*, Vol. 7, pp. 1103-1112.

Avrami, M., 1940, "Kinetics of Phase Change.II", *Journal of Chemical Physics*, Vol. 8, pp. 212-224.

Avrami, M., 1941, "Kinetics of Phase Change.III", *Journal of Chemical Physics*, Vol. 9, pp. 177-184.

Bassiouny, E., Ghaleb, A.F. and Maugin, G.A., 1988, "Thermodynamical Formulation for Coupled Electromechanical Hysteresis Effects$\longrightarrow$ I and II", *International Journal of Engineering Science*, Vol. 26, pp. 1279-1306.

Bassiouny, E., Ghaleb, A.F. and Maugin, G.A., 1989, "Thermodynamical Formulation for Coupled Electromechanical Hysteresis Effects$\longrightarrow$ III and IV", *International Journal of Engineering Science*, Vol. 27, pp. 975-1000.

Chen, P.J. and Peercy, P.S., 1979, "One Dimensional Dynamic Electromechanical Constitutive Relations of Ferroelectric Materials", *Acta Mechanica*, Vol. 31, pp. 231-241.

Chen, P.J. and Montgomery, S.T., 1980, "A Macroscopic Theory for the Existence of the Hystersis and Butterfly Loops in Ferroelectricity", *Ferroelectrics*, Vol. 23, pp. 199-208.

Devonshire, A.F., 1949, "Theory of Barium Titanate", *Philosophical Magazine*, Vol. 40. pp. 1040-63.

Fatuzzo, E. and Merz, W.J., 1967, *Ferroelectricity*, John Wiley & Sons, Inc., New York.

Gerthsen, P. and Krüger, G., 1976, " Coercive Field in Fine-Grained PLZT Ceramics", *Ferroelectrics*, Vol. 11, pp. 489-492.

Haun, M.J., Furman, E., Jang, S.J., McKinstry, H.A., and Cross, L.E., 1987, "Thermodynamic Theory of $PbTiO_3$", *Journal of Applied Physics*, Vol. 62, pp. 3331.

Janta,J., 1971, "The Influence of the Shape of Domains On the Ferroelectric Hysteresis Loop", *Ferroelectrics*, Vol. 2, pp. 299-302.

Landauer, R., Young, D.R. and Drougard, M.E., 1956, " Polarization Reversal in the Barium Titanate Hysteresis Loop", *Journal of Applied Physics*, Vol. 27, pp. 752-758.

Lazarus, K.B. and Crawley, E.F., 1989, "Induced Strain Actuation of Composite Plates", GTL Report # 97, MIT, Cambridge, MA 02139.

Merz, W.J., 1954, "Domain Formation and Domain Wall Motions in Ferroelecrtic $BaTiO_3$ Single Crystals", *Physical Review*, Vol. 95, pp. 690-698.

Pulvari, C.F. and Kuebler, W., 1958, "Phenomenological Theory of Polarization Reversal in $BaTiO_3$ Single Crystals", *Journal of Applied Physics*, Vol. 29, pp. 1315.

Rossetti, Jr., G.A., Udayakumar, K.R., Haun, M.J., and Cross, L.E., 1990, "Thermodynamic Theory of Single-Crystal Lead Titanate with Consideration of Elastic Boundary Conditions", *Journal of American Ceramic Society*, Vol. 73, pp. 3334.

Shaikh, A.S., Vest, R.W. and Vest, G.M., 1989, " Dielectric Properties of Ultrafine Grained $BaTiO_3$", *IEEE Transactions On Ultrasonics, Ferroelectrics, and Frequency Control*, Vol. 36, pp. 407-412.

Shigley, J.E. and Mitchell, L.D., 1983, *Mechanical Engineering Design*, McGraw-Hill Series in Mechanical Engineering, McGraw-Hill Book Company, New York.

Stadler, H.L. and Zachmanidis, P.J., 1963, "Nucleation and Growth of Ferroelectric Domains in $BaTiO_3$ at Fields From 2 to 450 KV/cm", *Journal of Applied Physics*, Vol. 34, pp. 3255-3260.

Tanaka, K., 1986, "A Thermomechanical Sketch of Shape Memory Effect: One-dimensional Tensile Behavior", *Res Mechanica*, Vol. 18, pp. 251-263.

Experimental Characterization and Constitutive Modeling of PMN-PT

Experimental Investigation of the Electrostrictive Relaxor Ferroelectric Lead Magnesium Niobate-Lead Titinate

Chet G. Namboodri, Jr.
Craig A. Rogers

Center for Intelligent Material Systems and Structures
Virginia Polytechnic Institute and State University
Blacksburg, Virginia 24061-0261
(703) 231-2900

Abstract

Fundamental to the design of intelligent material systems and structures are the realization of attributes of the constitutive materials—the sensors and actuators—and the ability to model the characteristics of these transducers. In this paper, electromechanical behaviors of the electrostrictive relaxor ferroelectric lead magnesium niobate-lead titinate (PMN-PT) are experimentally investigated. The dependencies of PMN-PT electromechanical transduction on temperature and frequency, characteristics of relaxor ferroelectrics, and on applied direct-current electric field, an attribute of electrostrictors which enables tunable transduction sensitivities, are examined with respect to electrical, sensing, and actuation properties. Results from these experiments are compared with phenomenological models explained in another paper. The objectives for these experiments are to understand the behaviors of PMN-PT sensors and actuators with respect to temperature, frequency, and bias field.

Nomenclature

d^e	Electrostrictive piezoelectric strain coefficient (m/V)
E	Electric field, vector (V/m)
E^{AC}	Dynamic (AC) contribution to electric field (V/m)
E^{DC}	Static (DC) contribution to electric field (V/m)
g^e	Electrostrictive piezoelectric voltage coefficient (V-m/N)
P	Polarization (C/m^2)
Q	Electrostrictive coefficients [transverse, Q_{13}] (m^4/C^2)
s	Applied mechanical strain (m/m)
T	Temperature (°C, K)
T_{max}	Curie temperature for maximum permittivity with relaxor ferroelectrics (°C, K)
Y	Young's modulus of elasticity (N/m^2)

Greek

ϵ'	Relative electric permittivity
ϵ''	Relative electric permittivity loss
ϵ_{max}, κ_{max}	Maximum relative permittivity of ferroelectrics

ϵ_o	Electric permittivity of free space, 8.85×10^{-12} F/m
κ	Dielectric constant, same as relative electric permittivity
Λ	Free-induced strain (m/m)
σ	Applied mechanical stress (N/m^2)
χ	Relative dielectric susceptibility
χ_{max}	Maximum relative susceptibility of ferroelectrics
ω	Frequency (Hz)

Introduction

In the past decade, interest in electroceramic transducers has been renewed by the conceptual advent of intelligent material systems and structures. Intelligent, or smart, material systems and structures are designed, via control capabilities and architected mechanics, to autonomously and judiciously sense and respond to their environments using transducer materials, i.e., sensors and actuators. Much progress has been made in the development of applications with electroceramic transducers and their integration into these systems; consequently, the need for appropriate mechanical characterization and useful, quantitative constitutive modeling for design applications has arisen.

Although electronic ceramics comprise a tremendous variety of sensors and actuators, the most common and pertinent to intelligent material systems and structures are those containing an electromechanical relationship. Application of these electroceramics are found in the areas of mechanical transduction, vibration, and acoustics. Piezoelectric and electrostrictive materials are used almost exclusively in these fields. Lead magnesium niobate doped with lead titinate ($Pb[Mg_{1/3}Nb_{2/3}]O_3$-$PbTiO_3$, or PMN-PT) is a ceramic which exhibits a strong electrostrictive effect. Electrostriction involves a nonlinear electromechanical coupling for which the material develops a strain proportional to the square of the polarization. Free-induced strains in PMN-PT as high as $4\text{-}5 \times 10^{-4}$ have been achieved for realizable fields on the order of 10^3 V/mm (Ealey and Davis, 1990). For comparison, a piezoceramic develops strain *proportional* to the electric-field-induced polarization. Strain levels for the best piezoelectrics are comparable to the best electrostrictors (Damjanovic and Newnham, 1992). When compared with a typical piezoceramic such as lead zirconate titinate ($Pb[ZrTi]O_3$, or PZT), PMN-PT distinguishes itself not only in the nonlinearity of its coupling, through which tunable transduction sensitivities can be achieved, but also in its electromechanical and thermal stability, its negligible dielectric aging, its repeatability under cyclic driving fields, and its dynamic response (Cieminski and Beige, 1991; Cross et al., 1980).

A description of the advantages of PMN-PT, however, would be remiss without relating its disadvantages. Because the response of PMN-PT is nonlinear, quadratic with respect to polarization, the useful actuator authority for AC applications is limited. Furthermore, the electromechanical response is highly frequency-dependent and is restricted to a temperature range in which the dielectric permittivity is large, namely the *relaxor phase transition* range. Finally, deformation for low applied electric fields is small (quadratic behavior), so that

electrostrictors such as PMN-PT somewhat exacerbate the desire for low-voltage devices.

Although much research into the constitutive behavior of PMN-PT has been reported, emphasis has been placed on material processing and dielectric behavior, due to attractive high permittivity values. The bridge of understanding from processing, composition, and dielectric properties to the mechanical domain has been qualitatively described and incompletely formulated. The electromechanical response of PMN-PT requires thorough investigation from an engineering perspective and sound, practical constitutive models for use in design and integration into intelligent material systems and structures. The objectives of this research are to characterize the electromechanical behaviors of PMN-PT, with an emphasis on engineering design utility. Investigations of the electrostrictive properties of PMN-PT have been performed with respect to temperature, frequency, and DC electric field. Experimentation with this electroceramic has included macroscopic mechanical studies of the material as both a sensor and an actuator and investigations into its dielectric behavior.

Electrostrictive Phenomenology

According to Landau-Ginzburg-Devonshire (LGD) thermodynamic formalism, relating dielectric and elastic properties of solids, electrostriction arises from free energy terms (Newnham, 1991; Namboodri and Rogers, 1992a). Three different but equivalent effects arise when the three possible partial derivatives of the electrostrictive free energy terms are taken in different orders. Integration of these relations yields constitutive equations for electrostrictive behavior.

With the so-called 'direct effect,' free-induced strain varies with the square of polarization:

$$\Lambda_i = Q_{ijk} P_j P_k + d_{ij}^o P_j + \Lambda_i^o. \tag{1}$$

Physically, the piezoelectric coefficient in eq. (1) relates any effects from spontaneous polarization of an electrostrictor. One converse effect describes the electric field developed when an electrostrictor is stressed,

$$E_i = (Q_{ijk} P_k + g_{ij}^o)\sigma_j + E_i^o. \tag{2}$$

The second converse electrostrictive effect involves the linear stress dependence of susceptibility.

Equations (1) and (2) represent the electrostrictive actuation and sensing constitutive relations. For practical engineering design and implementation, the polarization term prevalent in these equations does not possess the parametric convenience of applied electric field. Conventionally, linear dielectric behavior is assumed for a parallel-plate capacitor, where induced polarization is described as the product of dielectric susceptibility and electric field:

$$P_i = \chi_{ij} E_j = (\epsilon'_{ij} - 1) E_j. \tag{3}$$

Therefore, dielectric properties are vital to the electrostrictive behaviors of eqs. (1) and (2).

Experimental Design and Procedure

PMN-PT Specimen History

To associate experiments herein described with results in the literature, the processing history of PMN-PT samples must first be considered. Specimens of the solid solution $0.9Pb[Mg_{1/3}Nb_{2/3}]O_3$-$0.1PbTiO_3$ (PMN-PT) were manufactured at AVX Corporation using mixed oxides calcined through the two-stage procedure introduced by Swartz et al. (1984). The calcined mixture was milled in a slurry and tape cast. Platinum electrodes were screen printed onto the green cast, and the composite was fired. The specimens were formed in the shape of plates, having dimensions approximately 0.0572 m x 0.0127 m x 0.00043 m; though, there was some curvature observed for most of the plates. Some of these plates were tested as prepared, and some were scribed and fractured to produce smaller specimens. The edges of fractured pieces were sanded with emery paper and cleaned with acetone to ensure there was no short between electrodes.

Actuation Property Experiments

Actuation with PMN-PT involves the direct electrostrictive effect, described by the derivation of LGD phenomenology in eq. (1). In this equation, free-induced strain is related to applied polarization. However, polarization is not a practical measure; whereas, the applied electric field which induces polarization is. Experimental studies of actuation are thus conducted with respect to applied field, and dielectric studies described later are correlated with actuation results, in order to separate and quantify the electrostrictive coefficient of eq. (1).

As indicated in eq. (1), the electrostrictive coefficient is a tensor quantity. Because of symmetry of the cubic perovskite PMN-PT and planar isotropy with respect to polarization direction, this tensor can be described by only two quantities for a unidirectionally applied electric field. Electric field applied in the direction of one material Cartesian coordinate will result in strain both parallel and transverse to the direction of induced polarization (applied field). Bi-directional transverse strain is uniform because of planar isotropy of dielectric and electrostrictive properties. In these studies, only transverse behaviors were investigated.

As illustrated in Fig. 1, transverse electromechanical properties of PMN-PT were determined by monitoring both the electric field applied across parallel-plate electrodes and the corresponding free-induced strain, measured by a strain gage bonded to the monomorph surface. It is important to note that the strain gage was bonded to the grounded electrode of the specimen, to avoid capacitive feed-through of voltage to strain measurements. Strain was measured to within ± 1 μm/m.

Two sets of experimental apparatus, illustrated in Fig. 2, were utilized for two types of measurement, static and dynamic. As shown in Fig. 2 (a), static measurements were obtained by stepping DC voltage applied to PMN-PT specimens up and down with a potentiometer and by measuring the steady-state strain response at each step. Frequency response measurements were acquired through digital conversion of voltage and strain signals, as in Fig. 2 (b), and Fast (Discrete) Fourier Transform spectral analysis of digitized data. High levels of applied voltage were resistively divided for proportional measurement of electric field with a data acquisition board, which is limited to ± 10 V inputs. The input impedance of the voltage divider was carefully selected with respect to the capacitance of PMN-PT specimens to ensure that electrical dynamics were unaffected. AC voltage was measured to an accuracy of ± 5 mV for a ± 10 V range, while DC voltage was measured to ± 1 mV.

In both experimental setups, temperature of PMN-PT specimens was varied with an oven to investigate thermal (phase transition) effects. Specimens were placed next to the controlling thermocouple of the oven to ensure temperature accuracy within ± 0.5°C. To simulate free boundary conditions in the transverse plane, specimens were suspended in the oven by their electrode solder connections. Although this configuration created local stress variation near the solder joints, the magnitude of these variations were negligible, because of the PMN-PT ceramic's stiffness and relatively low density.

For dynamic measurements, a moderate AC electric field was used to electromechanically excite the PMN-PT specimens, while a DC bias field was concurrently applied and stepped, so that bias-field effects on PMN-PT behavior could be surmised. The amplifier used in these experiments was capable of providing simultaneous DC and AC high-gain, low-current amplification of voltages supplied to specimens. Broad-band frequency responses were created using a noise generator as the AC input, whose amplified signals were limited to 75 kV/m amplitudes. FFT spectral analysis of electromechanical data from PMN-PT required A/D conversions at 5 kHz to avoid aliasing at 2 kHz.

The thicknesses of all specimens were identical, at around 0.43 mm; however, the electrode areas, thus specimen capacitances, varied. Specimens ranged in dimensions from 0.0589 m x 0.0125 m to 0.0289 m x 0.0126 m. Nevertheless, the lowest fundamental extensional-mode frequency was at 28.4 kHz, well above 2 kHz, such that any modal effects on dynamic measurements were designed to be negligible.

To summarize, the actuation experiments were intended to investigate free-induced-strain electromechanical responses of PMN-PT with respect to temperature, bias field, and frequency. Specifications for these experiments are outlined in Table 1, and the test matrix is shown in Table 2. Thermal effects between 25°C and 85°C, corresponding with the diffuse ferroelectric-paraelectric phase transition of PMN-PT, were studied. Influences of bias field levels between 0 and 814 kV/m were determined, and frequency responses between 0 and 2 kHz were investigated.

Sensing Property Experiments

Similar to the actuator experiments, the sensor experiments with PMN-PT involved investigation of transverse electrostrictive properties, specifically the charge developed on parallel-plate electrodes resulting from the stress applied transverse to the direction of polarization. As is evident in eq. (2), the level of electric field generated by a stressed electrostrictor depends on how much the sensor is polarized. Contributions to the transduction sensitivity, the collective terms between applied stress and generated field in eq. (2), arise from the electrostrictive effect of applied polarization, as well as any piezoelectric effects due to spontaneous polarization. Since applied polarization varies with applied electric field, there is a bias-field dependence of the transduction sensitivity apparent in the LGD phenomenological derivation of eq. (2). The experimental arrangement for observing transverse electrostrictive sensing properties using the strain-gage technique is shown in Fig. 3.

As indicated in Fig. 4, PMN-PT monomorphs were bonded to the base of a cantilever beam, which was excited using an electromagnetic shaker with random noise input. Strain gages were attached to the exposed, unbonded surface of a PMN-PT specimen and to the opposite, unbonded surface on the beam. Transfer function analysis was performed for each strain signal with respect to the sensor output, while care was taken to ensure that the strain gage of interest was on an electrically grounded surface. The average of these two analyses for each sensor test was chosen to represent the sensor transduction capabilities; thus, an average, uniform strain field was determined and assumed to represent the input to PMN-PT sensor specimens.

Specifications for sensing experiments are provided in Table 3, and the test matrix is listed in Table 4. As in the actuation studies, bias fields ranged from 0 to 814 kV/m. Data were digitally collected at 2 kHz, with anti-alias frequency of 500 Hz. Beam dimensions were designed so that the first bending mode was larger than the maximum frequency of interest for the studies, in this case 500 Hz. Since only bending mode vibration occurred in the beam, only flexural stresses were transmitted to the PMN-PT sensing specimens. Frequencies of 2 kHz were not feasibly studied in this configuration, due to the difficulty of exciting structural elements at such high frequencies. Furthermore, thermal effects could not be reliably tested using the shaker-beam configuration, so that thermal and high frequency results on sensing properties were waived for analytical correspondence to actuation and dielectric experiments.

Dielectric Property Investigations

In order to quantify the individual parameters contributing to the electrostrictive effects, dielectric properties between parallel plates of specimens used for actuation and sensing investigations were distinguished. The dielectric response of PMN-PT monomorphs were examined using an impedance analyzer, which was capable of examining electrical response functions from 100 Hz to 100 MHz. For these experiments, testing frequencies ranged from 100 Hz to 10 kHz, and the parameters investigated included capacitance and permittivity ratio. Relative permittivity was readily determined from capacitance measurements, including analytical adjustments for edge effects. As exhibited in the test matrix of Table 5, temperatures of PMN-PT specimens were varied between 15°C and 85°C, which encompasses the range of the diffuse

phase transition. Bias field effects were not examined during this test, mainly because the impedance analyzer was not equipped to handle such large DC bias fields.

Experimental Results and Discussion

Dielectric Results

Since polarization is an extrinsic parameter used to describe electrostrictive relations for actuation and sensing in equations (1) and (2) and since electric field is related and is more practical for engineering design, the dielectric properties which associate field and polarization are essential to a model-based description of electrostriction with the relaxor ferroelectric PMN-PT. For this reason, experimental results for dielectric properties are described prior to actuation and sensing results. Although much of the existing literature pertaining to PMN-PT involves characterization of electric permittivity relations, it was important to identify the relations for specimens used in the present study, so that electromechanical results can be appropriately interpreted.

In Fig. 5, results for the weak-field (2.3 kV/m) relative permittivity and permittivity ratio of PMN-PT specimens are shown with respect to temperature. The broad and frequency-dispersive thermal phase transition typical of relaxor ferroelectrics (Cross, 1987) is evident in this figure. Values and shapes of curves in Fig. 5 correspond well with results obtained by Swartz et al. (1984) for PMN-PT with a processing history similar to the specimens in this study. It should be noted here that the standard deviation ranged from 50 to 180 for relative permittivity data and from 0.0001 to 0.0026 for permittivity ratio data.

Characteristically, higher frequency excitations result in a reduced, or dispersed, dielectric constant and increased dielectric loss for the ferroelectric-dominated phases prior to the dielectric maximum. With the onset of paraelectric phases, frequency dependence is negligible. These frequency relations are notable in the dielectric frequency response plots of Fig. 6. For temperatures past the Curie maximum temperature, T_{max}, of around 45-50°C, the relative permittivity and permittivity ratio are flat with respect to frequency. For temperatures below T_{max}, there is a linear decay of the dielectric constant and an increase in permittivity ratio with respect to the logarithm of frequency.

AC Actuation Results

In Table 2, the test matrix for investigating the actuation response of PMN-PT specimens shows that electromechanical properties were simultaneously investigated with respect to temperature, frequency, and electric bias field. These investigations have prompted some interesting results, especially when compared with dielectric results previously described. For example, in the plots of Fig. 7, frequency dispersion is much more pronounced in the actuator transduction thermal responses than in the dielectric thermal responses of Fig. 5. Furthermore, the maxima of the broad thermal phase transition appear shifted, when comparing the actuator transduction with the dielectric response, from between 45°-50°C to between 25-30°C. The actuator transduction sensitivity described in these figures is equivalent to the *d*-coefficient for piezoelectrics; it is the

ratio of induced strain to applied AC electric field.

The apparent shift in the phase transition maxima can be explained by the temperature dependence of the electrostrictive coefficient described by Zhang et al. (1989). The net effect of Q decreasing, while the dielectric constant increases to a maximum near 45°C, as in Fig. 5, is that the maximum electrostrictive actuator transduction is shifted, compared to the maximum permittivity. Pronouncement of the frequency dependence of the actuator transduction sensitivity compared with the frequency dependence of the dielectric response can be explained by examining the LGD phenomenology of eq. (1). By combining eqs. (1) and (3) and by ignoring initial conditions and neglecting contributions from the electrostrictive piezoelectric term, the free-induced strain,

$$\Lambda_i = Q_{ij}(\epsilon_o \chi_{jm} E_m)^2. \tag{4}$$

According to eq. (3), the relative dielectric susceptibility and relative permittivity are practically identical for high permittivity materials like PMN-PT. In eq. (4), free-induced strain varies with the square of relative susceptibility, thus the square of relative permittivity. Therefore, variation of dielectric properties due to frequency is more pronounced in the actuator strain transduction curves of Fig. 7 than the dielectric responses of Fig. 5. This variation is likewise evident in the frequency response plots of Fig. 8, which contains results at a different bias field.

In Fig. 8, the flat response of about 0.1 x 10^{-10} (m/m)/(V/m) at 85°C corresponds with the flat response for the 85°C dielectric permittivity curve of Fig. 6 and relates to the introduction of paraelectric material phases. The frequency response plots of Fig. 9, demonstrating bias-field dependence, have similar shapes to those of Fig. 8. In both of these figures, the response levels out at higher frequencies. Both figures also indicate anomalous results between 400 and 600 Hz. In Table 1, values for the first bending mode of the experimental actuators are indicated. Since some curvature was noted for these specimens and since asymmetric material properties about the neutral axis were introduced by bonding strain gages, the apparent resonant/anti-resonant results between 400 and 600 Hz occur due to bending.

In Fig. 9, the bias-field dependence of actuator transduction sensitivity is also introduced. Constant frequency plots in Fig. 10 confirm this dependence and indicate a law of diminishing returns for the transduction sensitivity with respect to higher bias fields. For actuation studies, applied electric field was composed of a DC component, ranging to very large values of 814 kV/m, and a moderate AC component having an amplitude of at most 75 kV/m. If the electric field is algebraically separated into these two components and if the separate effects of field on the dielectric susceptibility are considered, eq. (4) becomes, after assuming unidirectional field and considering only the transverse strain component,

$$\Lambda_1 = Q_{13}\epsilon_o^2[(\chi_{33}^{DC}E_3^{DC})^2 + 2\chi_{33}^{DC}E_3^{DC}\chi_{33}^{AC}E_3^{AC} + (\chi_{33}^{AC}E_3^{AC})^2]. \tag{5}$$

Actuator transduction sensitivity represents the free strain induced by AC field, or the partial derivative of eq. (5) with respect to E_{AC},

$$\frac{\partial \Lambda_1}{\partial E_3^{AC}} = 2Q_{13}\epsilon_o^2[\chi_{33}^{DC}\chi_{33}^{AC}E_3^{DC} + (\chi_{33}^{AC})^2 E_3^{AC}]. \quad (6)$$

In eq. (6), both AC and DC components contribute to the actuator transduction. The AC component is constant, except for frequency dependence, so that for each constant frequency plot in Fig. 10, the DC, or bias field, component evokes change in the sensitivity. According to eq. (6), a rise in DC field will increase the transduction sensitivity; however, as described by Pan et al. (1989), decreased permittivities (susceptibilities) accompany increased bias fields, so that the net effect on actuator transduction is the peak demonstrated by data of Fig. 10. Frequency effects on the AC permittivity demonstrate shifts in the bias field associated with maximum transduction and variation in transduction amplitudes.

Thermal considerations for bias-field-dependent actuator transduction results are typified by the plots of Fig. 11. For temperatures above T_{max}, the paraelectric phase dominates behavior, such that the relaxor ferroelectric effects of reversible polarization and direct electrostriction are not revealed until very high fields, at which remaining ferroelectric phases are field-excited enough to induce aggregate strain. Beneath T_{max}, the electrostrictive actuator specimens exhibit different bias-field response shapes and maxima at different temperatures.

Finally, the sixth permutation in the temperature-frequency-bias field co-dependent, direct electrostrictive behavior of PMN-PT is illustrated by the varying bias-field plots in the thermal responses of Fig. 12. Shape changes of the thermal responses through the phase transition due to bias field differences result from the effective interactions between the bias-field dependent permittivity and the bias field itself. Examination of eq. (6) indicates that actuator transduction sensitivity relies on this interaction. Data displayed for all dynamic actuation tests represent specimen averages, ranging in standard deviation from 5×10^{-13} to 8×10^{-11} (m/m)/(V/m).

DC Actuation Results

As described earlier, DC actuation tests were also performed with PMN-PT specimens. Results from these investigations are plotted in Fig. 13, whose data represent averages consisting of standard deviations between 0 and 20 μm/m. In Fig. 13, among the most noticeable characteristics is the decrease in hysteresis, which is considerably less than that of the more commonly used piezoelectric PZT, with increased paraelectric material phase (higher temperatures). Another notable characteristic is the nonlinear, yet non-parabolic relation between applied DC field and induced strain.

According to eq. (6), there is a quadratic relationship between applied field and induced strain; however, there is also a quadratic relationship between susceptibility and induced strain. As described above, the net effect of the product of the square of a permittivity declining with applied field and the square of that field appears in the shapes of the curves in Fig. 13. As introduced by Zhang and Rogers (1992), the ferroelectric relation between polarization and electric field can be described using a hyperbolic tangent phenomenological model. The results

from and implications of using this model are described in another paper (Namboodri and Rogers, 1992b).

Sensing Results

Results from the sensor experiments with PMN-PT specimens described earlier are graphed in Figs. 14 and 15. Differences between using PMN-PT as a sensor and as an actuator are readily apparent in these figures. One noticeable difference is that the frequency responses for the PMN-PT sensors between 0 and 500 Hz are flat, compared with the responses of Figs. 8 and 9 for PMN-PT actuators. The shape of plots in Figs. 8 and 9 are readily explained by the shapes of responses in Fig. 5 for the dielectric permittivity, a constituent of PMN-PT transduction. The difference in Fig. 14 is a consequence of the relative levels of induced polarization. For the dielectric and actuation studies, moderate levels of AC polarization were induced by electric fields; however, in the PMN-PT sensing studies, the stress-induced polarization levels were millionths-to-billionths of the other two. Because the swings in polarization magnitudes were far less during sensing tests, the frequency of these swings and its effect on dielectric properties were negligible, so that frequency responses appear flat.

The insignificant frequency effects on sensing transduction are again apparent in Fig. 15, which indicates bias-field dependence. Sensing transduction represents a modified version of terms in the parentheses of eq. (2), whose collection is equivalent to the piezoelectric g-coefficient. By assuming a linear, symmetric stress-strain law for PMN-PT and neglecting any feed-through or initial conditions represented by E^o, eq. (2) can be rewritten,

$$E_i=[(Q_{ijk}P_k+g_{ij}^o)Y_{jm}]s_m. \tag{7}$$

The bracketed terms of eq. (7) symbolize the sensor transduction sensitivity depicted in Figs. 14 and 15.

The electrostrictive piezoelectric voltage coefficient g^o of eq. (7) appears in Fig. 15 as non-zero transduction values for zero applied bias field. The nonlinearity of the curves of Fig. 15 arises from P-E nonlinearity. According to LGD phenomenology of eq. (7), sensor transduction is linearly related to applied polarization. Since electric bias field of the abscissa of Fig. 15 is used to induce that polarization, the nonlinearity, as previously alluded for other tests, must result from the nonlinear electric field-polarization relations.

Conclusions and Recommendations

In this paper, electromechanical behavior of the relaxor ferroelectric PMN-PT was experimentally characterized. Dielectric, sensing, and actuation behaviors of PMN-PT monomorphs were investigated. Based on Landau-Ginzburg-Devonshire (LGD) phenomenology for electrostrictive effects, the relative susceptibility is of utmost importance, since electrostriction is related to polarization. As such, aspects of polarization, including dielectric susceptibility, were carefully considered for electrostrictive sensing and actuation constitutive

relations with PMN-PT.

Although this research includes results which account for the behaviors of PMN-PT very well, these results describe only transverse transduction, i.e., only actuation and sensing perpendicular to applied or measured electrical quantities. Furthermore, there are other aspects of the findings in this paper which require further investigations. Approaches discussed herein for modeling PMN-PT behavior could be generalized and improved by the following suggestions:

- Processing effects on grain size should be studied for 0.9PMN-0.1PT specifically, to realize the relations between grain size and dielectric properties proposed by Shrout et al. (1987).
- Frequency dependence of the electrostrictive coefficient should be further characterized and validated, since there are no other research endeavors in the literature to confirm this behavior.
- The electrostrictive piezoelectric coefficients developed from LGD phenomenology require better understanding. For example, the relation of the electrostrictive piezoelectric voltage coefficient to spontaneous polarization could be researched.
- The tensor behavior should be robustly investigated and modeled, like the transverse transduction studies of this paper, for design of PMN-PT sensors and actuators in configurations utilizing other tensor properties, for example, a stack geometry.

References

von Cieminski, J. and H. Beige, 1991. "High-signal electrostriction in ferroelectric materials," *Journal of Physics D* **24**[7], 1182-1186.

Cross, L.E., 1987. "Relaxor Ferroelectrics," *Ferroelectrics* **76**, 241-267.

Cross, L.E., S.J. Jang, R.E. Newnham, S. Nomura and K. Uchino, 1980. "Large electrostrictive effects in relaxor ferroelectrics," *Ferroelectrics* **23**, 187-192.

Damjanovic, D. and R.E. Newnham, 1992. "Electrostrictive and piezoelectric materials for actuator applications," *Journal of Intelligent Material Systems and Structures* **3**, 191-209.

Ealey, M.A. and P.A. Davis, 1990. "Standard SELECT electrostrictive lead magnesium niobate actuators for active and adaptive optical components," *Optical Engineering* **29**[11], 1373-1382.

Namboodri, C.G. and C.A. Rogers, 1992a. "Tunable Vibration/Strain Sensing with Electrostrictive Materials," *Proceedings of the Conference on Recent Advances in Adaptive and Sensory Materials and their Applications*, Blacksburg, VA, 285-297.

Namboodri, C.G. and C.A. Rogers, 1992b. "Constitutive Modeling of the Electrostrictive Relaxor Ferroelectric Lead Magnesium Niobate-Lead Titinate," Center for Intelligent

Material Systems and Structures, Blacksburg, VA.

Newnham, R.E., 1991. "Tunable transducers: nonlinear phenomena in electroceramics," *NIST Special Publication 804, Chemistry of Electronic Ceramic Materials*, Proceedings of the International Conference, Jackson, WY.

Pan, W.Y, W.Y. Gu, D.J. Taylor and L.E. Cross, 1989. "Large piezoelectric effect induced by direct current bias in PMN:PT relaxor ferroelectric ceramics," *Japanese Journal of Applied Physics* **28**[4], 653-661.

Shrout, T.S., U. Kumar, M. Megherhi, N. Yang and S.J. Jang, 1987. "Grain size dependence of dielectric and electrostriction of $Pb(Mg_{1/3}Nb_{2/3})O_3$-based ceramics," *Ferroelectrics* **76**, 479-487.

Swartz, S.L., T.R. Shrout, W.A. Schulze and L.E. Cross, 1984. "Dielectric properties of lead-magnesium niobate ceramics," *Journal of the American Ceramic Society* **67**[5], 311-314.

Zhang, Q., W. Pan, A. Bhalla and L.E. Cross, 1989. "Electrostrictive and dielectric response in lead magnesium niobate-lead titinate (0.9PMN:0.1PT) and lead lanthanum zirconate titinate (PLZT 9.5/65/35) under variation of temperature and electric field," *Journal of the American Ceramic Society* **72**[4], 599-604.

Zhang, X.D. and C.A. Rogers, 1992. "A macroscopic phenomenological formulation for coupled electromechanical effects in piezoelectricity," *Proceedings of the Conference on Recent Advances in Adaptive and Sensory Materials and their Applications*, Blacksburg, VA, 183-203.

Table 1. Specifications for PMN-PT transverse actuation experiments.

Specimens	28.9 - 58.9 x 12.5 x 0.43 mm^3 28.4 - 47.9 kHz first extensional mode 427 - 1,773 Hz first bending mode
Strain Gages	0 μm/m thermal expansion compensation $\pm$ 1 μm/m accuracy
Strain Gage Conditioner	Quarter bridge configuration 0.496 mV/μm/m transduction
Oven	25 - 85°C experimental operating range $\pm$ 0.5°C accuracy
DC Supply	0 - 400 V (DC tests) 0 - 18 V (AC tests)
Noise Generator (AC Supply)	$\pm$ 1.5 V maximum amplitude 0 - 20 kHz random noise
Amplifier	20(x) gain 0 - 5 κHz frequency response
Voltage Divider	1:10 ratio 56 kΩ input impedance
Anti-alias Filter	8-pole, 6-zero elliptical 2 kHz cutoff setting 100 - 189(x) gain on strain signal 1(x) gain on voltage signal
PC Computer and A/D Board	Two channels 0 - 14 kHz sampling range 1024-point FFT, 60 averages

Table 2. Text matrix for PMN-PT transverse actuation experiments.

		Temperature (°C)					
		25	35	45	55	65	85
Bias Field (kV/m)	116	0-2 kHz	0-2 kHz	0-2 kHz	0-2 kHz	0-2 kHz	0-2 kHz
	233	0-2 kHz	0-2 kHz	0-2 kHz	0-2 kHz	0-2 kHz	0-2 kHz
	349	0-2 kHz	0-2 kHz	0-2 kHz	0-2 kHz	0-2 kHz	0-2 kHz
	465	0-2 kHz	0-2 kHz	0-2 kHz	0-2 kHz	0-2 kHz	0-2 kHz
	581	0-2 kHz	0-2 kHz	0-2 kHz	0-2 kHz	0-2 kHz	0-2 kHz
	698	0-2 kHz	0-2 kHz	0-2 kHz	0-2 kHz	0-2 kHz	0-2 kHz
	814	0-2 kHz	0-2 kHz	0-2 kHz	0-2 kHz	0-2 kHz	0-2 kHz

Table 3. Specifications for PMN-PT transverse sensing experiments.

Specimens	23.6 - 57.2 x 12.5 x 0.43 mm^3
Strain Gages	0 $\mu m/m$ thermal expansion compensation $\pm$ 1 $\mu m/m$ accuracy
Strain Gage Conditioner	Quarter bridge configuration 0.496 $mV/\mu m/m$ transduction
DC Supply	0 - 350 V
Voltmeter	$\pm$ 1 mV
Noise Generator (AC Supply)	$\pm$ 1.5 V maximum amplitude 0 - 20 kHz random noise
Shaker	17.8 N force, $\pm$ 2.50 mm stroke 0 - 12.5 kHz frequency range
Beam	Aluminum, 63.5 x 20.3 x 3.1 mm^3 4.0 kHz fundamental bending mode
Amplifier	0 - 5 kHz frequency response
Anti-alias Filter	8-pole, 6-zero elliptical 500 Hz cutoff setting 100(x) gain on strain signal 2 - 100(x) gain on voltage signal
PC Computer and A/D Board	Two channels 0 - 14 kHz sampling range 1024-point FFT, 60 averages

Table 4. Text matrix for PMN-PT transverse sensing experiments.

Bias Field (kV/m)	Frequency (Hz)
0	0 - 500
116	0 - 500
233	0 - 500
349	0 - 500
465	0 - 500
581	0 - 500
618	0 - 500
814	0 - 500

Table 5. Text matrix for PMN-PT dielectric experiments.

Temperature (°C)	Frequency (kHz)
15	0.1 - 10
25	0.1 - 10
35	0.1 - 10
45	0.1 - 10
55	0.1 - 10
65	0.1 - 10
75	0.1 - 10
85	0.1 - 10

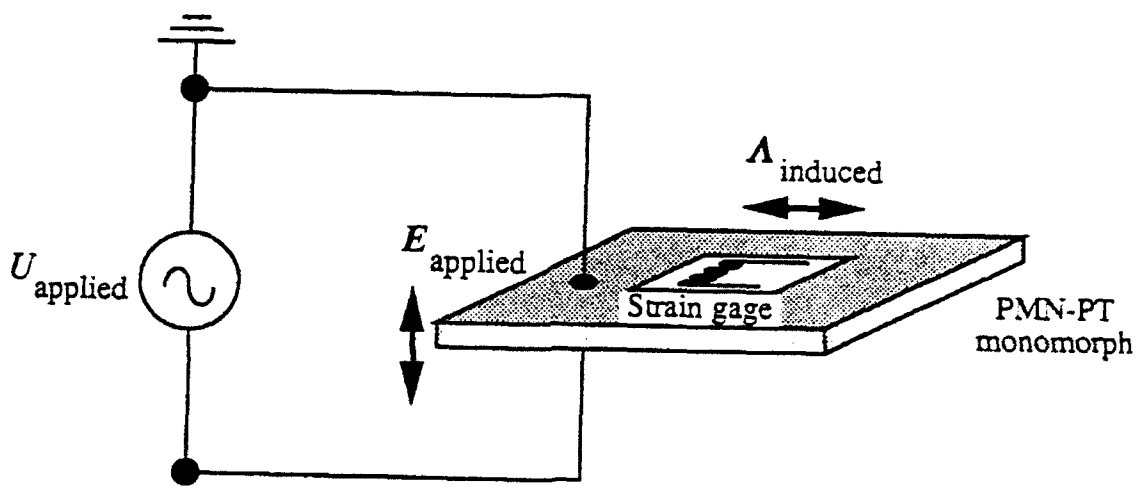

Figure 1 Strain-gage technique for observing the transverse direct electrostrictive effect in PMN-PT.

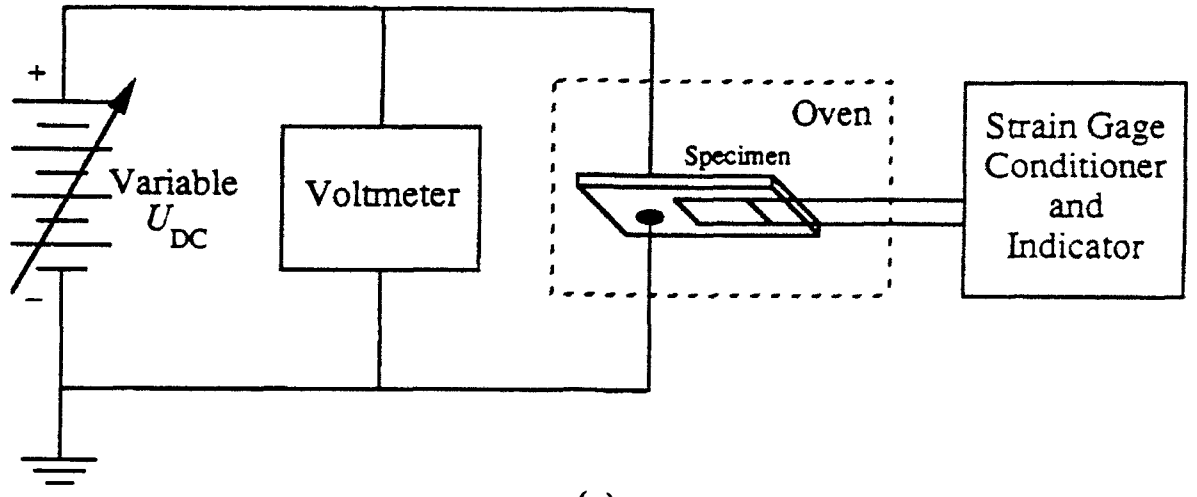

(a)

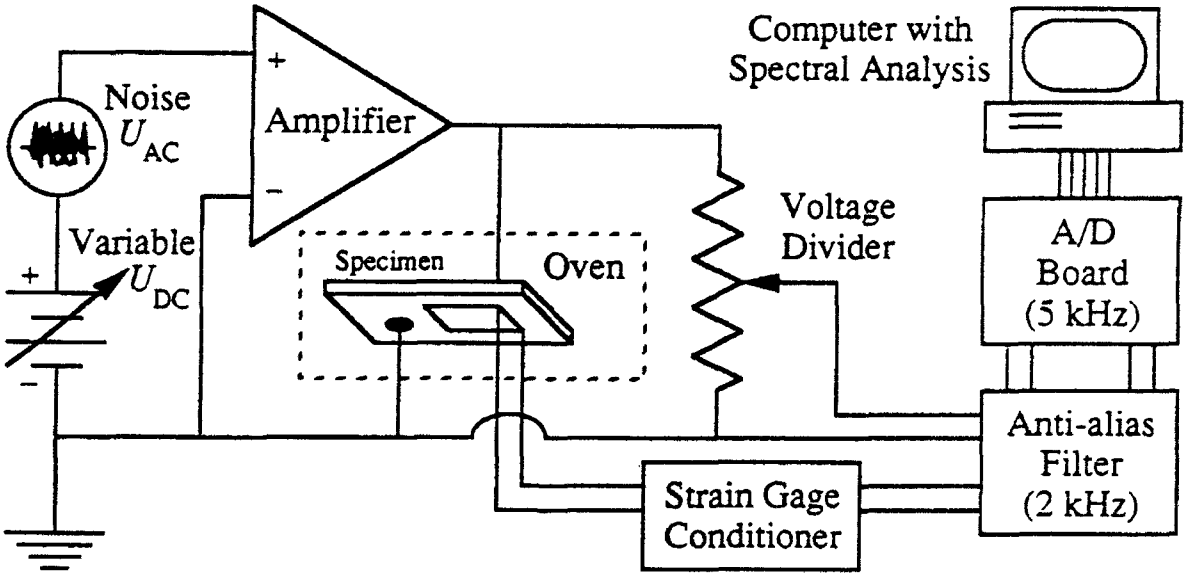

(b)

Figure 2 Experimental apparatus for (a) static and (b) dynamic measurement of transverse direct electrostrictive effect with PMN-PT.

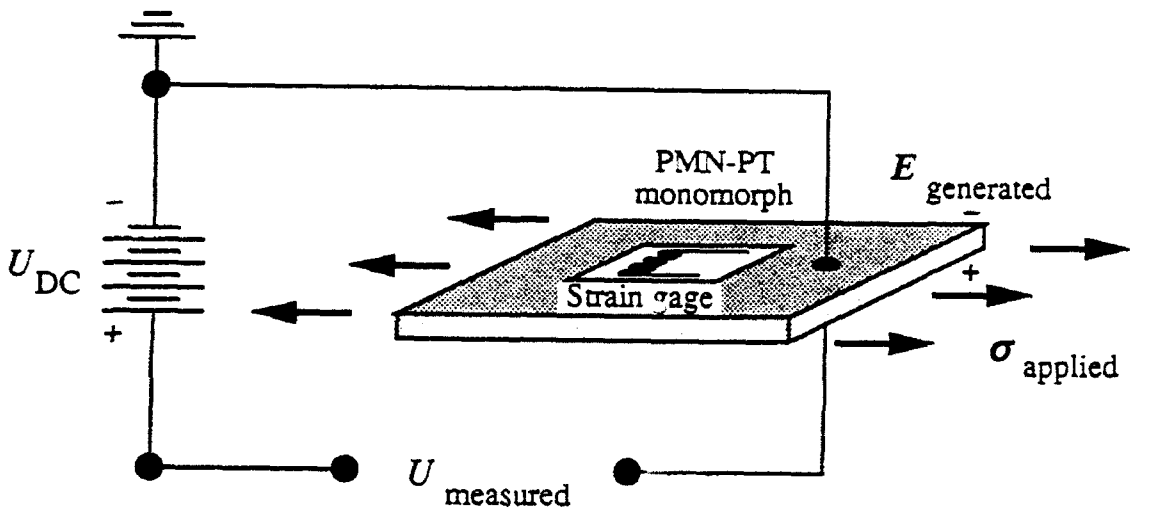

Figure 3 Strain-gage technique for observing transverse electrostrictive sensing properties of PMN-PT with respect to applied bias field.

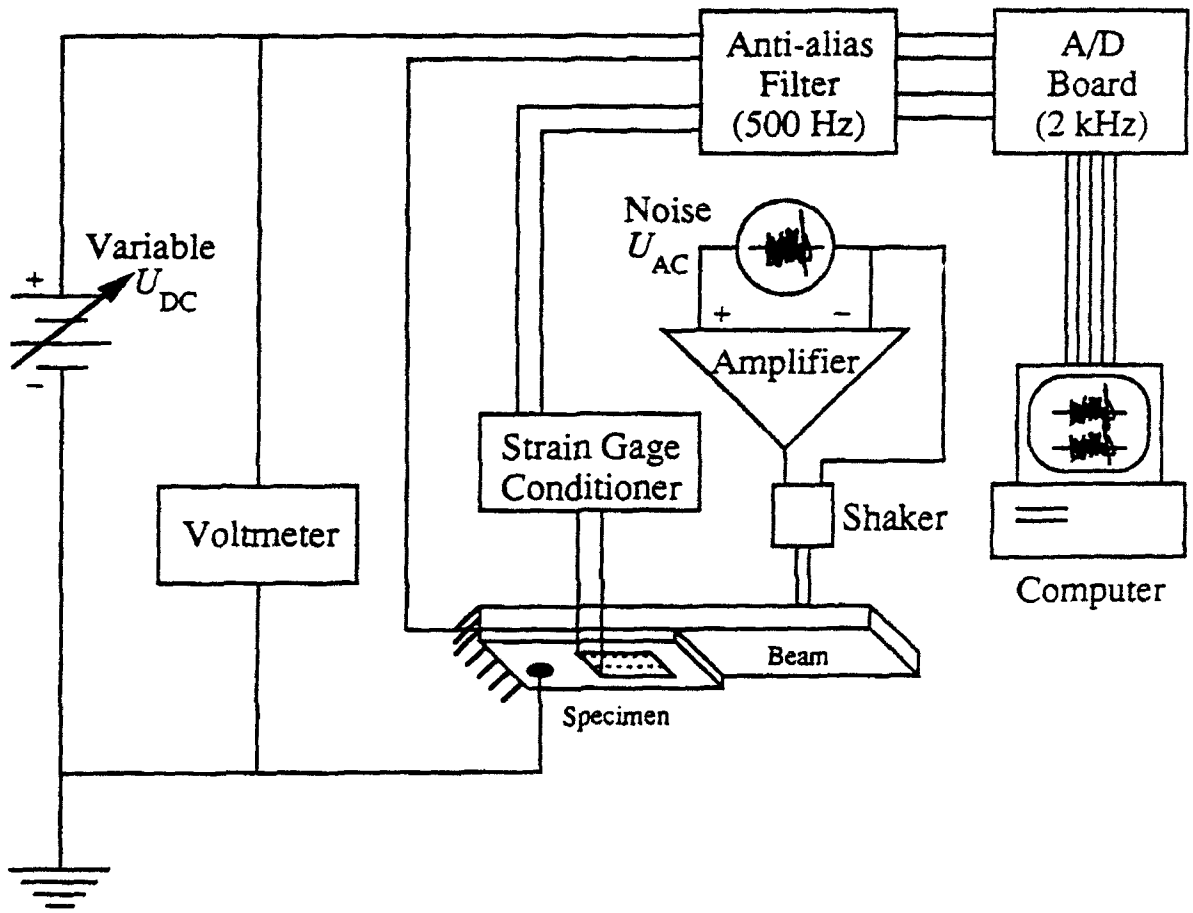

Figure 4 Experimental apparatus for measurement of transverse electrostrictive sensing properties of PMN-PT.

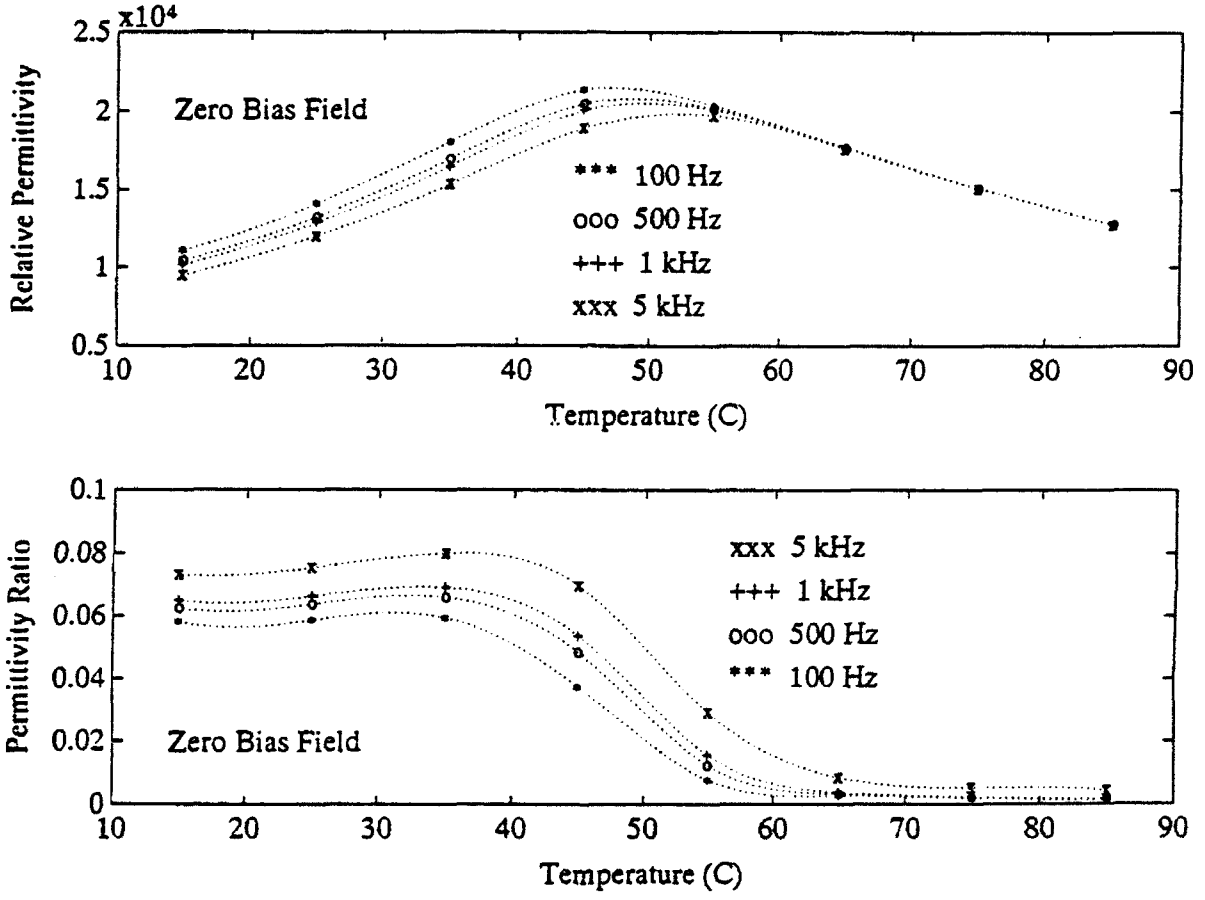

Figure 5 Dielectric results versus temperature for various frequencies.

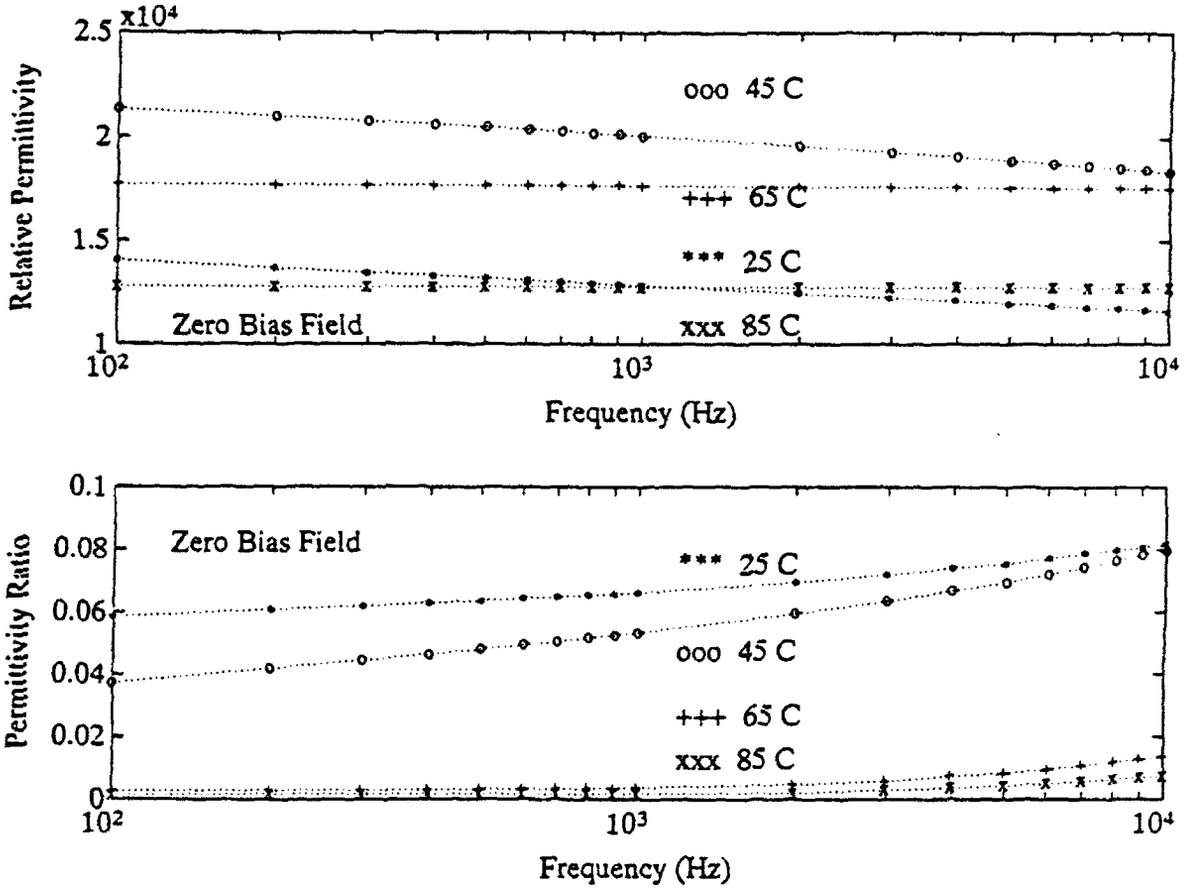

Figure 6 Dielectric frequency-response at various temperatures.

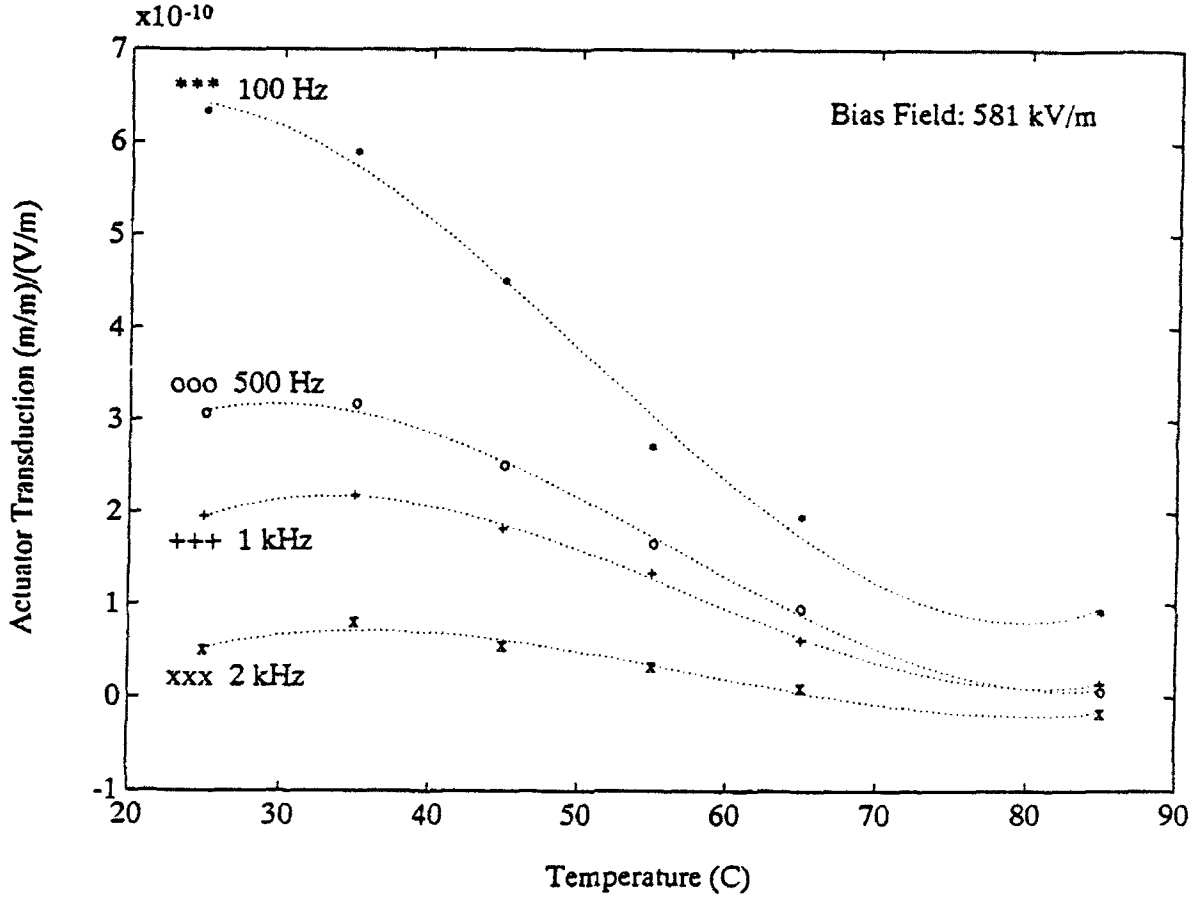

Figure 7 Actuator transduction sensitivity versus temperature for various frequencies at constant bias field.

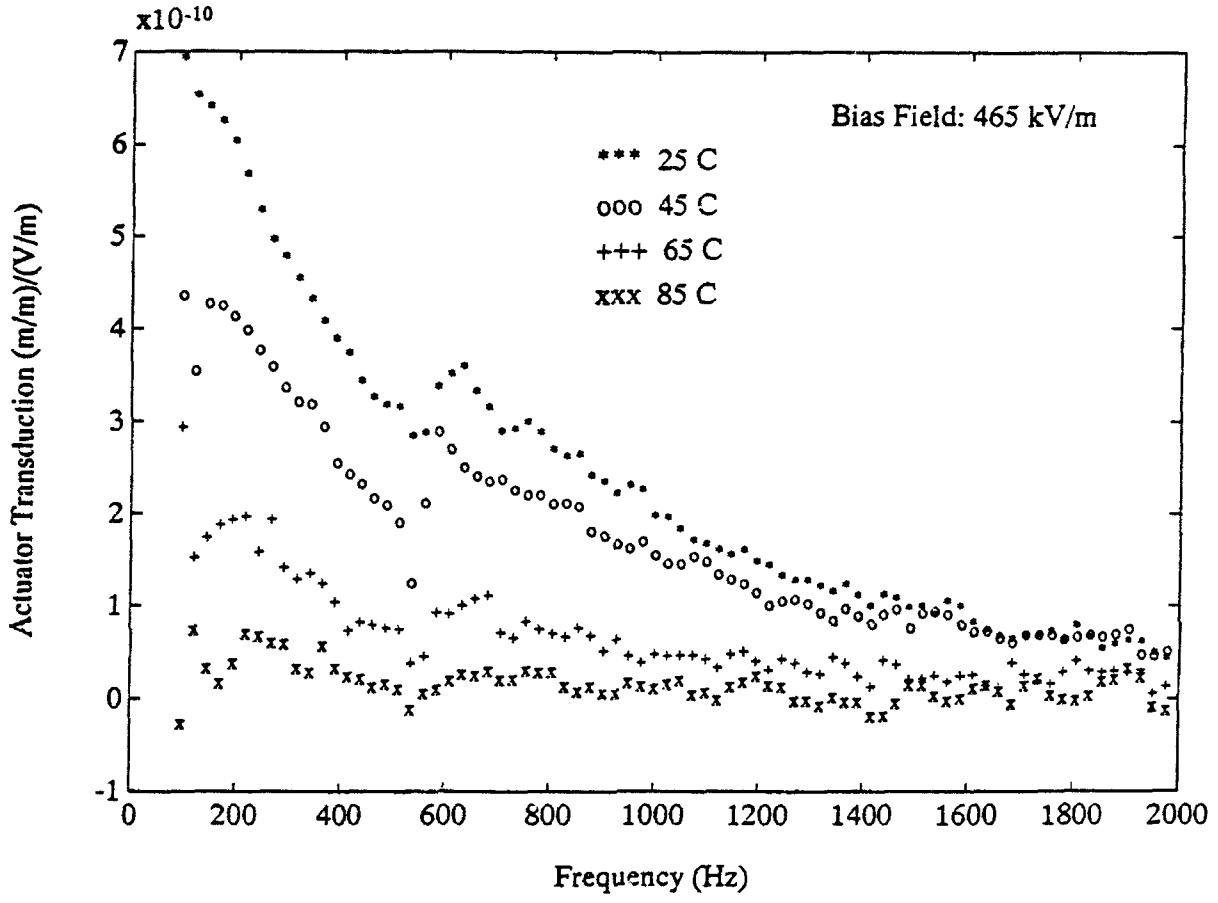

Figure 8 Frequency response of actuator transduction sensitivity for various temperatures at constant bias field.

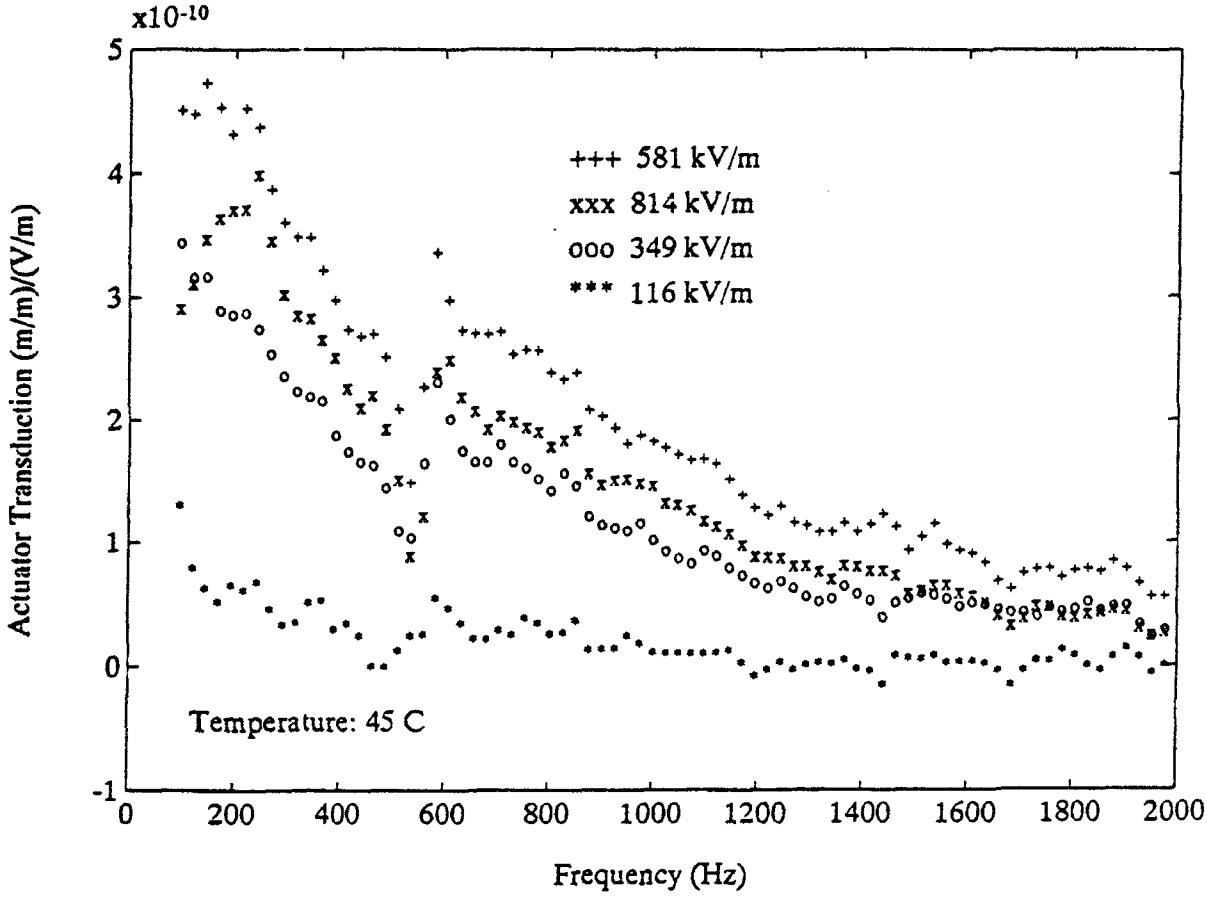

Figure 9 Frequency response of actuator transduction sensitivity for various bias fields at constant temperature.

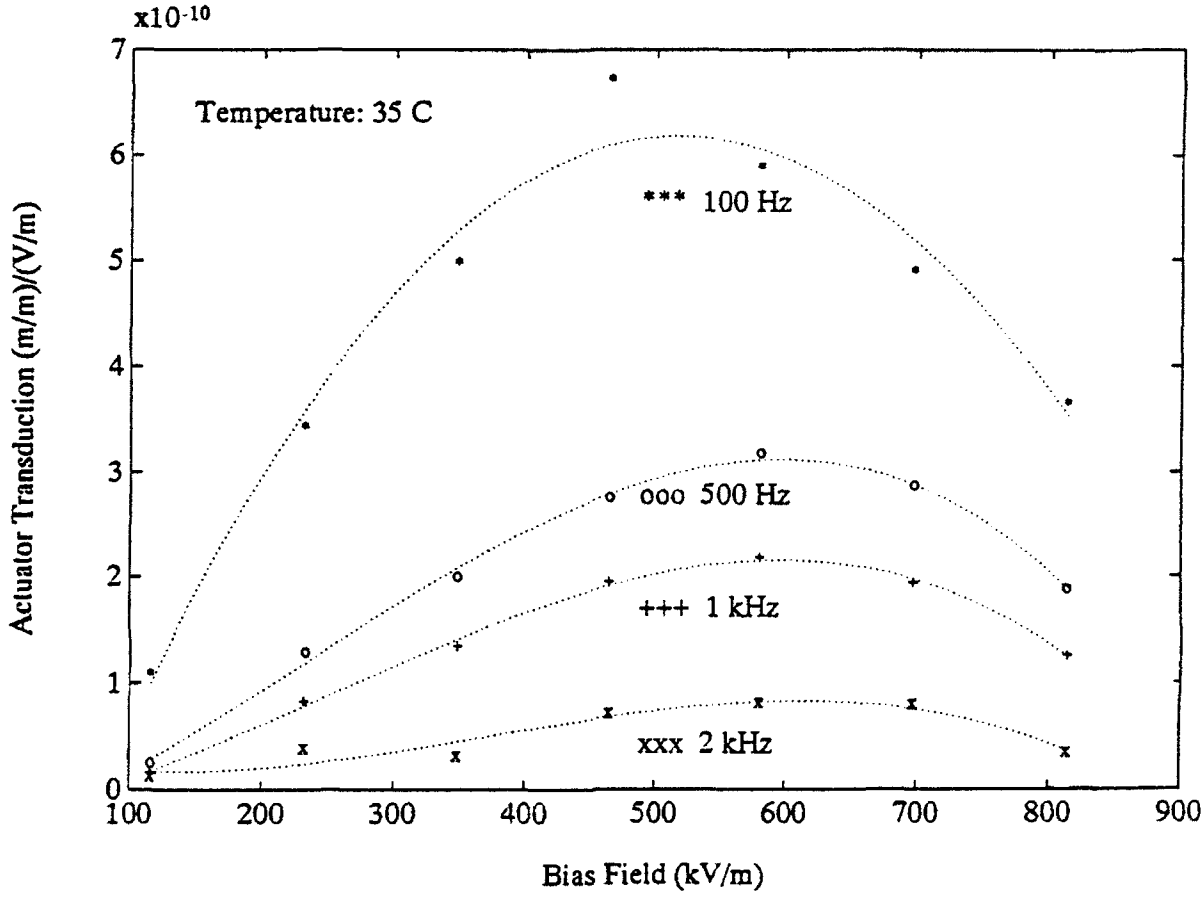

Figure 10 Actuator transduction sensitivity versus bias field for various frequencies at constant temperature.

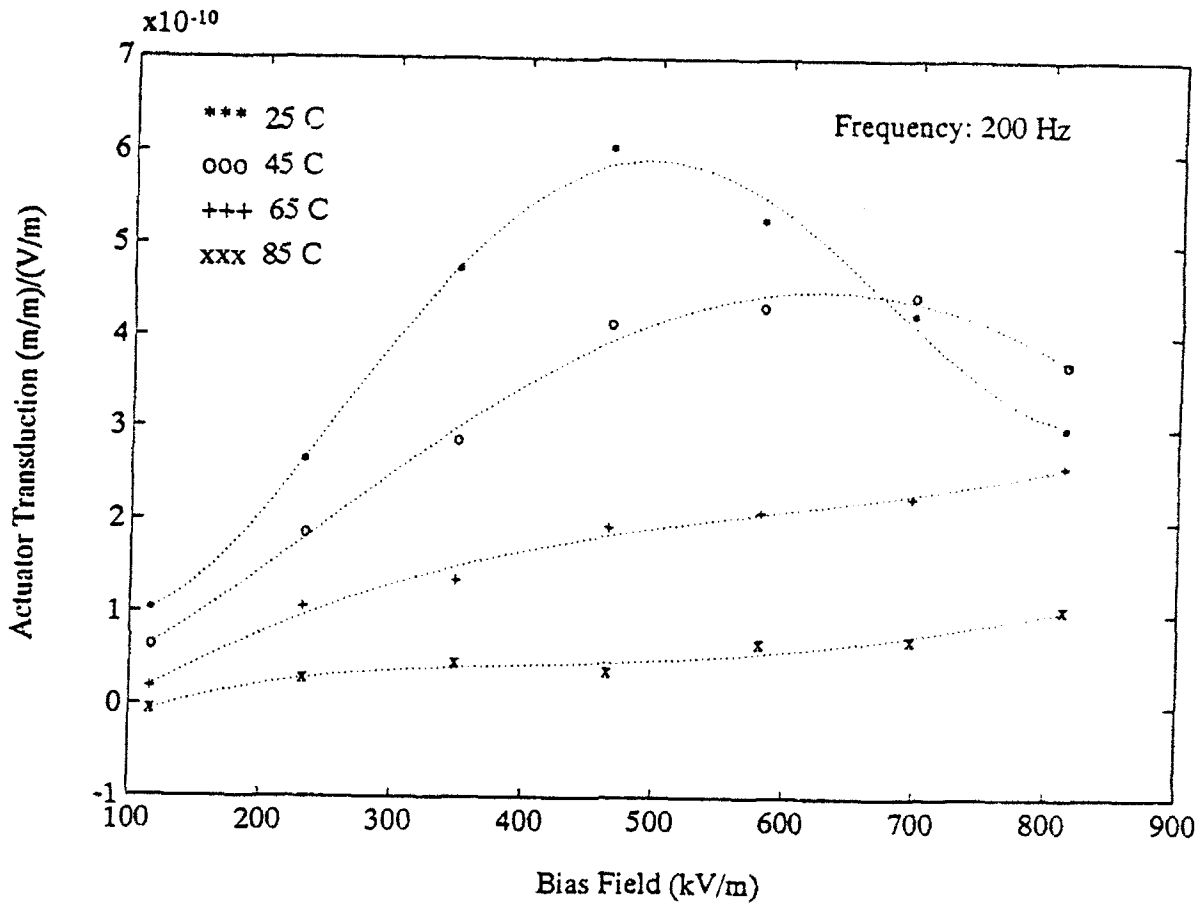

Figure 11 Actuator transduction sensitivity versus bias field for various temperatures at constant frequency.

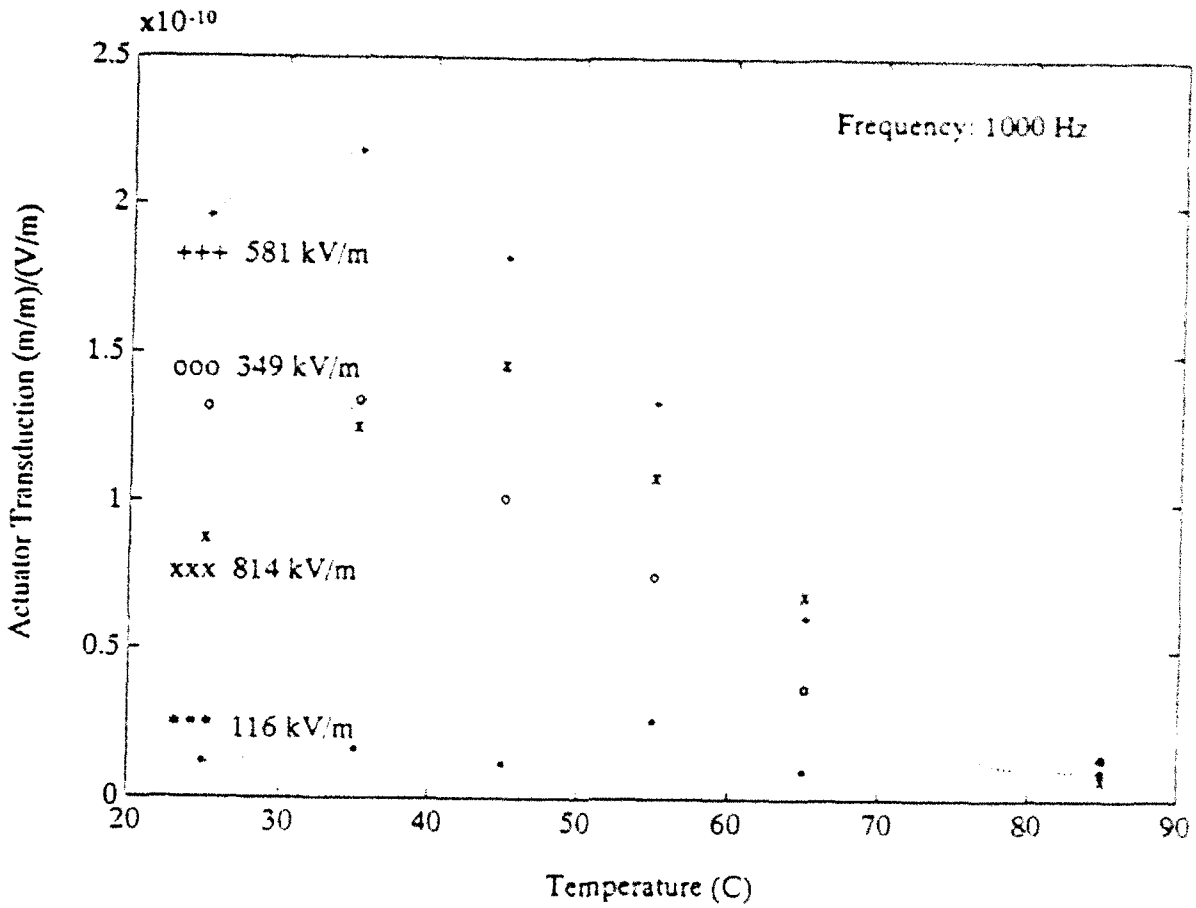

Figure 12 Actuator transduction sensitivity versus temperature for various bias fields at constant frequency.

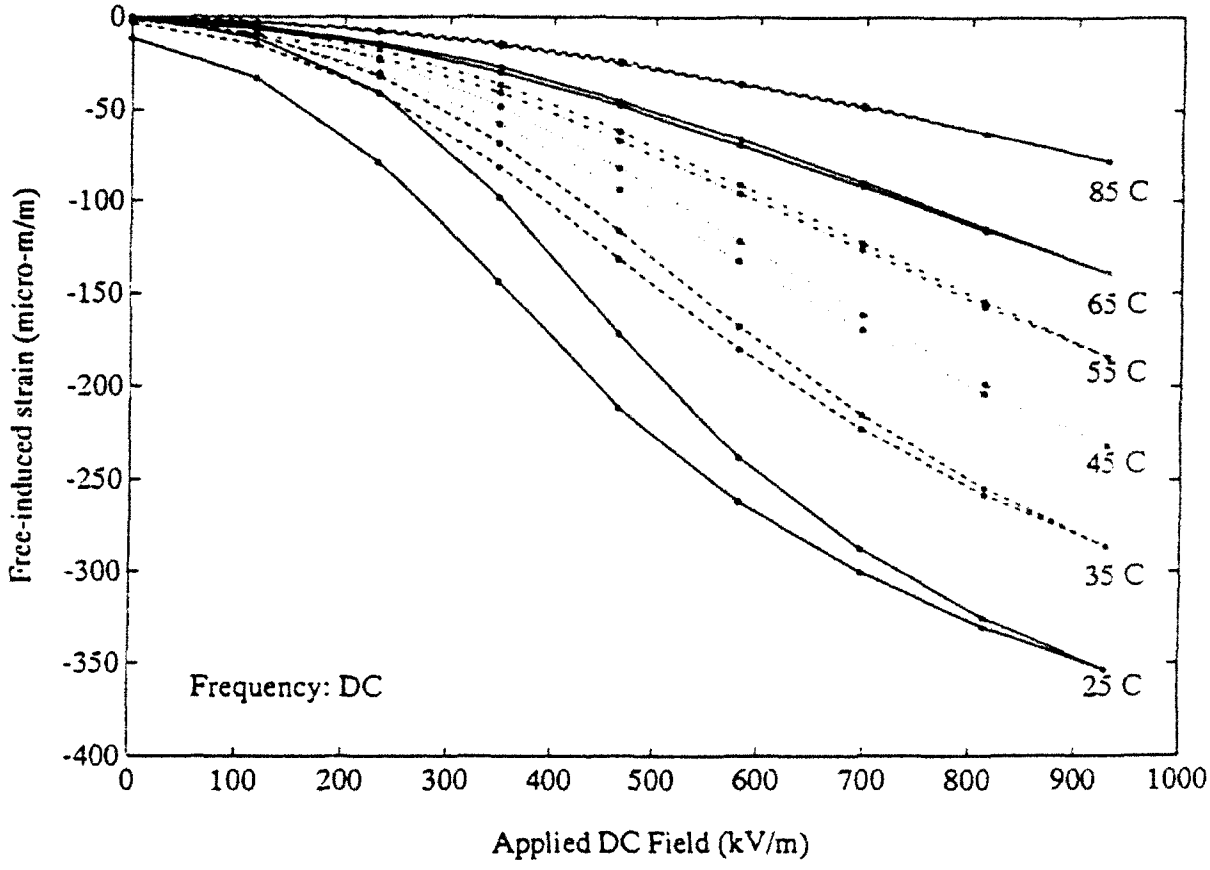

Figure 13 Free-induced strain resulting from the application of DC electric fields at various temperatures.

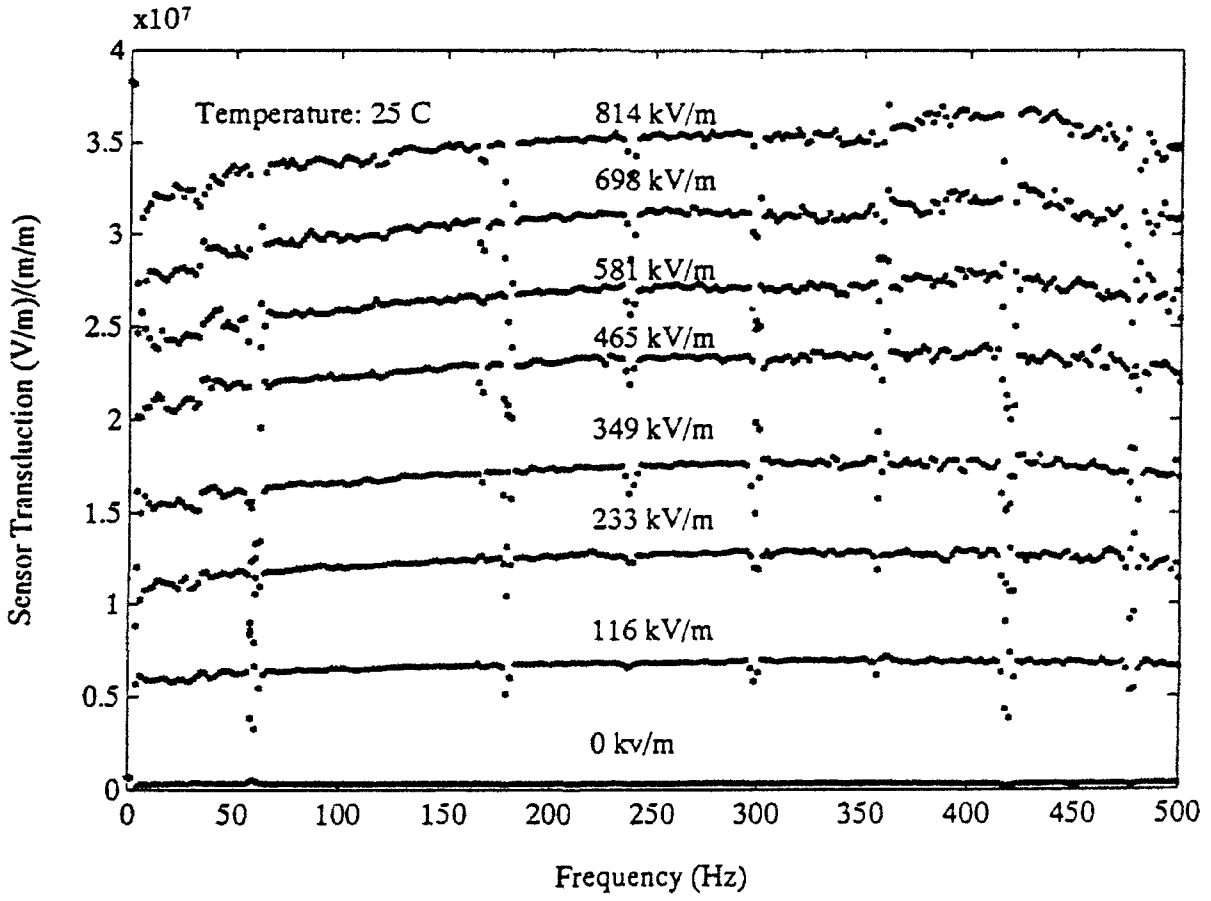

Figure 14 Frequency response of sensor transduction sensitivity at various temperatures.

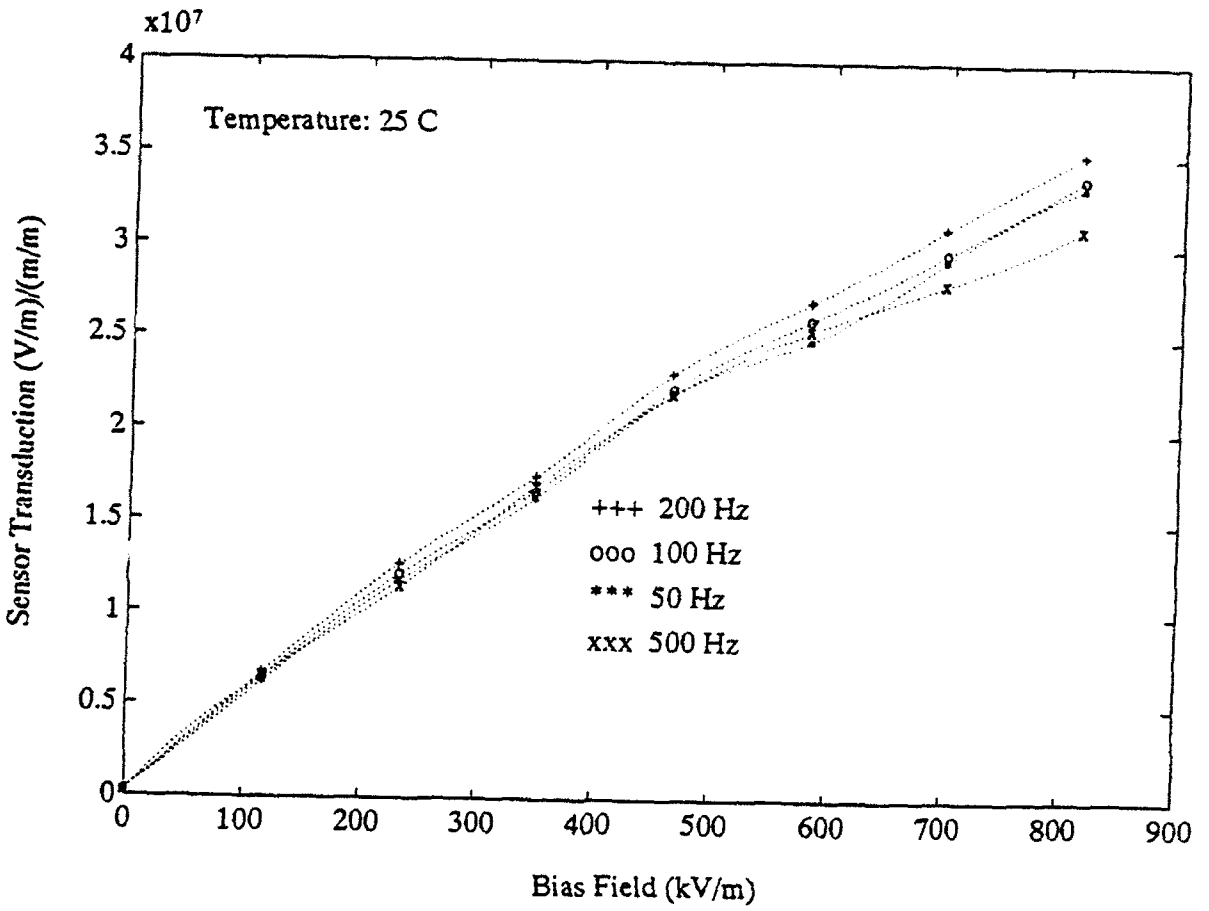

Figure 15 Sensor transduction sensitivity versus temperature for various frequencies.

Constitutive Modeling of the Electrostrictive Relaxor Ferroelectric Lead Magnesium Niobate-Lead Titinate

Chet G. Namboodri, Jr.
Craig A. Rogers

Center for Intelligent Material Systems and Structures
Virginia Polytechnic Institute and State University
Blacksburg, Virginia 24061-0261
(703) 231-2900

Abstract

Fundamental to the design of intelligent material systems and structures are the realization of attributes of the constitutive materials—the sensors and actuators—and the ability to model the characteristics of these transducers. In this paper, electromechanical behaviors of the electrostrictive relaxor ferroelectric lead magnesium niobate-lead titinate (PMN-PT) are phenomenologically modeled. The dependencies of PMN-PT electromechanical transduction on temperature and frequency, characteristics of relaxor ferroelectrics, and on applied direct-current electric field, an attribute of electrostrictors which enables tunable transduction sensitivities, are modeled with respect to electrical, sensing, and actuation properties. A general procedure for using the developed constitutive models to quantitatively describe the behavior of PMN-PT is introduced for sensing and for the three types of actuation—servo, on/off, and AC. The objective for this research is to model the behaviors of PMN-PT sensors and actuators with respect to temperature, frequency, and bias field for practical use in mechanical design.

Nomenclature

d^e	Electrostrictive piezoelectric strain coefficient (m/V)
E	Electric field, vector (V/m)
E^{AC}	Dynamic (AC) contribution to electric field (V/m)
E^{DC}	Static (DC) contribution to electric field (V/m)
g^e	Electrostrictive piezoelectric voltage coefficient (V-m/N)
L_i	Maximum permittivity-diffuseness model coefficients (K)
k	Constant in hyperbolic tangent polarization model (m/V)
k_i	Polarization model temperature coefficients (m/V-K^i)
P	Polarization, vector (C/m^2)
P^s	Saturation polarization (C/m^2)
Q	Electrostrictive coefficients [transverse, Q_{13}] (m^4/C^2)
q	Electrostrictive frequency model coefficient (m^4/C^2)
s	Applied mechanical strain (m/m)
T	Temperature (°C, K)
T_{max}	Curie temperature for maximum permittivity with relaxor ferroelectrics (°C, K)

X	Susceptibility temperature-frequency model coefficient
X_{AC}	Susceptibility paraelectric temperature-frequency model coefficient
X_E	Susceptibility temperature-frequency-bias model coefficient (V/m)
X_i	Susceptibility grain-size model coefficients (μm^{-i})
X_{max}	Maximum susceptibility temperature-frequency model coefficient
Y	Young's modulus of elasticity (N/m^2)

Greek

ϵ'	Relative electric permittivity
ϵ''	Relative electric permittivity loss
ϵ_m, κ_m	Integral mean relative permittivity for relaxor phase transition
ϵ_{max}, κ_{max}	Maximum relative permittivity of ferroelectrics
ϵ_o	Electric permittivity of free space, 8.85×10^{-12} F/m
κ	Dielectric constant, same as relative electric permittivity
Λ	Free-induced strain (m/m)
λ	Level of diffuseness of relaxor phase transition (°C, K)
σ	Applied mechanical stress (N/m^2)
τ_i	Maximum Curie temperature-grain size model coefficients ($K/\mu m^i$)
τ_{max}	Maximum Curie temperature-frequency model coefficient (°C, K)
χ	Relative dielectric susceptibility
χ_m	Integral mean relative susceptibility for relaxor phase transition
χ_{max}	Maximum relative susceptibility of ferroelectrics
ω	Frequency (Hz)

Introduction

In the past decade, interest in electroceramic transducers has been renewed by the conceptual advent of intelligent material systems and structures. Intelligent, or smart, material systems and structures are designed, via control capabilities and architected mechanics, to autonomously and judiciously sense and respond to their environments using transducer materials, i.e., sensors and actuators. Much progress has been made in the development of applications with electroceramic transducers and their integration into these systems; consequently, the need for appropriate mechanical characterization and useful, quantitative constitutive modeling for design applications has arisen.

Although electronic ceramics comprise a tremendous variety of sensors and actuators, the most common and pertinent to intelligent material systems and structures are those containing an electromechanical relationship. Application of these electroceramics are found in the areas of mechanical transduction, vibration, and acoustics. Piezoelectric and electrostrictive materials are used almost exclusively in these fields. Lead magnesium niobate doped with lead titinate ($Pb[Mg_{1/3}Nb_{2/3}]O_3$-$PbTiO_3$, or PMN-PT) is a ceramic which exhibits a strong electrostrictive effect. Electrostriction involves a nonlinear electromechanical coupling for which the material develops a strain proportional to the square of the polarization. Free-induced strains in PMN-PT

as high as $4\text{-}5 \times 10^{-4}$ have been achieved for realizable fields on the order of 10^3 V/mm (Ealey and Davis, 1990). For comparison, a piezoceramic develops strain *proportional* to the electric-field-induced polarization. Strain levels for the best piezoelectrics are comparable to the best electrostrictors (Damjanovic and Newnham, 1992). When compared with a typical piezoceramic such as lead zirconate titinate ($Pb[ZrTi]O_3$, or PZT), PMN-PT distinguishes itself not only in the nonlinearity of its coupling, through which tunable transduction sensitivities can be achieved, but also in its electromechanical and thermal stability, its negligible dielectric aging, its repeatability under cyclic driving fields, and its dynamic response (Cieminski and Beige, 1991; Cross et al., 1980).

A description of the advantages of PMN-PT, however, would be remiss without relating its disadvantages. Because the response of PMN-PT is nonlinear, quadratic with respect to polarization, the useful actuator authority for AC applications is limited. Furthermore, the electromechanical response is highly frequency-dependent and is restricted to a temperature range in which the dielectric permittivity is large, namely the *relaxor phase transition* range. Finally, deformation for low applied electric fields is small (quadratic behavior), so that electrostrictors such as PMN-PT somewhat exacerbate the desire for low-voltage devices.

Although much research into the constitutive behavior of PMN-PT has been reported, emphasis has been placed on material processing and dielectric behavior, due to attractive high permittivity values. The bridge of understanding from processing, composition, and dielectric properties to the mechanical domain has been qualitatively described and incompletely formulated. The electromechanical response of PMN-PT requires thorough investigation from an engineering perspective and sound, practical constitutive models for use in design and integration into intelligent material systems and structures. The objective of this research is to model the electromechanical behaviors of PMN-PT, with an emphasis on engineering design utility. Constitutive modeling of the electrostrictive properties of PMN-PT have been performed with respect to temperature, frequency, and DC electric field.

In another paper, the authors have experimentally established the transverse dielectric and electrostrictive behaviors of PMN-PT (Namboodri and Rogers, 1992b). In this paper, the ultimate objective for this research, to develop a model which can be used for the electro-mechanical design of intelligent material systems which incorporate PMN-PT electrostrictors, will be fulfilled. As alluded in quotes of Moulson's and Herbert's Electroceramics: Materials, Properties, Applications (1990), it is nearly impossible to theoretically account for the precise behaviors of electroceramics. For this reason, an empirical approach to modeling has been undertaken. Electrostrictive phenomenology finally formulated by Devonshire is first described for a fundamental basis of PMN-PT constitutive modeling (Grindlay, 1970). Then, the diffuse phase transition characteristic of relaxor ferroelectrics (Cross, 1987) is considered by interpreting a model put forth by Shrout et al. (1987). Frequency dispersion of dielectric properties is considered in this model. Next, effects of bias field on permittivity are examined and modeled, and the impact of frequency on electrostrictive properties is appraised. The paper concludes with model results and a procedural summary for modeling PMN-PT electromechanical behavior.

Electrostrictive Phenomenology

According to Landau-Ginzburg-Devonshire (LGD) thermodynamic formalism, relating dielectric and elastic properties of solids, electrostriction arises from free energy terms (Newnham, 1991; Namboodri and Rogers, 1992a). Three different but equivalent effects arise when the three possible partial derivatives of the electrostrictive free energy terms are taken in different orders. Integration of these relations yields constitutive equations for electrostrictive behavior.

With this so-called 'direct effect,' free-induced strain varies with the square of polarization:

$$\Lambda_i = Q_{ijk} P_j P_k + d_{ij}^o P_j + \Lambda_i^o. \tag{1}$$

Physically, the piezoelectric coefficient in eq. (1) relates any effects from spontaneous polarization of an electrostrictor. One converse effect describes the electric field developed when an electrostrictor is stressed,

$$E_i = (Q_{ijk} P_k + g_{ij}^o)\sigma_j + E_i^o. \tag{2}$$

The second converse electrostrictive effect involves the linear stress dependence of susceptibility.

Equations (1) and (2) represent the electrostrictive actuation and sensing constitutive relations. For practical engineering design and implementation, the polarization term prevalent in these equations does not possess the parametric convenience of applied electric field. Conventionally, linear dielectric behavior is assumed for a parallel-plate capacitor, where induced polarization is described as the product of dielectric susceptibility and electric field:

$$P_i = \chi_{ij} E_j = (\epsilon_{ij}' - 1) E_j. \tag{3}$$

Therefore, not only are the actuation and sensing properties in eqs. (1) and (2) important, but also dielectric properties are important to electrostrictive behavior.

Frequency Dispersion of Dielectric Properties

From grain-size studies of a composition of PMN-PT, Shrout et al. (1987) introduced a model for the Gaussian appearance of the relative dielectric permittivity through the ferroelectric-paraelectric phase transition,

$$\epsilon'(T) = \frac{2\epsilon_{max}\epsilon_m\lambda^2}{2\epsilon_m\lambda^2 + \epsilon_{max}[T - T_{max}]^2}. \tag{4}$$

T_{max}, ϵ_{max}, and λ are all parameters that can be experimentally obtained at a given frequency or as Shrout suggested, can be related to grain size. Thus, the only parameter unrealized for the model of eq. (4) is ϵ_m. No data exist in Table 1.1 to relate ϵ_m to grain size. Regardless, this

constant, which represents the integrated mean of relative permittivity across the phase transition, can be determined through eq. (4) by measuring the permittivity at one temperature, for example 25°C. Therefore, the permittivity phase transition (at a given frequency) of a solid solution of PMN-PT can be modeled with eq. (4) by measuring grain size and permittivity at one temperature.

As shown in Fig.1, model of eq. (4) compares well with data from Namboodri and Rogers (1992b) up to and just past the Curie maximum temperature, T_{max}. Values of model parameters for this plot include T_{max} = 47.5°C and ϵ_{max} = 21500, λ = 27°C, and ϵ_m = 14500. The Gaussian nature of the model dictates that the distribution be symmetric about T_{max}, which is not the case for PMN-PT data of Fig. 1. Although the quadratic, Gaussian model of eq. (4) represents behavior very well for ferroelectric phases of the thermal transition, the linear, paraelectric behavior past the Curie maximum is not well-modeled.

Furthermore, frequency dispersion of permittivity is not incorporated. Both of these problems are the subject of the next section. In addition to the insufficiency of representing permittivities past the Curie maximum temperature, the model of eq. (4) neglects a major contributor to the dielectric response, frequency. Frequency-dependence is prevalent in the experimental results of Namboodri and Rogers (1992b). From these curves, one can surmise that the parameters of eq. (4)—T_{max}, ϵ_{max}, and ϵ_m—vary with frequency. Viehland et al. (1990) observed the similarities of the microscopic compositional fluctuation behavior of relaxor ferroelectrics to the spin-glass behavior of superparamagnetic relaxors and derived a 'spin-glass-analogous model,' which indicates frequency dependence of T_{max}. In this equation, Viehland proposed a logarithmic relation between the Curie maximum and frequency, supported by experimental data. In this vein, the Curie maximum and maximum relative permittivity (thus, susceptibility) are proposed as functions of the logarithm of frequency:

$$T_{max}(\omega)=T_{max}(\omega_o)+\tau_{max}\ln(\omega_o/\omega) \tag{5}$$

$$\chi_{max}(\omega)=\chi_{max}(\omega_o)+X_{max}\ln(\omega_o/\omega). \tag{6}$$

With respect to the model of eq. (4), three of the four parameters necessary to determine the relative permittivity at a given frequency and temperature—T_{max}, ϵ_{max}, and λ—can be determined experimentally or determined against grain size.

The remaining parameter, ϵ_m or χ_m, can be determined from the other three and from a known relative susceptibility at a known temperature. However, χ_m will certainly vary with frequency, since it represents an integral mean of susceptibility. To account for this probable frequency dependence, a logarithmic relation similar to those of eqs. (5) and (6) is proposed:

$$\chi(T_o,\omega)=\chi(T_o,\omega_o)+X\ln(\omega_o/\omega), \tag{7}$$

where $\chi(T_o,\omega_o)$ is a measured susceptibility at a known temperature and interrogation frequency.

Again, only the grain size number and one susceptibility measurement are required to use this frequency-dispersive, dielectric phase transition model.

The problem of accuracy for increased paraelectric phase temperatures still remains with the model of eq. (4), upon which everything is based. In Fig. 1, these permittivities (susceptibilities) seem to be linearly related to temperature. However, this linear relationship begins at temperatures somewhat past the Curie maximum. Empirically, the onset of linear thermal-permittivity variance occurs at a temperature about 10% greater than the maximum Curie temperature, which is frequency dependent. From eq. (4) and from these empirical observations, the AC susceptibility can be described by the following equations:

$T \leq 1.1\ T_{max}(\omega)$,

$$\chi^{AC}(T,\omega)=\frac{2\chi_{max}(\omega)\chi_m(\omega)\lambda^2}{2\chi_m(\omega)\lambda^2+\chi_{max}(\omega)[T-T_{max}(\omega)]^2} \tag{8}$$

$T > 1.1\ T_{max}(\omega)$,

$$\chi^{AC}(T,\omega)=\chi^{AC}(1.1T_{max}(\omega),\omega)+X_{AC}[T-1.1T_{max}(\omega)]. \tag{9}$$

By implementing eqs. (5)-(7) and presuming $T_o \leq 1.1\ T_{max}(\omega_o)$, the term $\chi_m(\omega)$ can be determined, as described above, from the following expression:

$$\chi_m(\omega)=\frac{\chi(T_o,\omega)\chi_{max}(\omega)[T_o-T_{max}(\omega)]^2}{2\lambda^2[\chi_{max}(\omega)-\chi(T_o,\omega)]}. \tag{10}$$

Results from this complete frequency-dispersive, dielectric phase transition model are compared with experimental data in Fig. 2. Model results were generated using the following constants: T_o = 25°C, ω_o = 100 Hz, $T_{max}(\omega_o)$ = 47.5°C, τ_{max} = -1.3°C, $\chi_{max}(\omega_o)$ = 21500, $\chi(T_o,\omega_o)$ = 14063, X_{max} = 400, X = -532, X^{AC} = -255, and λ = 27°C.

The frequency-dispersive, dielectric phase transition model embodied by eqs. (8) and (9) has been developed so that only two measurements are required, grain size and permittivity at a known temperature and frequency. With grain size, $T_{max}(\omega_o)$, $\chi_{max}(\omega_o)$, and λ can be determined, as proposed by Shrout et al. (1987). With these values, $T_{max}(\omega)$ and $\chi_{max}(\omega)$ can be ascertained using eqs. (5) and (6). The measurement of relative susceptibility at known temperature and frequency is required to complete the models of eqs. (7) and (10), for $\chi(T_o,\omega)$ and $\chi_m(\omega)$, respectively. Finally, the AC relative susceptibility with respect to both frequency and temperature, within the phase transition region, can then be obtained using eqs. (8) and (9).

Bias Field Considerations

Experimental results in Namboodri and Rogers (1992b) for PMN-PT actuation indicate that

applied DC electric bias field contributes significantly to the electrostrictive response of PMN-PT. Equations (1) and (2), based on the LGD phenomenology, indicate direct influences of DC bias field on transduction sensitivities. Additionally, Pan et al. (1989) suggest an influence of bias field on dielectric properties and support this assertion by the experimental findings.

Zhang's and Rogers' (1992) proposed hyperbolic tangent relation for polarization attempts to model the nonlinear polarization-electric field (P-E) coupling of ferroelectrics. DC actuation investigations described by Namboodri provide a means for evaluating the hyperbolic tangent expression. Although indirect, the P-E relation can be compared with free-induced strain data from DC actuation experiments by assimilating it into the LGD phenomenology of eq. (1):

$$\Lambda_1(E^{DC})=Q_{13}[P^s\tanh(kE_3^{DC})]^2, \tag{11}$$

Approximate values for saturation polarization and the hyperbolic tangent polarization model coefficient obtained from results by Pan et al. (1989) can be used. According to these results, since Q_{13} does not vary greatly with temperature (Zhang et al., 1989), it appears that either P^s or k must vary thermally, based on a comparison with eq. (11). Because the shapes of different isothermal plots vary with respect to bias field, it is more likely that k, not the scaling factor P^s of eq. (11), changes with temperature. A value for the saturation polarization, $P^s = 0.23$ C/m^2, and an algebraic expression for the hyperbolic tangent model coefficient temperature dependence,

$$k(T)=\sum_{i=0}^{N=2} k_i T^i, \tag{12}$$

have been chosen for comparison of DC actuation data with results from eq. (11).

Free-induced-strain results from experiments and from the model of eqs. (11) and (12) are compared in Fig. 3. Values for Q, P^s, and k as described above were used, where k_0 = 3.694x10^{-5} V/m, k_1 = -2.008x10^{-7} V/m-K, and k_2 = 2.768x10^{-10} V/m-K^2. These plots indicate that the hyperbolic tangent model for polarization fits experimental data very well and can perhaps be relied upon for modeling bias field effects on relative dielectric susceptibility.

By comparing the hyperbolic tangent P-E expression with that of the conventional eq. (3), the hyperbolic tangent polarization model can be related to the relative dielectric susceptibility:

$$\chi^{DC}(T,E^{DC})=\frac{P^s\tanh[k(T)E^{DC}]}{\epsilon_o E^{DC}}. \tag{13}$$

To correlate this formulation with experimental DC actuation data for further analyses, it is necessary to derive an expression to reduce free-induced strain data to dielectric information. Based on the electrostrictive and dielectric phenomenology of eqs. (1) and (3), the relative susceptibility realized from free-induced transverse strain,

$$\chi_{33}^{DC}(T,E_3^{DC})=\sqrt{\frac{\Lambda_1(T,E_3^{DC})}{Q_{13}\epsilon_o^2[E_3^{DC}]^2}}. \tag{14}$$

Up to this point, models have been proposed for the AC dielectric susceptibility dependence on both temperature and frequency and for the DC dielectric susceptibility dependence on bias field and temperature. These models have been corroborated by experimental results. Regarding conservative dielectric properties, only one other relation must be addressed to complete the temperature-frequency-bias field co-dependent models for PMN-PT dielectric properties. The AC dielectric susceptibility has not been considered with respect to bias field. A logical conclusion from results with the DC susceptibility is to incorporate the hyperbolic tangent formulation into the AC susceptibility models:

$$\chi^{AC}(T,\omega,E^{DC})=\chi^{AC}(T,\omega)\frac{\tanh[k(T)E^{DC}]}{X_E E^{DC}}. \tag{15}$$

Equation (15) will be used in modeling AC actuation with PMN-PT, as later discussed.

Electrostrictive Coefficient Relations

The transverse electrostrictive coefficient cited in models introduced by eqs. (11) and (14) has been assumed constant with respect to temperature and bias field. Although previous studies have indicated variation with these parameters (Zhang et al., 1989), the degree is sufficiently minor, less than ten percent, to warrant neglect of their effects. This assumption is supported by the results of Fig. 3. However, one other parameter considered in this study, frequency, has not yet been affiliated with the electrostrictive coefficient.

The experimental actuator responses in Namboodri and Rogers (1992b) show a rather drastic reduction of transduction sensitivity with respect to increased frequency. The large change cannot be explained by the dispersion of relative permittivity. Thus, one might surmise that the electrostrictive coefficient decreases with respect to frequency. It is here proposed that, like the variance of permittivity, Q decreases with the logarithm of frequency:

$$Q(\omega)=Q(\omega_o)+q\ln(\omega_o/\omega). \tag{16}$$

Equation (16) completes a constitutive model for the electrostrictive response of PMN-PT, so that results from actuation tests can be directly compared.

Dielectric and Actuator Transduction Responses

From eq. (1), while considering the separate effects of applied AC and DC fields, the actuator transduction sensitivity can be derived:

$$\frac{\partial \Lambda(T,\omega,E)}{\partial E^{AC}} = 2Q(\omega)\epsilon_o^2[\chi^{DC}(T,E^{DC})\chi^{AC}(T,\omega,E^{DC})E^{DC} + [\chi^{AC}(T,\omega,E^{DC})]^2 E^{AC}]. \qquad (17)$$

Equations (14) through (16) model how dielectric susceptibility and electrostrictive parameters vary with temperature, frequency, and bias field. Equations (4) through (13) support these models and accentuate relations buried in the three equations.

Using eq. (17), results from the actuation experiments can be directly compared with constitutive models introduced in this chapter. In Fig. 4, the DC relative susceptibility model of eqs. (12) and (13) is compared with DC free-strain actuation data reduced by eq. (14). Values for constants used to evaluate these expressions are given earlier. Data and model results are plotted with respect to temperature at a given bias field. Frequency does not pertain to DC relative permittivity.

As compared with AC results, most notable in Fig. 4 are the extremely large values of relative permittivity, derived from both DC free-induced strain data and from the constitutive model. Another difference is that the thermal response of DC susceptibility does not have the characteristic Gaussian shape in the range of temperatures that the AC susceptibility does. The experimental data do indicate, as does the model of eq. (5), that for lower frequencies, the Curie maximum shifts to lower temperatures. Nevertheless, reduced data based on the electrostrictive phenomenology-derived expression of eq. (14) corroborate the high permittivity values and thermal response shape for DC electric field stimuli. The discernment of relative susceptibility in experimental results arises from AC field inputs. According to the differences between AC and DC results, frequency dispersion of dielectric properties excited by any AC source drastically reduces the realized permittivity of DC-induced polarization.

In Fig. 5, the AC relative susceptibility for constitutive models embodied primarily by eqs. (8), (9), and (15) are compared with experimental results. It should be noted here that data in Fig. 5 have been reduced by eq. (15), since bias field effects could not be implemented in dielectric experiments. All constants for the constitutive models illustrated in plots of Fig. 5 are identical to those introduced earlier. Again, there is very strong correspondence between experimental and model results for the thermal AC permittivity responses, both in shape and amplitude.

A final test of empirical, phenomenological modeling introduced in this chapter with respect to temperature variation is to compare model results with PMN-PT AC actuator experimental data. This comparison requires the use of eqs. (16) and (17), in addition to the permittivity model equations. In Fig. 6, actuator transduction sensitivity experimental data is plotted with respect to temperature at various frequencies and is compared with constitutive model results, which incorporate results of Figs. 4 and 5. All constants used to formulate values for actuator

transduction have been introduced, except for those of eq. (16), which are $Q(100\ \text{Hz}) = -0.014\ \text{m}^4/\text{C}^2$ and $q = 4.0057\text{x}10^{-3}\ \text{m}^4/\text{C}^2$. The shapes and amplitudes of formulated plots in Figure 6 fit data remarkably well. Based on these results, the constitutive models of this chapter appear to successfully relate the behavior of PMN-PT relaxor ferroelectrics as electrostrictive actuators.

As described in Namboodri and Rogers (1992b), since the co-dependent effects of three extrinsic parameters—temperature, frequency, and bias field—on dielectric and electrostrictive performance of PMN-PT are studied, there are six permutations to describe the material behaviors. However, only three of these are necessary to fully comprehend the responses since the other three are simply converse relations. One of these three, the thermal response at different frequencies and constant bias field, is illustrated for DC susceptibility, AC susceptibility, and actuator transduction in Figs. 4 through 6, respectively. The other two responses must be examined to completely compare constitutive modeling efforts with experimental actuation results.

One of these two, frequency response at different bias fields and constant temperature, precludes the DC permittivity, since it cannot vary with frequency. Nonetheless, the AC relative susceptibility certainly varies with respect to frequency, and plots comparing experimental and model results are provided in Fig. 7. The model, which is based on linear variation of permittivity parameters with respect to the logarithm of frequency, compares exceedingly well to data from dielectric experiments. Again, all constants used to evaluate model equations have been provided earlier in this chapter.

Amplitudes of frequency response plots in Fig. 8 for model results do not compare so favorably with actuator transduction experimental data. However, shapes of model curves do correspond with the data trends in this figure, and relative amplitudes for different bias fields match reasonably well. If the maximum standard deviation of $8\text{x}10^{-11}$ (m/m)/(V/m) for actuator transduction sensitivity data is considered, plots representing the model are well within empirical variation. Regardless, shapes and relative amplitudes, both of which are satisfactory in Fig. 8, are the two most important aspects of model responses with regard to mechanical and control design.

A final comparison of experimental results with formulations introduced in this chapter involves variation of PMN-PT material properties with respect to applied bias field. In Fig. 9, relations for the DC relative permittivity are plotted against bias field at different temperatures. The differences between experimental data and model results for relatively low bias fields illustrates a failing of the hyperbolic tangent polarization model. According to DC free-induced strain data reduced by eq. (14), the relative susceptibility is much larger for low bias fields than predicted by the hyperbolic tangent model of eq. (13). The shape of responses with respect to smaller bias fields is ill-represented by the model. One other problem with this model is that values for zero applied DC field do not exist. Nevertheless, for larger values of bias field the model is sufficiently accurate, according to Fig. 9.

In Fig. 10, experimental and model results for AC relative susceptibility are displayed with

respect to bias field at different temperatures and constant frequency. This figure and Fig. 9 both illustrate the reduced effects of bias field with increased temperatures, or the onset of the paraelectric phase of PMN-PT. Slopes of isothermal plots decrease drastically with higher temperatures; in fact, at 85°C the susceptibility is almost constant versus bias field. Again, it should be noted that data from dielectric experiments have been adjusted by bias field, as in eq. (15), since such data were not experimentally obtained. This step was necessary to contrast model results and data.

The plots of Fig. 11 complete the comparison of actuator transduction data with values from constitutive models. Plots in this figure truly exemplify the accuracy and utility of the dielectric and electrostrictive models introduced earlier in this chapter. Although formulated amplitudes do not match exactly with experimental data, trends illustrated by model plots with respect to bias field are notably consistent with data.

Figs. 4 through 11 illustrate the utility of the temperature-frequency-bias field co-dependent models for DC susceptibility, AC susceptibility, and AC actuator transduction sensitivity embodied in eqs. (4) through (17). Although amplitudes for these material behaviors do not correspond precisely with experimental values, these models illustrate trends exceedingly well, within the ranges of data. Amplitude differences can be the result of many factors, such as improper selection of model constants, variation of experimental conditions and procedure, and material property variation due to processing. However, the correspondences of response shapes and relative amplitudes are important with regard to mechanical design of PMN-PT actuators for intelligent material systems. Design and performance optimization really precludes absolute values in favor of relative improvements. Constants are of little consequence; although, the ratio of constants can be extremely important. These ratios are reasonably portrayed by the models and constants presented in this chapter for PMN-PT electrostrictive behavior.

Sensor Transduction Response

In the discussion of Namboodri and Rogers (1992b), there was attention given to fundamental differences between employing PMN-PT as an actuator and using it as a sensor. It was noted that for sensing a[illegible]ication, the extent of polarization is minute. Since stress-induced polarization amplitudes are very small, the unlikelihood that frequency affects polarization reversal was recognized theoretically and observed experimentally. This insignificance must be reflected in the modeling of PMN-PT behavior, as well.

All of the tools for modeling sensing behavior, even most of the material constants, have been introduced. Essentially, the hyperbolic tangent polarization model, including the temperature relations of eq. (12), are incorporated into the electrostrictive phenomenology for sensing. As such, an expression for the sensor transduction sensitivity, disregarding tensor subscripts, is derived:

$$\frac{\partial E(T,E^{DC})}{\partial s} = QP^2 Y \tanh[k(T)E^{DC}] + g^o(T)Y, \qquad (18)$$

where $k(T)$ is described by eq. (12).

Most of the constants of eq. (18)—Q, P^s, Y, k_t, and g^o—have been appraised for PMN-PT used in the present investigations, except for Young's modulus and the electrostrictive piezoelectric voltage coefficient. Technical specifications from AVX Corporation (Galvagni and Duprè, 1990) show values for the compressive Young's modulus as high as 112 GPa for stack geometries of their PMN-PT solid solution. However, present studies empirically indicate that for the monomorph configuration, the tensile modulus of elasticity is far less, at Y = 20 GPa. For ceramic materials, this large difference between tensile and compressive moduli is not unusual.

The empirically derived value for the transverse electrostrictive piezoelectric term of eq. (18) is around $g^o(25°C) = 2\text{x}10^{-5}$ V-m/N. Actually, this value is related to the spontaneous polarization of PMN-PT and thus depends on temperature. Viehland et al. (1990) have suggested a model for spontaneous polarization that relates to the 'freezing temperature,' analogous to polar spin-glass magnetic behavior. However, electrostrictive piezoelectric-spontaneous polarization relations are beyond the scope of this paper, so that the empirical value provided above suffices for modeling efforts.

Based on these constants, the model of eq. (18) compares fairly well in Fig. 12 with data from experimental sensing results of Chapter 3. Scatter in data results from 60-Hz noise and FFT aliases of that noise. Since frequency was not modeled as influential on dielectric properties, it was also considered to have a negligible effect on electrostrictive properties, so that a constant value of Q = -0.008 m^4/C^2 was chosen. In these plots, the independence of frequency is illustrated by both experimental and model results. Furthermore, relative amplitudes of the hyperbolic tangent model of eq. (18) compare favorably with data. Thermal responses for PMN-PT sensing were not investigated, but the temperature-dependent coefficient k of eq. (12) can be confidently used to model sensor transduction, based on results previously obtained. However, the temperature-dependent constant g^o must be considered in such modeling.

Summary: A Constitutive Model for PMN-PT

Since the order of model equations in this paper does not necessarily best fit the order with which a designer might employ them, the following summary is offered as somewhat of a procedure for using the proposed models for PMN-PT transduction.

Sensing with PMN-PT

The model proposed for sensing is completely independent of the separate descriptions for DC and AC relative susceptibility. Furthermore, there is no frequency dependence for either dielectric or electrostrictive terms in this model. As such, if PMN-PT is used as a sensor only,

there is no reason to bother with models for such terms. Equation (18) models the transduction sensitivity of PMN-PT sensors, which is the voltage generated per unit of applied alternating strain. This transduction sensitivity varies with applied bias field and with temperature. In this equation, the electrostrictive, saturation polarization, and elastic modulus coefficients are assumed constant. The hyperbolic tangent polarization model coefficient k varies with temperature by the relation of eq. (12). The electrostrictive piezoelectric term varies with spontaneous polarization, or temperature, and has not been modeled, since no experiments were designed to investigate its behavior.

Servo Actuation with PMN-PT

The other electrostrictive effect involving use of PMN-PT with intelligent material systems and structures is actuation. Three types of actuation have been classified—servo, on/off, and AC. As with sensing, servo actuation with PMN-PT does not necessitate modeling frequency dependence of dielectric and electrostrictive terms. Instead, a relation identical to eq. (11), without tensor subscripts and including temperature variation, is all that is required:

$$\Lambda(T,E^{DC})=Q[P^s\tanh[k(T)E^{DC}]]^2, \tag{19}$$

where Q and P^s are constants, and $k(T)$ is given by eq. (12).

DC Dielectric Susceptibility

Since DC dielectric susceptibility pertains to bias fields with both on/off and AC actuation with PMN-PT, its appraisal is a reasonable first step in realizing a model for frequency-dependent actuator behavior. Equation (13) represents the temperature and bias field dependence of the DC dielectric susceptibility. Again, the temperature variation of k is described by eq. (12).

AC Dielectric Susceptibility

If the design involves implementation of PMN-PT as a servo actuator, this section is of little consequence, and the designer can skip to the next section on actuator transduction, unless there are dynamic concerns. If an on/off or AC actuator is considered, the procedure in this section should be consulted to model the temperature-frequency-bias field co-dependent AC dielectric susceptibility. The proposed model begins with eq. (15), which really just describes the bias field variation. The k polarization parameter comes from eq. (12), and X_E is a constant.

To evaluate the variable $\chi^{AC}(T,\omega)$ of eq. (15), eqs. (8) and (9) need to be consulted. Variables arising in these equations which must be accounted include χ_m, χ_{max}, T_{max}, and λ; χ^{AC} is a constant. Equations (8) and (9) are designed so that grain size and a permittivity at known temperature and frequency are the only material measurements required, in addition to realizing values for constants. For the frequency-dependent χ_m, eqs. (10) and (7) are utilized. $\chi(T_o,\omega_o)$ describes the value of susceptibility measured at a known temperature and frequency, and X is a constant.

The frequency dispersive relations for T_{max} and χ_{max} are provided by eqs. (5) and (6) respectively. τ_{max} and X_{max} are constants in these relations. $T_{max}(\omega_o)$, $\chi_{max}(\omega_o)$, and λ can be related to grain

size. Evaluation of these equations with their appropriate constants completes models for the AC permittivity, so that dynamic actuation with PMN-PT can be perceived.

Dynamic Actuation with PMN-PT

The transduction sensitivity for cyclic driving of a PMN-PT actuator with a moderate alternating electric field is modeled in eq. (17). Dielectric parameters in this model are found from relations described above. Additionally, for moderate to large AC driving fields, the frequency-dispersive electrostrictive coefficient is modeled by eq. (16). As with dielectric terms, this relation involves a linear decay of the coefficient with respect to the logarithm of frequency.

Conclusions

In this paper, electromechanical behavior of the relaxor ferroelectric PMN-PT was phenomenologically modeled. Dielectric, sensing, and actuation behaviors of PMN-PT monomorphs were investigated. Based on Landau-Ginzburg-Devonshire (LGD) phenomenology for electrostrictive effects, the relative susceptibility is of utmost importance, since electrostriction is related to polarization. As such, aspects of polarization, including dielectric susceptibility, were carefully considered and modeled for electrostrictive sensing and actuation constitutive relations with PMN-PT. These models, based on phenomenological and empirical equations, agree very well with data acquired from experiments with the PMN-PT monomorphs. Highlights of results discussed are presented below:

- Phenomenology based on LGD thermodynamic formalism, which relates transduction sensitivity with applied DC bias field, was developed for electrostrictive sensing. A hyperbolic tangent model was introduced to relate bias field with polarization and to include temperature variation of sensor transduction sensitivity. Comparison of experimental data with PMN-PT monomorphs showed that results with this model conform very well.
- LGD phenomenology for DC, or servo, actuation with electrostrictors was again related to the hyperbolic tangent polarization model. Temperature and bias field dependencies of PMN-PT servo actuation were experimentally demonstrated and were well represented by constitutive models.
- Relations for DC dielectric susceptibility of PMN-PT were derived from the hyperbolic tangent polarization model and included temperature dependencies. The model agreed very well with experimental data, except at low bias fields values. It underpredicted DC susceptibility for bias fields less than 250 kV/m.
- Temperature-frequency-bias field co-dependence on the AC dielectric susceptibility modeled phenomenologically. The model embodies hyperbolic tangent polarization relations for bias field described above, Gaussian relations for the primarily ferroelectric phases of the thermal transition, linear relations with respect to temperature for the paraelectric phases after the Curie maximum temperature, and logarithmic frequency relations to account for dispersion of dielectric properties. The co-dependent model fit data extremely well.
- Logarithmic frequency dispersive relations similar to those modeled for AC susceptibility

were incorporated in models for the electrostrictive coefficient associated with moderate cyclic-field driving of PMN-PT actuators.

- Models for the frequency-dependent electrostrictive coefficient, temperature- and field-dependent DC susceptibility, and temperature-frequency-field co-dependent AC susceptibility were tested by coupling them with LGD actuator phenomenology and comparing the model results with experimental data. The constitutive model for cyclic actuation of PMN-PT compared favorably with experimental results. Response shapes and relative amplitudes were very accurate.
- Finally, since an objective for the research was to develop models for PMN-PT which can be readily utilized by intelligent material system designers, a procedural summary for using the constitutive relations was included in the text.

Although results from this research include models which account for the behaviors of PMN-PT very well, these models describe only transverse transduction, i.e., only actuation and sensing perpendicular to applied or measured electrical quantities. Furthermore, there are other aspects of the findings and models in this paper which require further investigations. Approaches discussed herein for modeling PMN-PT behavior could be generalized and improved by the following suggestions:

- Processing effects on grain size should be studied for 0.9PMN-0.1PT specifically, to realize constants for the algebraic relations between grain size and dielectric properties.
- Frequency dependence of the electrostrictive coefficient should be further characterized and validated, since there are no other research endeavors in the literature to confirm this behavior.
- The electrostrictive piezoelectric coefficients developed from LGD phenomenology require better understanding. For example, the relation of the electrostrictive piezoelectric voltage coefficient to spontaneous polarization could be researched.
- The tensor behavior should be robustly investigated and modeled, like the transverse transduction studies of this thesis, for design of PMN-PT sensors and actuators in configurations utilizing other tensor properties, for example, a stack geometry.
- Finally, constitutive equations introduced in this thesis and perhaps augmented by future studies should be applied both computationally and experimentally to control and mechanical design of smart material systems, in order to better evaluate their utility.

References

von Cieminski, J. and H. Beige, 1991. "High-signal electrostriction in ferroelectric materials," *Journal of Physics D* **24**[7], 1182-1186.

Cross, L.E., 1987. "Relaxor Ferroelectrics," *Ferroelectrics* **76**, 241-267.

Cross, L.E., S.J. Jang, R.E. Newnham, S. Nomura and K. Uchino, 1980. "Large electrostrictive effects in relaxor ferroelectrics," *Ferroelectrics* **23**, 187-192.

Damjanovic, D. and R.E. Newnham, 1992. "Electrostrictive and piezoelectric materials for actuator applications," *Journal of Intelligent Material Systems and Structures* **3**, 191-209.

Ealey, M.A. and P.A. Davis, 1990. "Standard SELECT electrostrictive lead magnesium niobate actuators for active and adaptive optical components," *Optical Engineering* **29**[11], 1373-1382.

Galvagni, J. and D. Duprè, 1990. "Electrostrictive actuators, precision electromechanical components," Technical Information, AVX Corporation, Myrtle Beach, SC.

Grindlay, J., 1970. An Introduction to the Phenomenological Theory of Ferroelectricity, Pergamon Press, New York, New York.

Moulson, A.J. and J.M. Herbert, 1990. Electroceramics: Materials, Properties, Applications, Chapman & Hall, New York, New York.

Namboodri, C.G. and C.A. Rogers, 1992a. "Tunable Vibration/Strain Sensing with Electrostrictive Materials," *Proceedings of the Conference on Recent Advances in Adaptive and Sensory Materials and their Applications*, Blacksburg, VA, 285-297.

Namboodri, C.G. and C.A. Rogers, 1992b. "Experimental Investigation of the Electrostrictive Relaxor Ferroelectric Lead Magnesium Niobate-Lead Titinate," submitted to the *Journal of Material Science*, November 1992.

Newnham, R.E., 1991. "Tunable transducers: nonlinear phenomena in electroceramics," *NIST Special Publication 804, Chemistry of Electronic Ceramic Materials*, Proceedings of the International Conference, Jackson, WY.

Pan, W.Y, W.Y. Gu, D.J. Taylor and L.E. Cross, 1989. "Large piezoelectric effect induced by direct current bias in PMN:PT relaxor ferroelectric ceramics," *Japanese Journal of Applied Physics* **28**[4], 653-661.

Shrout, T.S., U. Kumar, M. Megherhi, N. Yang and S.J. Jang, 1987. "Grain size dependence of dielectric and electrostriction of $Pb(Mg_{1/3}Nb_{2/3})O_3$-based ceramics," *Ferroelectrics* **76**, 479-487.

Viehland, D., S.J. Jang, L.E. Cross and M. Wuttig, 1990. "Freezing of the polarization fluctuations in lead magnesium niobate relaxors," *Journal of Applied Physics* **68**[6], 2916-2921.

Zhang, Q., W. Pan, A. Bhalla and L.E. Cross, 1989. "Electrostrictive and dielectric response in lead magnesium niobate-lead titinate (0.9PMN:0.1PT) and lead lanthanum zirconate titinate (PLZT 9.5/65/35) under variation of temperature and electric field," *Journal of the American Ceramic Society* **72**[4], 599-604.

Zhang, X.D. and C.A. Rogers, 1992. "A macroscopic phenomenological formulation for coupled electromechanical effects in piezoelectricity," *Proceedings of the Conference on Recent Advances in Adaptive and Sensory Materials and their Applications*, Blacksburg, VA, 183-203.

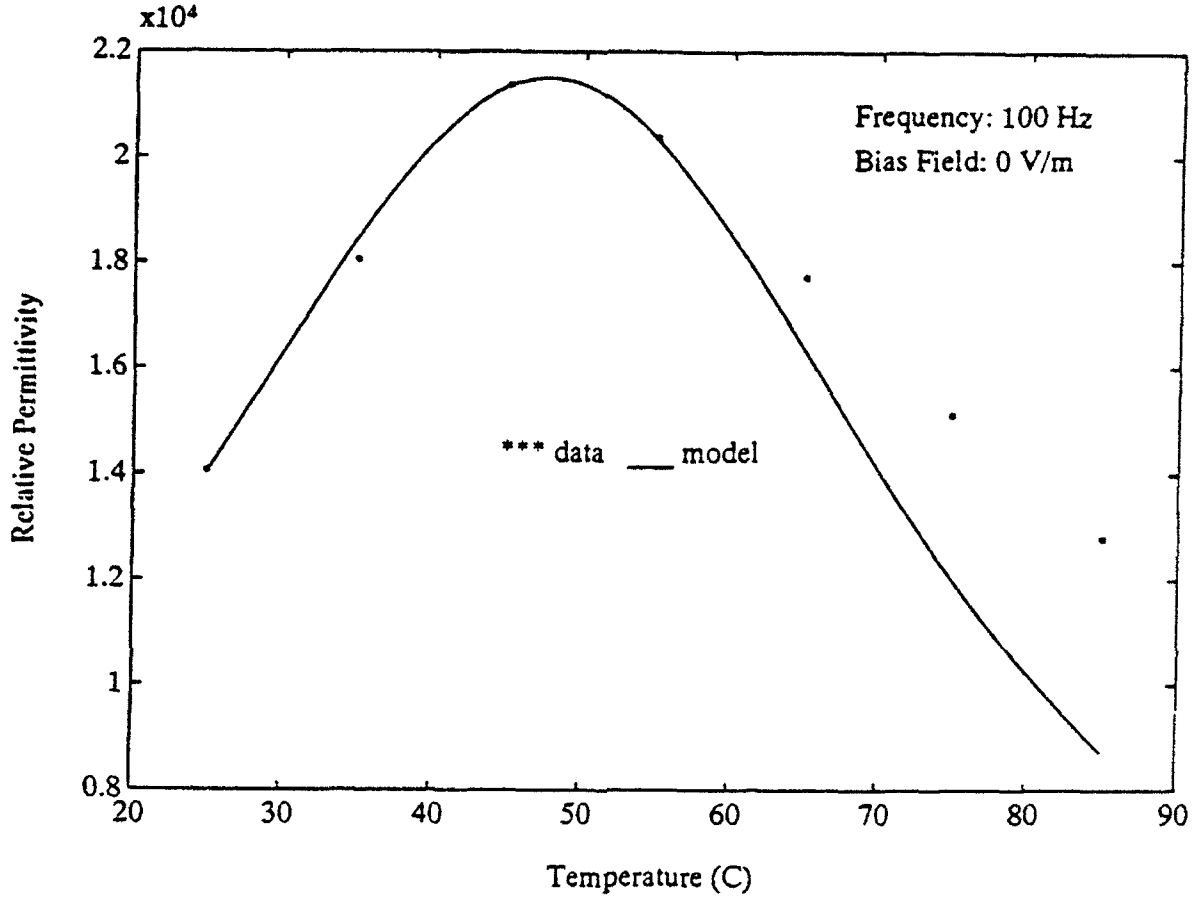

Figure 1 Comparison of Shrout's dielectric phase transition model with experimental data.

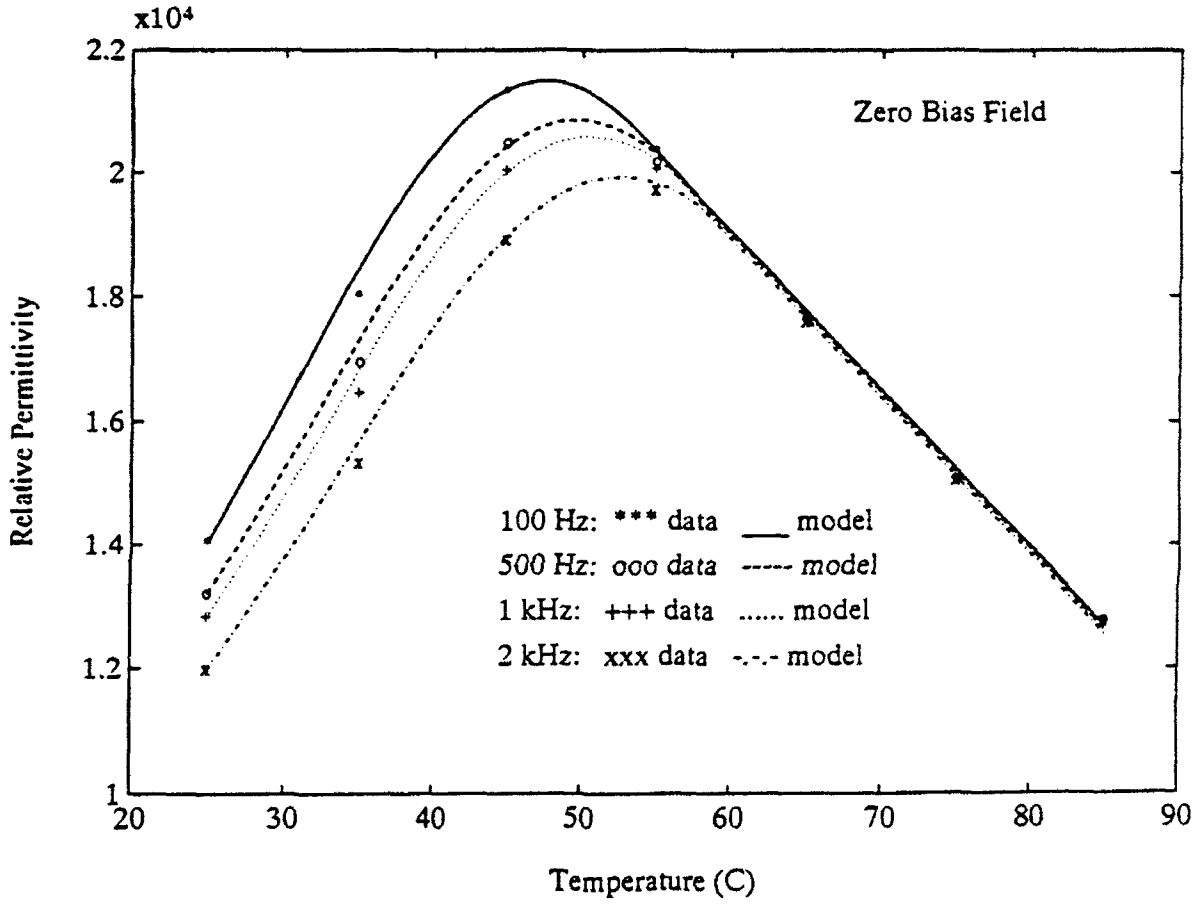

Figure 2 Comparison of frequency-dispersive, dielectric phase transition model with experimental data.

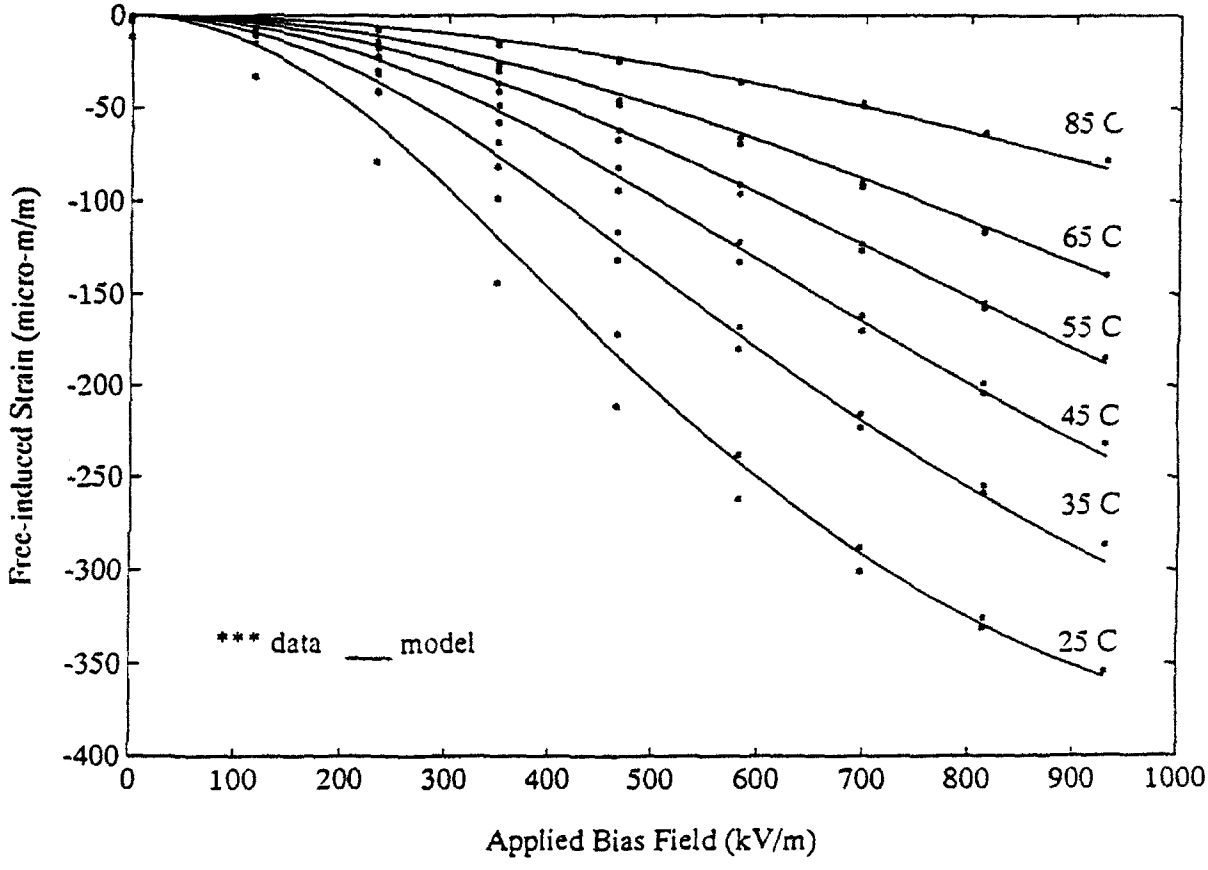

Figure 3 Comparison of hyperbolic tangent polarization model with DC free-induced strain experimental data.

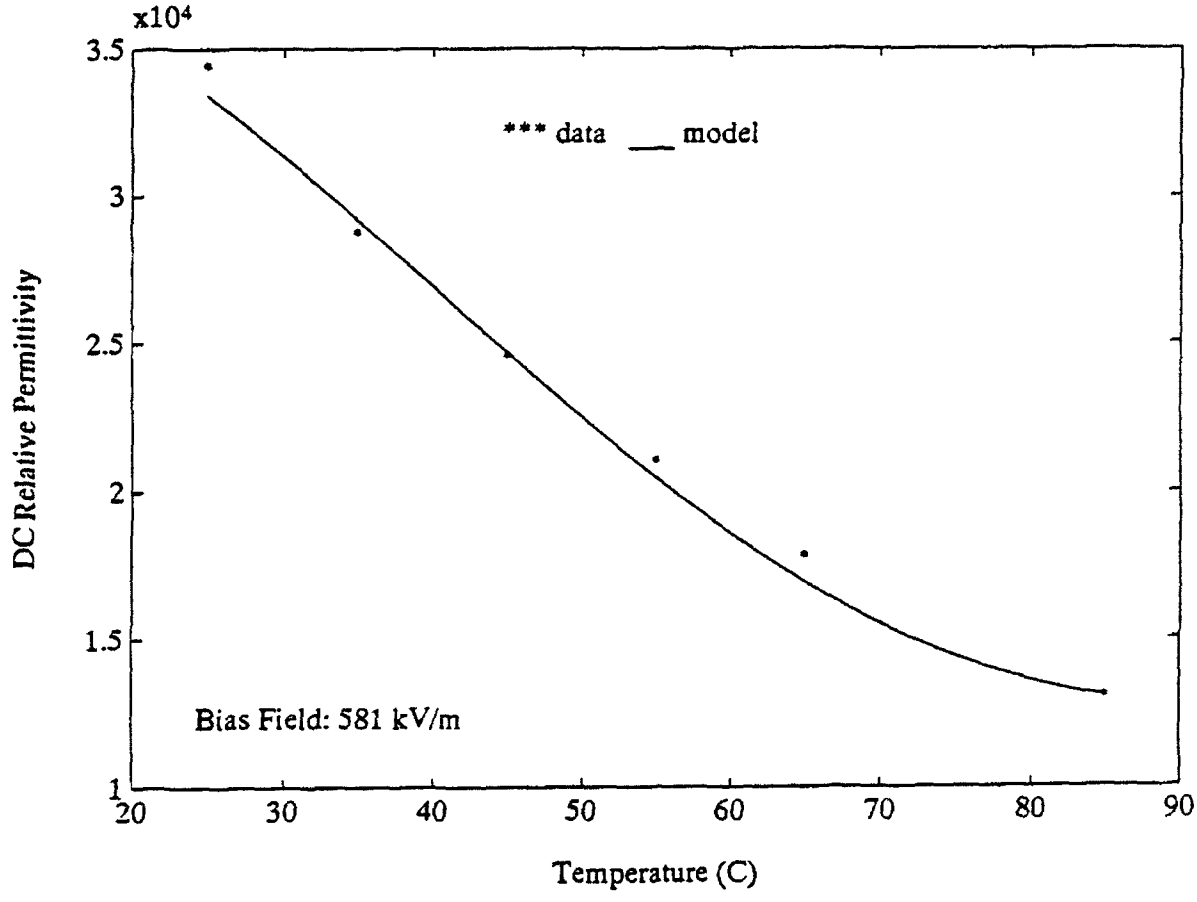

Figure 4 Comparison of DC relative susceptibility model results with reduced data from DC free-induced strain response experiments versus temperature.

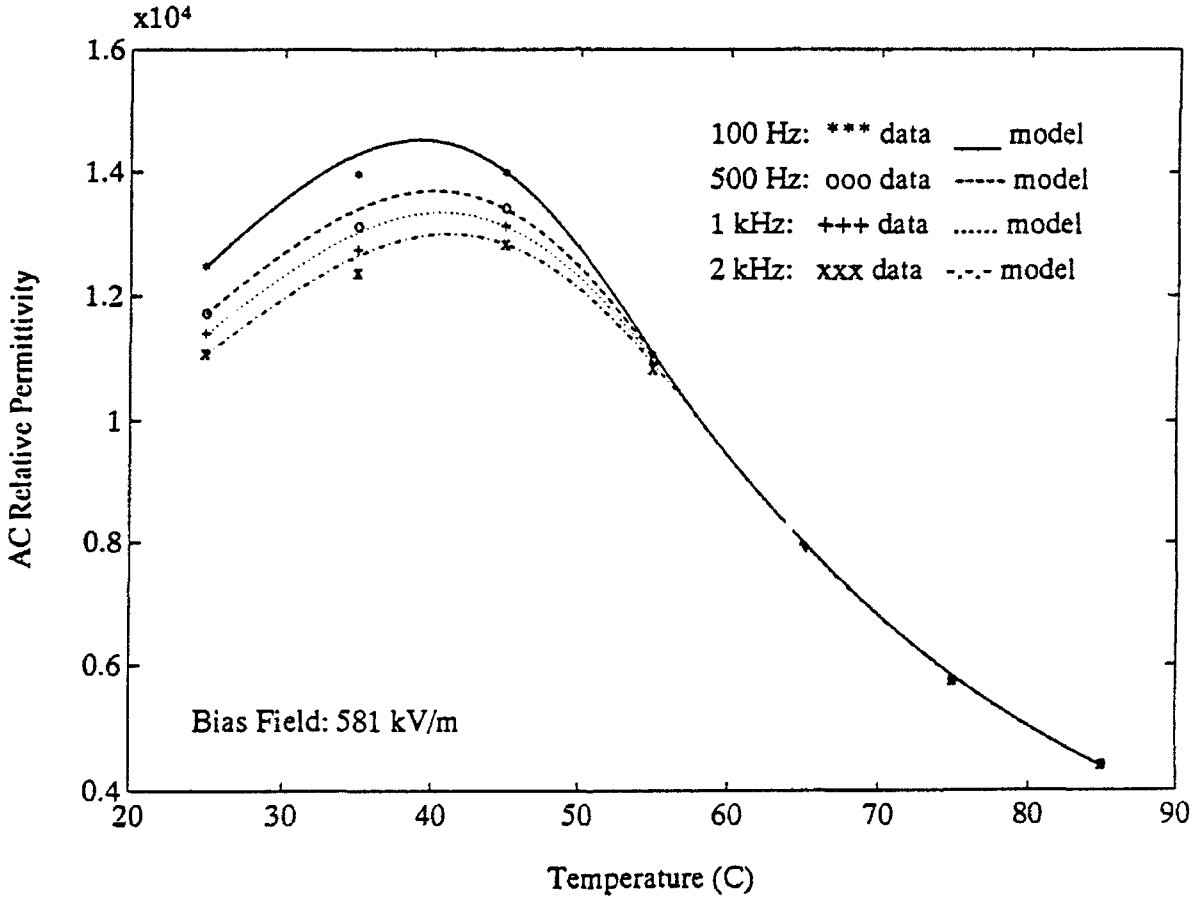

Figure 5 Comparison of AC relative susceptibility model results with reduced data from permittivity response experiments versus temperature at various frequencies.

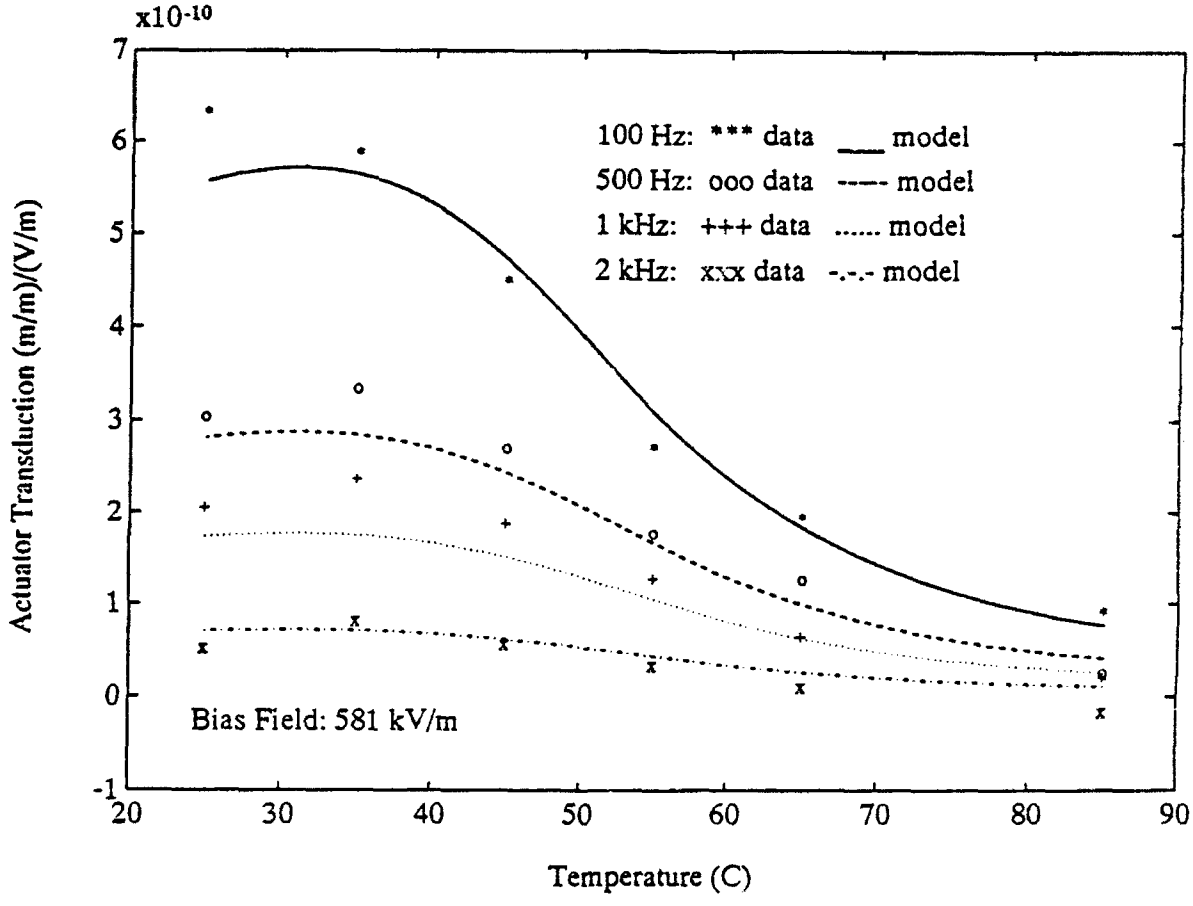

Figure 6 Comparison of electrostrictive constitutive model results with data from AC actuator response experiments versus temperature at various frequencies.

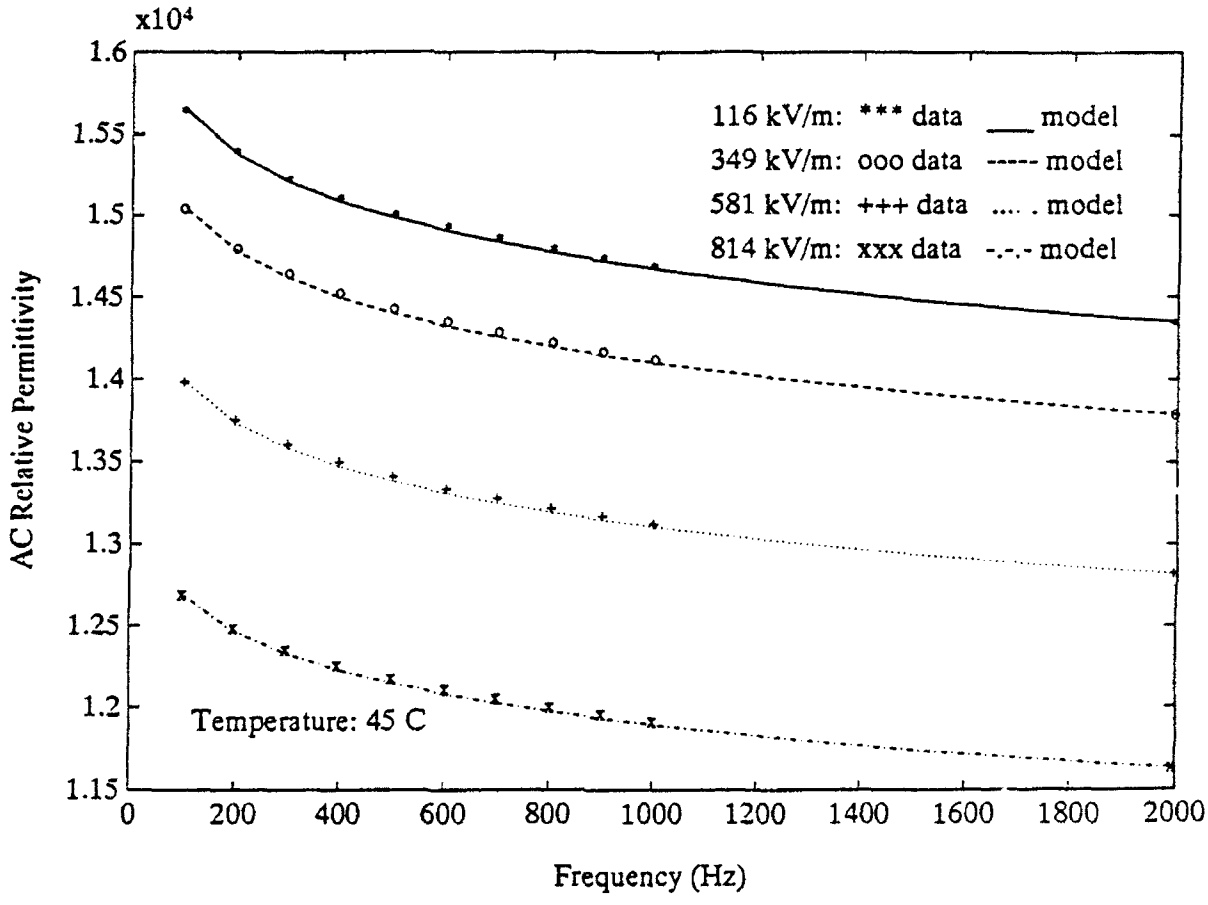

Figure 7 Comparison of AC relative susceptibility model results with reduced data from permittivity response experiments versus frequency at various bias fields.

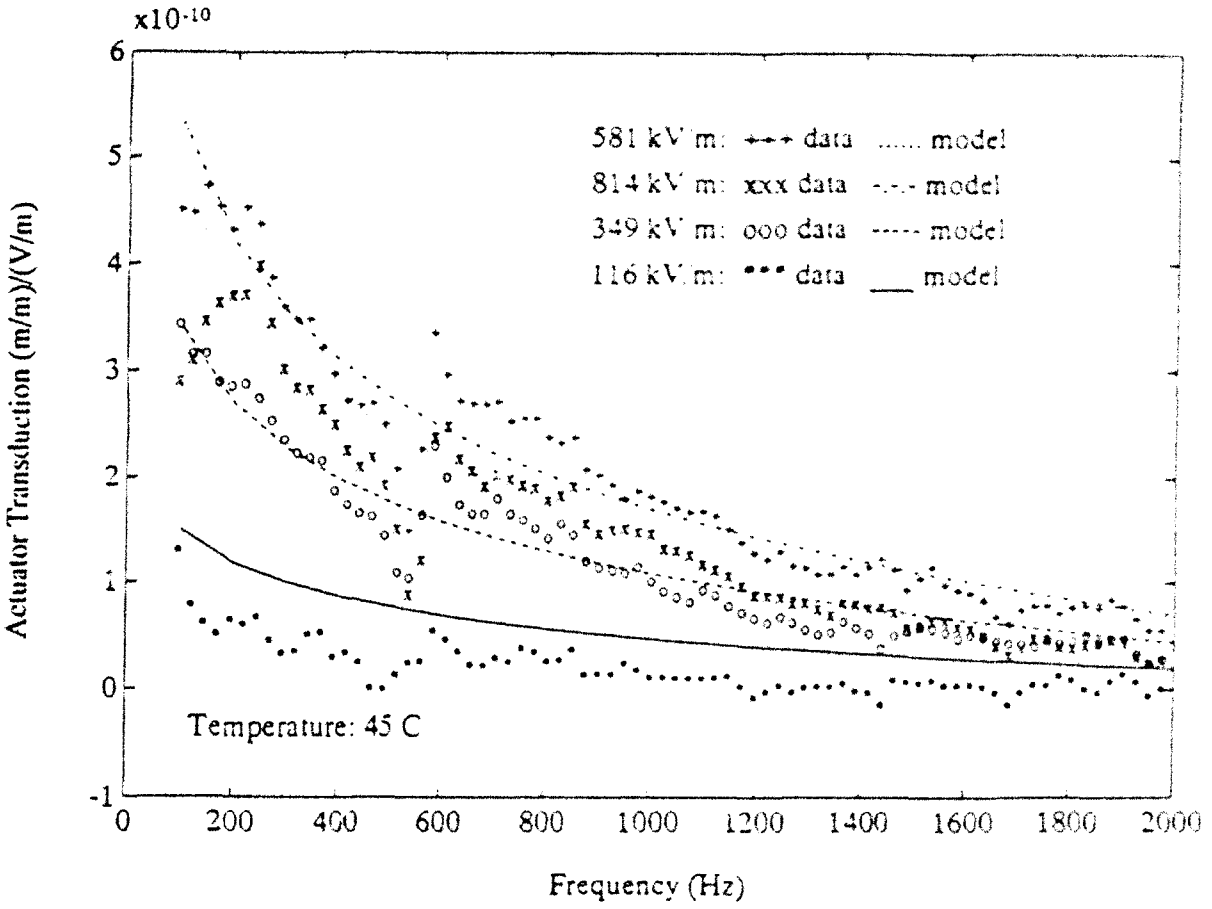

Figure 8 Comparison of electrostrictive constitutive model results with data from AC actuator response experiments versus frequency at various bias fields.

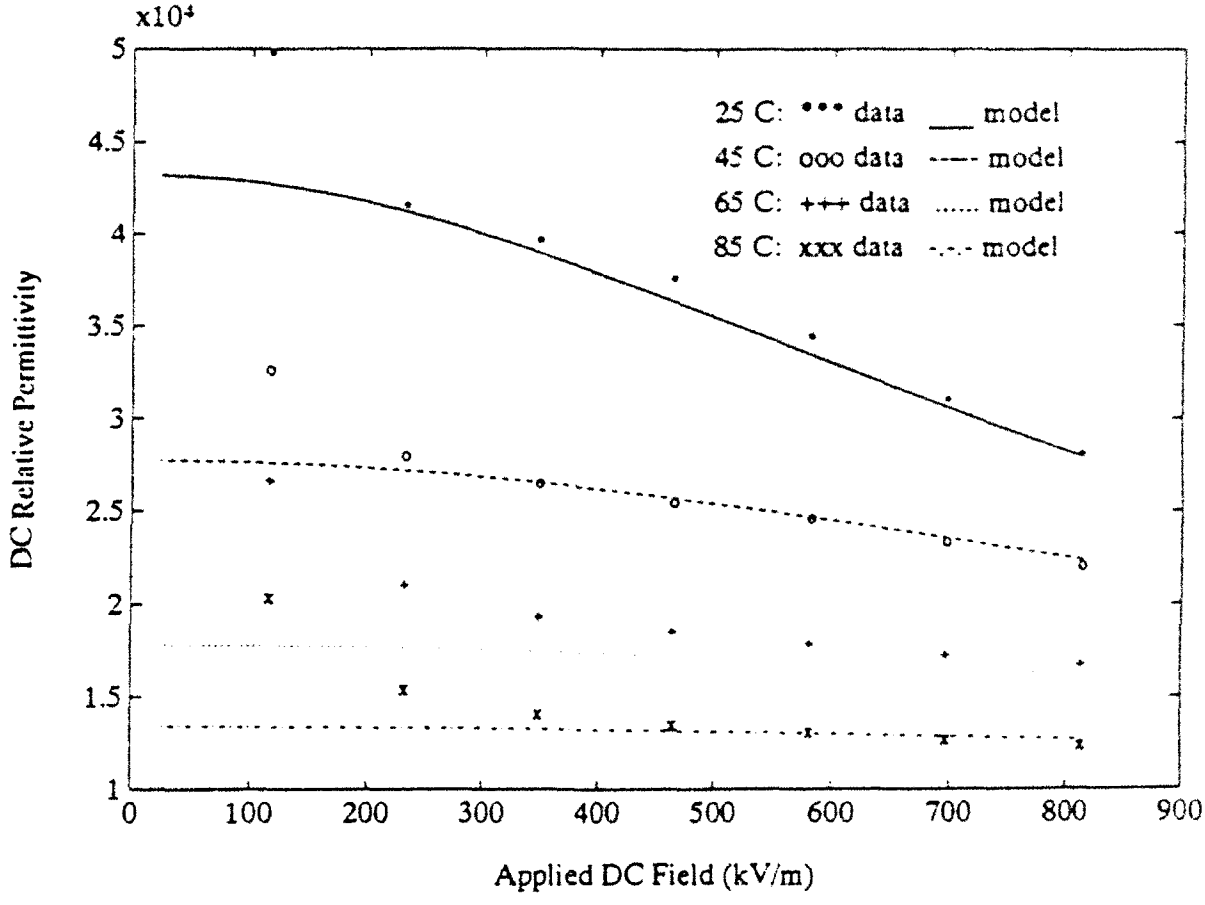

Figure 9 Comparison of DC relative susceptibility model results with reduced data from DC free-induced strain response experiments versus bias field.

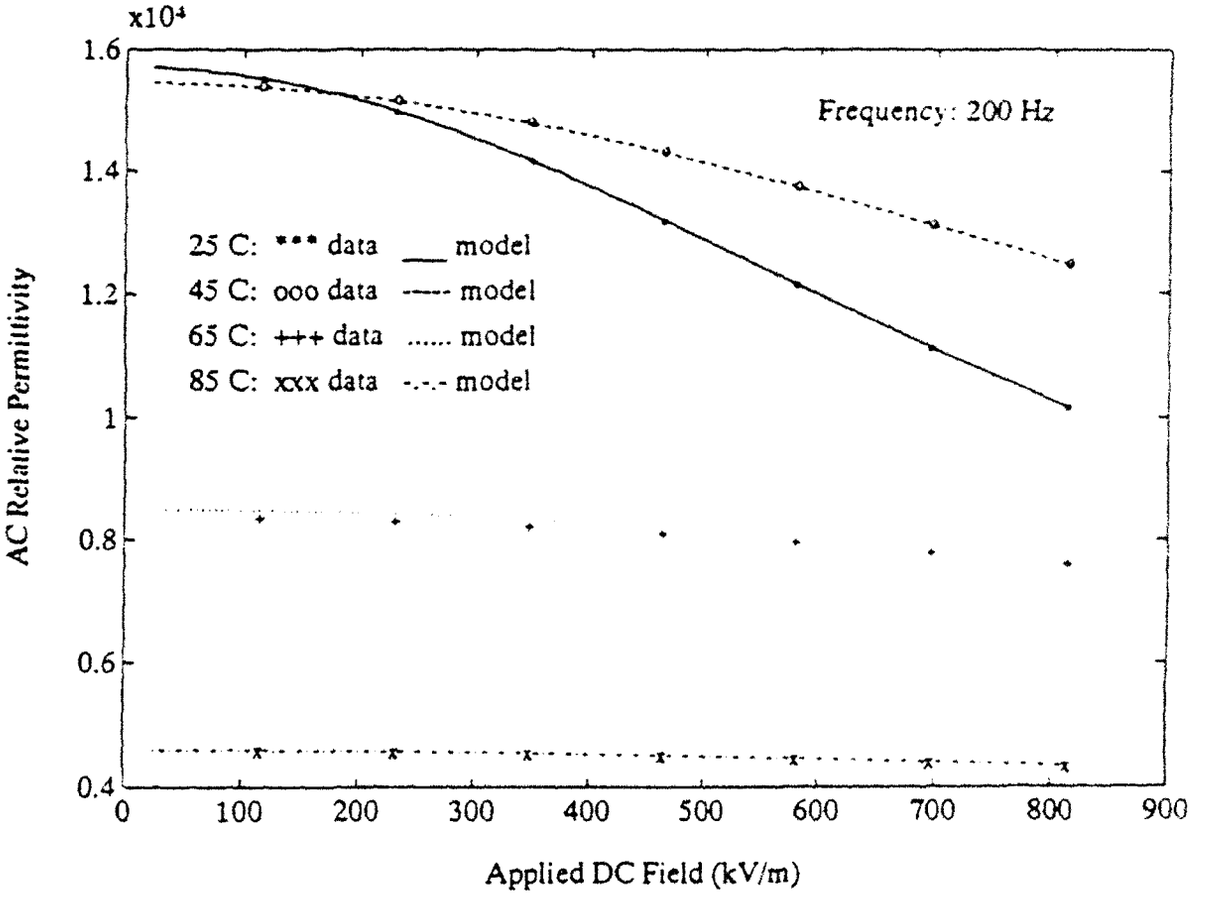

Figure 10 Comparison of AC relative susceptibility model results with reduced data from permittivity response experiments versus bias field at various temperatures.

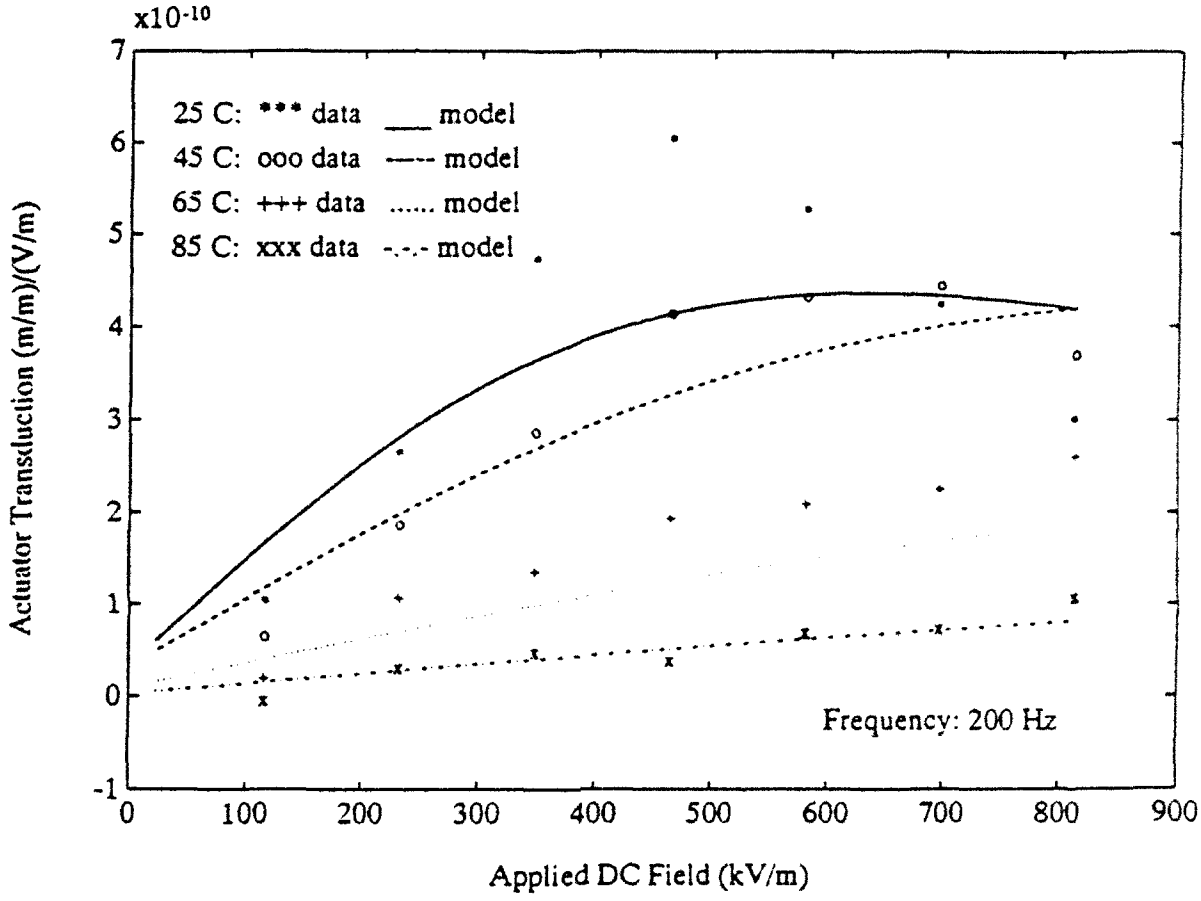

Figure 11 Comparison of electrostrictive constitutive model results with data from AC actuator response experiments versus bias field at various temperatures.

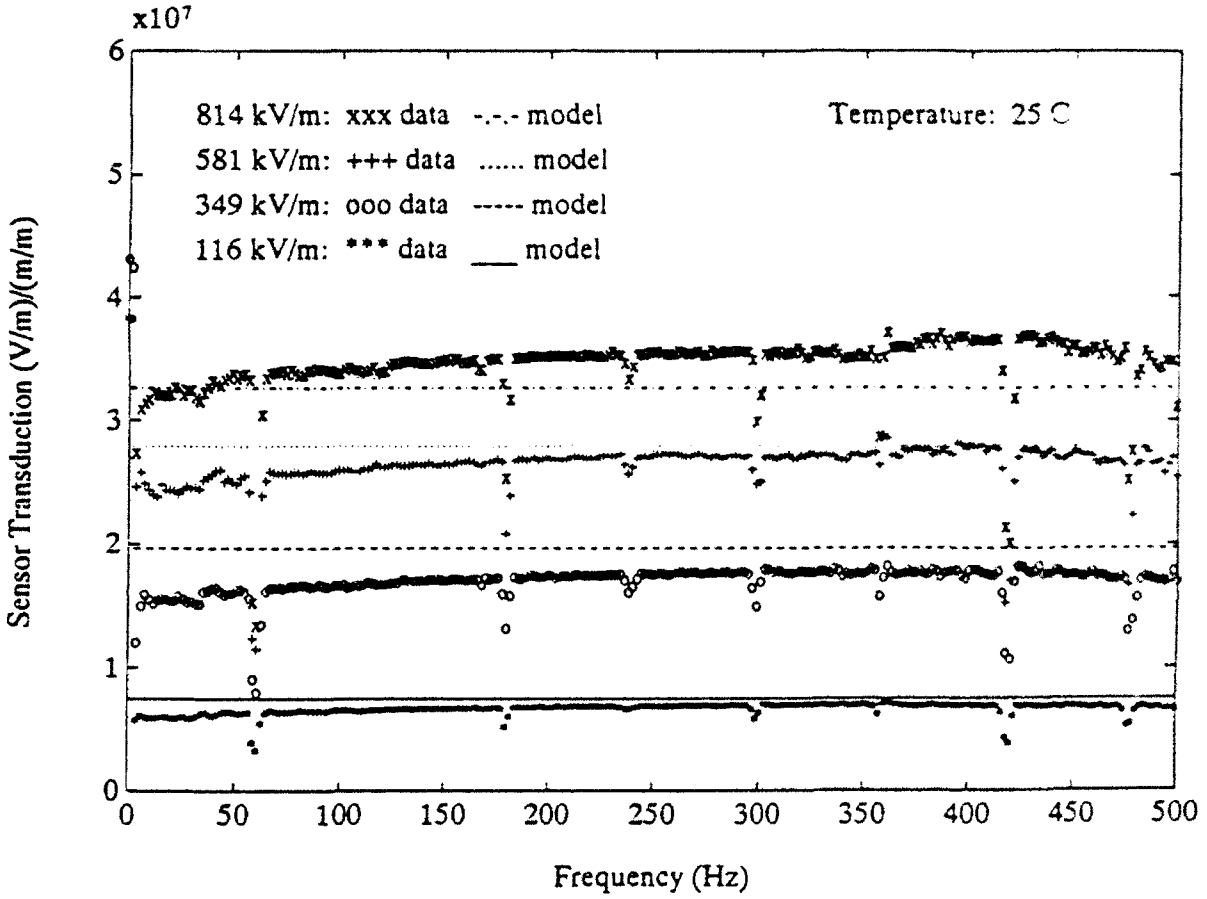

Figure 12 Comparison of electrostrictive constitutive model results with data from AC sensor response experiments versus frequency at various bias fields.

An Impedance Modeling Technique for Dynamic Analysis of Adaptive Materials

An Impedance Method for Dynamic Analysis of Adaptive Material Systems

C. Liang, F. P. Sun, and C. A. Rogers
Center for Intelligent Material Systems and Structures
Virginia Polytechnic Institute and State University
Blacksburg, VA 24061-0261
Tel. (703)231-2900, Fax (703)231-2903

Abstract

This paper describes a new approach to analyzing the dynamic response of active material systems with integrated induced strain actuators, including piezoelectric, electrostrictive, and magnetostrictive actuators. This approach, referred to as the impedance method, has many unique advantages compared with the conventional static approach and the equivalent thermal expansion approach, such as pin-force models and consistent beam and plate models. The impedance approach is presented using a simple example, a PZT actuator driven one-degree-of-freedom spring-mass-damper system, to demonstrate its ability to capture the physics of adaptive material systems and its utility and importance by means of an experimental example and a numerical case study.

The conventional static and equivalent thermal expansion approaches are briefly summarized. The impedance methodology is then discussed in comparison with the static approach. The basic elements of the impedance method, i.e. the structural impedance corresponding to actuator loading and the dynamic output characteristics of PZT actuators, are addressed. The advantages of using the impedance approach over conventional approaches are discussed using a simple numerical example. A comparison of the impedance method with the static and equivalent thermal expansion approaches are provided at the conclusion of this paper.

Introduction

There are two approaches currently used in the dynamic analysis of active material systems, one is referred to as a static approach and the other i. an equivalent thermal expansion approach. Both of these approaches have some drawbacks in analyzing the dynamic response of active material systems resulting from the activation of integrated induced strain actuators, such as PZT patches. A brief review of these two approaches is given below.

Static Approach

The static approach refers to the method of using a statically determined equivalent force or

moment as the amplitude of the forcing function to determine the dynamic response due to the activation of integrated induced strain actuators. There are several approaches to determining the equivalent force or moment from bonded PZT actuators. One widely used approach is the PIN force model. In the pin force model (Crawley and Deluis, 1989), it is assumed that the mechanical interaction between a bonded actuator and its host structure occurs at the ends of the actuator in the form of concentrated forces. This concentrated force can be determined based on the geometrical compatibility and *static* force equilibrium between the actuator and beam. This concentrated force or moment is then used to represent the effect of the induced strain actuator in static and dynamic analyses.

Another widely used approach for determining the static equivalent force or moment uses Euler-Bernoulli beam equations (Crawley and Deluis, 1989) or consistent plate equations which are fundamentally the same as the pin-force models except for a variation in the assumed strain field. The equivalent force or moment determined from Euler-Bernoulli beam theory is also more accurate than the pin-force model because it includes the mechanical stiffening and the bending of the bonded PZT actuators.

Lin and Rogers (1992) have developed a new model of the equivalent force and moment using an elasticity approach, which shows the nonlinear distribution of the equivalent induced force or moment. This model is very accurate for static analysis.

The static approach, as will be discussed in this paper, should be avoided in the dynamic analysis of active material systems.

Equivalent Thermal Expansion Approach

The equivalent thermal expansion approach is a new term used in this paper. It summarizes how finite element method determines the structural response resulting from the induced strain effect of various actuator, including piezoelectric ceramics, shape memory alloys, etc. (Liang and Rogers, 1989; Hagood et al., 1990; Sung et al., 1992).

The electric induced strain from any induced strain actuator (i.e., PZT or PMN) has the same effect as thermal expansion on the structural response. When using the equivalent thermal expansion approach to determine the dynamic response of an active material system, the actuators are treated as regular integrated structural components with associated mass, stiffness, and damping. The activation is represented by the excitation forces at the actuator locations. The amplitude of the forcing function is a *constant* and is equal to the blocking force of the induced strain actuators.

The equivalent thermal expansion approach does give accurate prediction of the dynamic response. However, there are some drawbacks associated this approach as will be discussed later.

In this paper, an impedance approach for dynamic analysis of active material systems will be

presented. Numerical results of the dynamic response of a beam excited by a PZT actuator based on various approaches discussed will be provided. This paper will also provides a comprehensive comparison between static, equivalent thermal expansion, and impedance approaches.

Impedance Methodology

The impedance method of analyzing the dynamic response of active material systems can be simply described: the interactions between actuators and structures are governed by the dynamic output characteristics of actuators and the dynamic characteristics of the structures, i.e., the structural impedance. Let us study the basic elements of this approach by examining the following example, a PZT actuator-driven one-degree-of-freedom spring-mass-damper (SMD) system.

Before we start, let us briefly discuss how the static response of a PZT/structure interaction is determined. Considering a PZT-driven spring system as shown in Fig. 1, the constitutive relation of PZT yields the following force-displacement relation:

$$F=K_A(x-x_{in}) \ , \tag{1}$$

where x is the displacement. F is the force exerted by the actuator. K_A is the static stiffness of the PZT given by $Y_{22}^E w_A h_A/l_A$ where w_A, h_A, and l_A are the width, thickness, and length of the PZT actuator, respectively. x_{in} is the free induced displacement of the actuator given by $d_{32}El_A$ where d_{32} is the piezoelectric constant and E is the electric field. The force and displacement relation for the spring is given by:

$$F=-K_S x \ , \tag{2}$$

where K_S is the spring constant of the spring. Equations (1) and (2) describe the force and displacement relations of the PZT actuator and spring. The force given by both equations is the force within the components. The force and displacement convention is positive for tension and negative for compression. If the induced displacement of the PZT actuator, x_{in}, is in the positive direction (also positive x direction as shown in Fig. 1), the resulting force in the spring is negative as expressed by Eq. (2).

Figure 2 illustrates the force-displacement relations of both the PZT actuator and spring. The intersection determines the static equilibrium of the actuator and spring system. A so-called "equivalent force" can be determined as:

$$F_{eq}=\frac{K_A K_S}{K_S+K_A} x_{in} \ . \tag{3}$$

The "equivalent force" is used to represent the presence and activation of the PZT actuator in the static approach. To determine the dynamic response of a mechanical system, as shown in Fig. 3, with the static approach, the governing equation is expressed by: $m\ddot{x} + c\dot{x} + K_s x = F_{eq}\sin(\omega t)$, where F_{eq} is determined from Eq. (3). Notice that the stiffness of PZT is not included and this "equivalent force" is a CONSTANT.

The impedance approach will treat the problem differently. As an example of how the impedance approach determines the dynamic response of an actuator-driven system, consider the PZT-driven one-degree-of-freedom spring-mass-damper (SMD) system shown in Fig. 3. On the spring side, the following relation based on the concept of mechanical impedance should be utilized:

$$F=-Z\dot{x}\ , \tag{4}$$

where Z is the mechanical impedance of the SMD system given by:

$$Z=c+m\frac{\omega^2-\omega_n^2}{\omega}i\ , \tag{5}$$

where i is $(-1)^{1/2}$, c is the damping coefficient, m the mass, ω the excitation frequency. The reason for the negative sign in Eq. (4) is the same as that in Eq. (2). ω_n, the resonant frequency of the SMD system, is given by:

$$\omega_n=\sqrt{K_S/m}\ . \tag{6}$$

Consider

$$\dot{x}=\omega i x\ , \tag{7}$$

the force-displacement for the SMD can be expressed as:

$$F=-K_D x=-[c\omega i-m(\omega^2-\omega_n^2)]x\ , \tag{8}$$

where K_D is called the dynamic stiffness.

In static analysis, the force-displacement relation of PZT, according to the constitutive equation, is given by Eq. (1). In the dynamic analysis, Eq. (1) is not longer adequate. The dynamic output characteristics of PZT actuators must be used, which can be determined based on a coupled electro-mechanical analysis.

Dynamic Output Characteristics of PZT Actuators

Consider the PZT actuator shown in Fig. 3, the electric field is applied in the z-direction and it is assumed that the PZT expands and contracts only in the y-direction. The constitutive relation of the PZT of the (T, E)-type (stress and electric field as independent variables) may be expressed as follows:

$$S_2=\overline{s}_{22}^{E}T_2+d_{32}E \tag{9}$$

and

$$D_3=\overline{\epsilon}_{33}^{T}E+d_{32}T_2\,, \tag{10}$$

where S_2 is the strain, T_2 the stress, $\overline{s}_{22}^{E}$ the complex compliance at zero electric field, d_{32} the piezoelectric constant, $\overline{\epsilon}_{33}^{T}$ the complex dielectric constant at zero stress given by $\epsilon_{33}^{T}(1-\delta i)$, δ the dielectric loss factor, and D_3 the electric displacement.

The equation of motion for a PZT vibrating in the y-direction may be expressed as follows:

$$\rho\frac{\partial^2 v}{\partial t^2}=\overline{Y}_{22}^{E}\frac{\partial^2 v}{\partial y^2}\,, \tag{11}$$

where v is the displacement in the y-direction, ρ is the density of the PZT, $\overline{Y}_{22}^{E} = Y_{22}^{E}(1+i\eta)$, is the complex modulus of PZT at zero electric field, and η is the mechanical loss factor of PZT.

Solving Eq. (11) by separating the displacement v into time and spatial domain solutions yields:

$$v=\overline{v}e^{i\omega t}=(A\sin ky+B\cos ky)\,e^{i\omega t}\,, \tag{12}$$

where

$$k^2=\omega^2\rho/\overline{Y}_{22}^{E}\,. \tag{13}$$

The PZT is connected to a structure which is represented by its impedance, Z. The equilibrium and compatibility relation between the structure and the PZT can be described by:

$$T_{2_{y=l_A}}=\overline{T}_{2_{y=l_A}}e^{i\omega t}=-\frac{Z\overline{v}_{y=l_A}i\omega}{w_A h_A}e^{i\omega t}\,, \tag{14}$$

The simplest expression for structural impedance is the one given by Eq. (5) for a one-degree-of-freedom SMD system.

Equation (14) provides one boundary condition for Eq. (12). Another boundary condition is given by $\overline{v}_{y=0} = 0$, which leads to B=0.

Substituting Eq. (14) into Eq. (9) yields:

$$\overline{S}_2=\frac{d\overline{V}}{dy}\Big|_{y=l_A}=-\overline{s}_{22}^{E}\frac{Z\overline{V}_{y=l_A}i\omega}{w_A h_A}+d_{32}\overline{E}\,. \tag{15}$$

Note: a bar over a variable indicates its spatial component except complex material properties, such as $\overline{s}_{22}^{E}$ and $\overline{Y}_{22}^{E}$. The coefficient, A, in Eq. (12) can be solved from Eq. (15) as:

$$A=\frac{d_{32}\overline{E}}{k\cos(kl_A)+\frac{\overline{s}_{22}^{E}Zi\omega}{w_A h_A}\sin(kl_A)} \tag{16}$$

In order to simplify further derivation and help us to explain the physics from a point of view of impedance matching, the mechanical impedance of PZT actuators is introduced here. If a constant force excitation is applied to a PZT actuator, such as the one shown in Fig. 3, the actuator response can be determined following the same derivation outlined in Eqs. (12) to (16). The mechanical impedance of the PZT actuator defined as the ratio of excitation force to velocity response may be expressed as:

$$Z_A=-\frac{K_A(1+\eta i)}{\omega}\frac{kl_A}{\tan(kl_A)}i\,, \tag{17}$$

Note, the mechanical impedance of the actuator defined above is based on the assumption that the PZT actuator behaves like a passive material and has no electric coupling.

The coefficient, A, given by Eq. (16) can then be simplified as:

$$A=\frac{Z_A d_{32}\overline{E}}{k\cos(kl_A)\,(Z_A+Z)}\,. \tag{18}$$

It is necessary to mention here that the second constitutive relation of PZT given by Eq. (10) is not used. Physically, this indicates that the power supply always satisfies the current requirement of the PZT actuators.

The output displacement of the PZT actuator and the strain and stress field, as well as the electric displacement field can then be solved as follows:

$$\overline{X}=\overline{V}_{y=l_A}=\frac{Z_A d_{32}\overline{E}l_A}{Z_A+Z}\frac{\tan(kl_A)}{kl_A}\,, \tag{19}$$

and the strain:

$$\overline{S}_2 = \frac{Z_A d_{32} \overline{E}}{Z_A + Z} \frac{\cos(ky)}{\cos(kl_A)} , \tag{20}$$

and the stress:

$$\overline{T}_2 = \left(\frac{Z_A}{Z_A + Z} \frac{\cos(ky)}{\cos(kl_A)} - 1 \right) d_{32} \overline{Y}_{22}^E \overline{E} , \tag{21}$$

and the electric displacement field:

$$\overline{D}_3 = \frac{Z_A \overline{Y}_{22}^E d_{32}^2 \overline{E}}{Z_A + Z} \frac{\cos(ky)}{\cos(kl_A)} - (\overline{e}_{22}^E - d_{32}^2 \overline{Y}_{22}^E) \overline{E} . \tag{22}$$

The force output from the actuator (within the actuator) can be obtained from Eq. (21) as:

$$\overline{F} = w_A h_A \overline{T}_{2_{y=l_A}} = - \frac{Z}{Z_A + Z} d_{32} \overline{E} \overline{Y}_{22}^E w_A h_A . \tag{23}$$

The output characteristics of a excitation device, such as a shaker, are usually expressed in terms of its free stroke and dynamic blocking force. The free stroke of a PZT actuator, $\overline{x}_f$, can be calculated from Eq. (19) by assuming the mechanical impedance, Z, to be zero, yielding:

$$\overline{x}_f = d_{32} \overline{E} l_A \frac{\tan(kl_A)}{kl_A} . \tag{24}$$

The dynamic blocking force, $\overline{F}_b$, can be determined from Eq. (23) by assuming an infinite mechanical impedance, Z, yielding:

$$F_b = - \overline{Y}_{22}^E d_{32} \overline{E} w_A h_A . \tag{25}$$

Equations (24) and (25) provide the dynamic output characteristics of PZT actuators. Based on Eq. (25), the dynamics blocking force of a PZT actuator is constant, regardless of the frequency variation, which is superior to shakers whose dynamic blocking force is constant in only a limited frequency range. However, it is necessary to state that, although a PZT actuator has a "constant" dynamic blocking force, the forces acting on a structure from integrated PZT actuators are not necessarily constant. The interaction forces from the integrated actuators are functions of the structural impedance, as will be discussed later.

The free stroke of a PZT actuator is a function of frequency. At the resonance of the PZT actuator corresponding to $kl_A=(n-1/2)\pi$, where n can be any positive integer, the displacement output for a PZT can be infinite if there is no damping (tangent function is infinite at these values). However, as a transducer, the operation frequency range should be far below its first resonant frequency, for example, below 1/5 of the resonant frequency as a rule-of-thumb. Thus, a PZT actuator may be treated as a constant displacement output device ($d_{32}\overline{E}l_A$). This approximation causes less than 3% error. For example, if the length of an actuator is 0.05 m, the Suggested Operation Frequency Range (SOFR) which is 1/5 of the first resonant frequency of the PZT actuator, will be from DC to around 2.8 kHz.

If a PZT actuator is driving a mechanical system, the output force and displacement of the PZT actuator are related. This relation can be determined by combining Eq. (19) and (23) to eliminate the structural impedance term, Z, yielding:

$$\overline{F}=K_A(1+i\eta)\frac{\tan(kl_A)}{kl_A}\overline{x}+F_b\,. \qquad (26)$$

Compared with the static force-displacement relation given by Eq. (1), Eq. (26) includes structural damping and the dynamics of the actuator. If the frequency is within the SOFR, $\tan(kl_A)/kl_A$ is about 1. A PZT actuator may be treated as a linear output device independent of frequency.

Determination of Actuator/Structure Dynamic Interaction

If the dynamic characteristics of the structure and actuators are known. The dynamic interaction between the structure and actuator can be determined from the Dynamic Actuator/Structure Interaction Chart (DASIC), as shown in Fig. 4. In Fig. 4, the dynamic output characteristics of a PZT actuator given by Eq. (26) is independent of frequency if the frequency is within the SOFR. The dynamic characteristics of the mechanical system a given by Eq. (8) are represented by a group of rotating lines, as shown in Fig. 4. The intersection of the rotating lines with the output characteristics of the PZT determines the dynamic response. Note that the damping is not included in the DASIC. When the excitation frequency is zero, the intersection of the dynamic force-displacement lines of the SMD and PZT is the same as the static response determined in Fig. 2. When frequency increases, the F-D lines of the SMD system rotates counter-clockwise around the origin of the coordinate system. The new intersection point of the F-D lines of the SMD system (non-zero frequency) and PZT actuator determines the dynamic response of the system. When the excitation frequency is the same as the resonant frequency of the SMD system, ω_n, the F-D line of SMD is coincident with the displacement axis. This indicates that the PZT actuator is free to expand and contract and the stress inside the actuator is zero, which implies that the induced force of the actuator is zero. When the excitation frequency is greater than ω_n, the mechanical displacement of the PZT actuator is larger than the free stroke, x_{in}. This indicates that the PZT actuator is stressed and deformed by the inertia of the mass and the recovery of the spring. If the excitation frequency is equal to the resonant frequency of the entire system (PZT + SMD), $\overline{\omega}_n$, which corresponds to the line parallel to the

F-D relation of the PZT, the force and displacement within the actuator and spring are infinite. $\bar{\omega}_n$ can be approximated from the following expression:

$$\bar{\omega}_n = \sqrt{\frac{K_A + K_S}{m_A + m}}, \qquad (27)$$

where m_A is the mass of the actuator.

If the excitation frequency is greater than $\bar{\omega}_n$, the displacement response is out-of-phase with respect to the displacement response before the frequency reaches $\bar{\omega}_n$. The dynamic equilibrium is in the third quadrant as shown in Fig. 4. If the frequency is infinite, the F-D line of the SMD is coincident with the force axis, which means that the SMD is dynamically rigid. The force provided by the actuator is the dynamic blocking force, F_b. However, it is necessary to remember that the excitation frequency needs to be within the SOFR in order to use this chart. If the excitation frequency is greater than the SOFR, the variation of the actuator output characteristics needs to be considered. This can be done by rotating the F-D line of the PZT actuator clockwise around the point corresponding to the blocking force.

The actuator/structure interaction can also be explained using the concept of mechanical impedance matching in Eq. (23). If the impedance of the mechanical system is at its lowest which corresponds to its resonance, the force provided by the PZT actuator is at its lowest. This corresponds to the case where the F-D line rotates to coincide with the displacement axis. If the structural impedance matches the actuator impedance, the actuator provides the maximum force. In DASIC, actuator and structure impedance matching is represented by their parallel F-D lines. It is necessary to state that the impedance matching between an output device and its load means that both impedances are complex conjugate.

Calculation of the Structural Impedance

In order to use the impedance approach, the structural impedance corresponding to actuator loading must be calculated first. The excitation force provided by integrated actuators can be very complicated. For example, the actuation provided by a PZT actuator bonded on a beam is shear force and its distribution may be expressed with a hyperbolic tangent function (Lin and Rogers, 1992). Determination of the structural impedance corresponding to a distributed actuator can be very difficult. In this paper, the structural impedance of beams corresponding to two types of actuator excitation will be discussed.

Consider a beam structure with a complex modulus of elasticity $\bar{Y}_B$, mass density ρ_B, and moment of inertia over area K^2. The equation of motion for the transverse deflection y(x,t) is:

$$\frac{\partial^2 y}{\partial t^2} = -\bar{c}^2 K^2 \frac{\partial^4 y}{\partial x^4} + \frac{p(x,t)}{\rho_B a}, \qquad (28)$$

where p(x,t) is the external dynamic loading, 'a' is the cross-sectional area of the beam, and $\overline{c}$ is the complex wave speed of the beam given by:

$$\overline{c}^2 = \frac{\overline{Y}_B}{\rho_B} \quad . \tag{29}$$

The governing Eq. (28) is solved by expanding the transverse displacements and external loads in terms of the eigenfunctions, $\chi_m(x)$, of the beam. The applied forcing function is harmonic and can be expressed as:

$$p(x,t) = \sum_{m=1}^{\infty} P_m \chi_m(x) \exp(i\omega t) \quad , \tag{30}$$

where ω is the driving frequency and $\chi_m(x)$ can be determined based on the boundary conditions of the beam. The transverse displacements can also be expressed in terms of the eigenfunctions of the beam as:

$$y(x,t) = \sum_{m=1}^{\infty} W_m \chi_m(x) \exp(i\omega t) \quad . \tag{31}$$

The modal amplitudes, W_m, can then be solved by substituting Eqs. (30) and (31) into Eq. (28). For example, if the boundary condition of the beam is simply-supported, the modal amplitude may be determined as:

$$W_m = \frac{P_m / \rho_B a}{\overline{c}^2 k^2 \left(\frac{m\pi}{L}\right)^4 - \omega^2} \quad , \tag{32}$$

where L is the length of the beam.

Consider a beam with two PZT actuators bonded on top and bottom. The actuators are activated out-of-phase, resulting in a pure bending excitation. The effect of the actuators can be represented by a pair of bending moments, M. If the two ends of the actuators are at ξ_1 and ξ_2, respectively, the moment distribution may be expressed as follows using the Heaviside functions:

$$M(x) = M[H(x-\xi_2) - H(x-\xi_1)] \quad . \tag{33}$$

The pressure function, p(x), can be expressed with the dipole function as:

$$p(x) = \frac{d^2M(x)}{dx^2} = M[\delta'(x-\xi_2) - \delta'(x-\xi_1)] \quad . \tag{34}$$

The modal amplitudes for the pressure expression, P_m, can be calculated using the following expression:

$$P_m = \frac{\int_0^L p(x)\,\chi_m(x)\,dx}{\int_0^L \chi_m^2(x)\,dx} \quad . \tag{35}$$

The modal amplitudes for the displacement expression can be calculated from Eq. (32). The equivalent rotational structural impedance corresponding to the pure bending moment of the actuators is defined to be:

$$Z_R = \frac{M}{(\dot{\theta}_2 - \dot{\theta}_1)} = \frac{M}{(\theta_2 - \theta_1)\,i\omega} \quad , \tag{36}$$

where θ_1 and θ_2 are the rotation angles at ξ_1 and ξ_2, respectively, which are found by differentiating the transverse deflection with respect to x:

$$\begin{aligned} \theta_1 &= \sum_{m=1}^{\infty} W_m \chi_m' \big|_{x=\xi_1} \\ \theta_2 &= \sum_{m=1}^{\infty} W_m \chi_m' \big|_{x=\xi_2} \quad . \end{aligned} \tag{37}$$

The equivalent structural impedance given by Eq. (36) needs to be modified in order to be used in Eqs. (19) to (23). The interaction between the beam and actuator previously discussed may be represented by a simple system of two actuators creating pure bending moment to drive a rotational mass-spring-damper system having the same rotational impedance as given by Eq. (36), as shown in Fig. 5. The two actuators have the same length l_A, width w_A, and thickness h_A, and they are h_B apart, where h_B is the thickness of the beam. If the rotation of mass is θ, the axial displacement of either of the actuators, x, will be $\theta h_B/2$ (assuming small deformation). The dynamic force equilibrium and geometrical compatibility together may be expressed as:

$$F = [2Z_R/(h_B+h_A)^2]\dot{x} = Z\dot{x} \quad . \tag{38}$$

The equivalent mechanical impedance determined from Eq. (38) can be directly used in Eqs. (19) to (23) to determine the stress, strain, force, displacement, and electric displacement of the PZT actuators. It is also necessary to mention that the mechanical impedance of the actuator, Z_A, used in those equations needs to be doubled since the thickness of the equivalent actuator

has been doubled considering two actuators on top and bottom of the beam.

For an actuator whose effect can be represented with a point loading, such as a stacked PZT actuator used in truss structures and a magnetostrictive actuator, as shown in Fig. 6, the definition of corresponding structural impedance to the actuator loading can be expressed as:

$$Z = \frac{F}{\dot{x}} . \tag{39}$$

This impedance is usually determined by calculating the structural response, $\dot{x}$, corresponding to an arbitrary force, F, at the actuator location.

Determination of Structural Dynamic Response

Once the structural impedance corresponding to the actuator load is calculated, the stress within the actuators can be determined from Eq. (21). The actuator excitation, whether it is a moment or force, can then be determined. For example, if the actuators create pure bending, the excitation moment can be determined as:

$$M_A = \bar{T}_2 w_A h_A h_B . \tag{40}$$

If the magnitude of moment in Eq. (33) is assumed to be unity, the corresponding modal amplitudes can be found to be $\bar{W}_m$ from Eq. (32). The actual dynamic response of the beam can then be determined based on the following modal amplitude:

$$W_m = M_A \bar{W}_m . \tag{41}$$

Numerical Example

Figure 6 shows a cantilever beam with a PZT actuator support vertically at 0.025 m away from its root. The d_{32} effect of the actuator is utilized to generate a vertical excitation. The beam is made of aluminum with a density, ρ_B = 2700 kg/m^3, elastic modulus Y_B = 60 GPa, length, l_B = 0.25 m, width, w_B = 0.02 m, and thickness h_B = 2 mm. The loss factor for the aluminum is assumed to be 0.005. The PZT actuator has a width w_A = 2 mm, length, l_A = 0.05 m, and thickness, h_A = 0.25 mm. The basic material properties for the PZT material (G1195) are listed in Table 1.

Table 1: Material Properties of G1195 PZT (from Piezo System, Inc.)

d_{32} (m/volt)	Y_{22}^E N/m^2	ρ kg/m^3	ϵ_{33}^T Farads/m	δ	η
-166x10^{-12}	6.3x10^{10}	7650	1.5x10^{-8}	0.00015	0.001

Assuming the electric voltage applied to the PZT actuator is 100 volts, the dynamic response of the beam at a point 0.1 m from the root of the beam is calculated using static, equivalent thermal expansion, and impedance method, and is illustrated in Fig. 7. The solid line is from the impedance approach, which is completely coincident with the dashed line predicted using the equivalent thermal expansion approach with BEAM VI program (Mitchell, 1992). The response predicted by the static approach is given by the dash-dotted line. It is apparent that the static approach fails to include the stiffening of the PZT actuator, which in this case is significant.

The electro-mechanical power can also be calculated based on the electric displacement given by Eq. (22). The resistive and reactive power of the coupled electro-mechanical system can then be determined, as shown in Fig. 8. The resistive power represents the actuator power consumption due to the mechanical damping of the PZT actuator and the beam as well as the dielectric loss of the PZT actuator. The reactive power reflects the transfer of the kinetic or potential energy of the entire mechanical system as well as the reactive electric field energy. Detailed discussion of power consumption and energy transfer can be found in previous work (Liang et al., 1992 and 1993).

Experimental Validation

Rossi et al. (1993) have applied the impedance approach presented in this paper to study the dynamic response of cylindrical structures. Experiments have also been conducted to verify the utility of the impedance model for shell structures. A brief discussion of the experimental results is provided here.

The test article is an aluminum ring with two bonded curved PZT actuators, as shown in Fig. 9. The out-of-plane displacements at point 1, 2, 3, and 4 are measured with VPI (vibration pattern image) laser system. The measured velocity response and the theoretical prediction based on the impedance and static approach at point #4 is plotted in Fig. 10. In Fig. 10, the solid line is the experimental results, the prediction using the impedance approach is given by the dashed line, and the result of using the static model is illustrated by the dash-dotted line. It is apparent that the results by the impedance approach agree extremely well with the experimental results while the static approach failed to predict the second and the forth mode. Detailed discussion on these experimental results can be found in the paper by Rossi et al. (1993) as well as in the following discussion.

Discussion of the Numerical Results

What are the dynamic mechanics of active material systems? The following discussion of the simple example above will establish an understanding of the dynamic interaction between actuators and their host structures. Figure 11 shows the mechanical impedance of the cantilever beam at the point of PZT actuator support (dashed line). The mechanical impedance of the PZT actuator according to Eq. (14) is also calculated (dash-dotted line). The valleys of the

mechanical impedance curve of the beam correspond to the resonances of the cantilever beam, which indicates that at the resonance, the beam is dynamically very soft. This is the reason why the force output from the PZT actuator is the lowest at the resonance of the beam, as shown by the solid line in Fig. 11. When the impedance of the actuator matches the impedance of the beam, the force output of the PZT actuator is maximum. Note: there are two intersections between the mechanical impedance curves of the PZT actuator and the beam around each peak; only the first intersection which corresponds to the complex conjugates of impedances is physically meaningful. The frequency corresponding to the first intersection is also the resonant frequency of the entire mechanical system (beam and PZT support) as explained in DASIC.

The stiffening effect on the resonant frequency due to the extra stiffness of the PZT actuator can be determined based on the actuator and structural impedance match. If the width of the actuator in the above numerical example increases, the mechanical impedance of the PZT actuator also increases. The frequency corresponding to the first intersection around every peak of the beam impedance curve will increase, as can be seen in Fig. 11. A higher resonant frequency indicates more stiffening from the PZT actuator. When the stiffness or impedance of the PZT actuator is so high that the actuator behaves like a rigid support, the resonant frequencies are those corresponding to the peak frequencies of the beam impedance curve. This happens when the actuator impedance curve intersects at the peak or is completely above the beam impedance curve.

The force applied to the beam by the actuator, referred to as the actuator force output in this paper (which is actually the force within the actuator), is apparently not a constant, as illustrated by the solid line in Fig. 11. The lower dotted line is the equivalent force used in static analysis, as determined from Eq. (3). The difference between the two clearly indicates the incorrect physical representation of the static model. The higher dotted line in Fig. 11 is the dynamic blocking force used in the equivalent thermal expansion approach. Using this constant force as the excitation does not make any sense in terms of the explaining the physics of the dynamic interaction between actuator and structure. Notice that around the resonances of the entire system (PZT actuator and beam), which correspond to the peaks of the PZT force curve predicted based on the impedance approach, the force inside the actuator (or the force acting on the beam provided by the actuator) can be larger than the dynamic blocking force illustrated by the higher dotted line. This has been observed experimentally and is due to the reactive nature of a vibrating system, and is clearly illustrated in DASIC. Another interesting thing to notice in Fig. 11 is that at the anti-resonant frequencies of the beam, the actuator output force is the same as the dynamic blocking force. This is shown in Fig. 9 by the second intersection point between the higher dotted line and the solid line around each peak of the force curve.

The impedance approach to determining the dynamic response is very different from the other two approaches. In experimental modal analysis, the resonance of a system is determined by the frequency response function which is the ratio of the response to the excitation force. This is simply because the excitation force provided by most excitation devices, such as shakers, is not a constant for the same reason stated in this paper. Using a response resulting from a variable force tends to provide misleading results. For example, if the excitation device is a

shaker, the frequency corresponding to a peak of the response curve is not the actual resonant frequency of that mode because of the extra mass loading from the shaker. Similarly, if the excitation device is a PZT actuator which has one end fixed as in the numerical example in this paper, the peak frequencies are higher than their corresponding resonant frequencies of the original mechanical system, such as the cantilever beam in the numerical example, because of the stiffening effect. Only when the excitation force is a constant the resonant frequencies determined from the peak frequencies are equal to the true resonance frequency. In the impedance approach, the frequency response function is first calculated by using a constant unit force, the dynamic response is then determined by multiplying the frequency response function with the actual actuator force output determined from the impedance approach. This is why the response predicted by the impedance approach can accurately reflect the mechanical stiffening of the actuators. It is necessary to say that induced strain actuators do not always stiffen the original mechanical system, even in the case where bonded PZT actuators are used to excite a structure. In this case, the impedance approach can still accurately predict the influence of actuator mass loading.

To further illustrate how the impedance approach predicts dynamic response, let us examine Fig. 12 which shows the actuator force output (dashed line), beam response (dash-dotted line) resulting from a unit force excitation (frequency response function), and the actual dynamic response (solid line) of the entire mechanical system (PZT actuator and cantilever beam). We already know from the force analysis above that the valleys of the force curve correspond to the resonant frequencies of the cantilever beam, while the peaks correspond to the resonant frequencies of the actuator and beam system. It is very clear that when multiplying the dashed line and dash-dotted line to yield the solid line, the peaks of the solid line will represent the resonance of the actuator and beam system.

Conclusions

The significant contribution of this paper is to introduce the impedance approach, which has been well studied in the modal analysis field, to the area of active material systems. This approach, compared with the static approach and the equivalent thermal expansion approach, has many advantages. The most important advantage of the impedance approach is that it reflects the physical essence of the mechanics of active material systems.

The work presented in this paper provides a methodology for analyzing the dynamics of active material systems with integrated actuators. This methodology can be used with any actuators, any material systems, and any structures as long as the structural impedance corresponding the actuator loading and the dynamic output characteristics of the actuators can be determined. This paper has also provided an approach to determining the structural impedance corresponding to two types of actuator loading. The concept of DASIC can virtually be used to describe any linear actuator/structure interaction.

This paper has used three approaches to determine the structural response. A comparison of the

three approaches, static, equivalent thermal expansion, and impedance, is provided below.

- Static approach

This approach is simple and easy to use, but it can yield very misleading results especially when the dynamic response is sensitive to actuator mass loading or stiffening. More importantly, this approach does not correctly capture the physical essence of the actuator/structure interaction in the dynamic scenario.

- Equivalent thermal expansion approach

The equivalent thermal expansion approach does predict the dynamic response accurately, but it does not represent the physical essence of the mechanics of active material systems. The thermal expansion approach requires including the mass and stiffness of the integrated actuator, which sometimes can be inconvenient.

- Impedance approach

The impedance approach provide a straightforward approach to accurately determine the dynamic response of active material systems. It represents the physical essence of the interaction between actuators and structures. As a discretized method, the impedance approach can provide much more information than the other descretized method, the static approach. This approach can easily be used in the electro-mechanical analysis of an adaptive material system to determine the electrical parameters, such as actuator power consumption and system power requirement. This approach has also provided a window for studying of the energy consumption and transfer in an active material system, which is a long-standing issue in the smart material system community.

Acknowledgment

This work is supported partially by Air Force Office of Scientific Research, Grant # AFOSR-91-0416 and Office of Naval Research, Grant ONR 00014-92-1170 The authors would like to thank Dr. Jim Chang from AFOSR and Dr. K. Ng from ONR for their kind support. The authors would also like to thank Dr. Z. Chaudhry for his valuable suggestions.

References

Crawley, E. F. and deLuis, J., 1989, "Use of Piezoelectric Actuators as Elements of Intelligent Structures", AIAA J. **25**(10).

Dimitriadis, E. K., Fuller, C. A., and Rogers, C. A., 1991, "Piezoelectric Actuators for Distributed Vibration Excitation of Thin Plates", J. Vib. Acoust. **113**(1), 100-107.

Ewins, D. J., 1984, Modal Testing: Theory and Practice, John Wiley & Son Inc., NY.

Ha, S. K., Keilers, C., and Chang, F. K., 1992, "Finite Element Analysis of Composite Structures Containing Distributed Piezoelectric Sensors and Actuators," AIAA Journal, Vol. 30, No. 3, March 1992.

Hagood, N. W., Ching, W. H., and von Flotow A., 1990, "Modeling of Piezoelectric Actuator Dynamics of Active Structure Control, " Proceedings, 31st SDM Conference, Long Beach, CA, AIAA-90-697-CP.

Liang, C and Rogers, C. A., 1989, "Behavior of Shape Memory Alloy Actuators Embedded in Composites," Proceedings of the 1989 International Composite Conference, Beijing, China, 1-4 Aug. 1989, pp. 475-482.

Liang, C., Sun, F. P., and Rogers, C. A., 1993, "Coupled Electric-Mechanical Analysis of Piezoelectric Ceramic Actuator Driven Systems - Determination of the Actuator Power Consumption", Proceedings, SPIE Smart Structures and Materials'93, Albuquerque, NM, 31 Jan to 4 Feb., 1993, in press.

Liang, C.,Sun, F. P., Rogers, C. A., and Stein, S., 1993, "Dynamic Output characteristics of Piezoelectric Actuators", Proceedings, SPIE Smart Structures and Materials'93, Albuquerque, NM, 31 Jan to 4 Feb., 1993, in press.

Liang, C., Sun, F. P., and Rogers, C. A., 1992, "Investigation of the Energy Transfer and Consumption of Adaptive Structures," Proceedings, IEEE Tuscon Conference, Tuscon, AZ, Dec. 1992, in press.

Lin, M. W. and Rogers, C. A., 1992, "Formulation of a Beam Structure with Induced Strain Actuators Based on an Approximated Linear Shear Stress Field, " Proceedings, 33rd SDM conference, Dallas, Texas, 13-15 April 1992, pp. 896-904.

Mitchell, L. D., 1992, User's Guide - BEAM VI, edition 6.1, AMDF Publication 08.05.92, Mech. Eng. Dept, Virginia Tech, Blacksburg, VA., Aug. 1992.

Pan, J, Hansen, C. H., and Snyder, S. D., 1991, "A Study of the Response of a Simply-Supported Beam to Excitation by a Piezoelectric Actuator, "Proceedings, Recent Advances in Active Control of Sound and Vibration," Blacksburg, VA, 15-17 April, 1991, Technomic Publishing Co., Inc, Lancaster, PA.

Wang, B. T., 1991, "Active Control of Sound Transmission/Radiation from Elastic Plates Using Multiple Piezoelectric Actuators", Ph.D. Dissertation, Dept. of Mech. Eng., Virginia Polytechnic Institute and State University, June.

Rossi, A., Liang, C., and Rogers, C. A., 1993, "A Coupled Electro-mechanical Analysis of PZT Actuator Driven Structures - An Application to Cylindrical Structures," Proceedings, 34th SDM Conference, LaJolla, CA, April 19-21, 1993

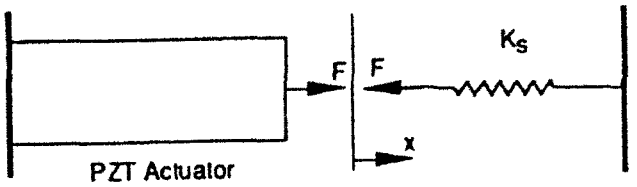

Figure 1. A spring driven by a PZT actuator.

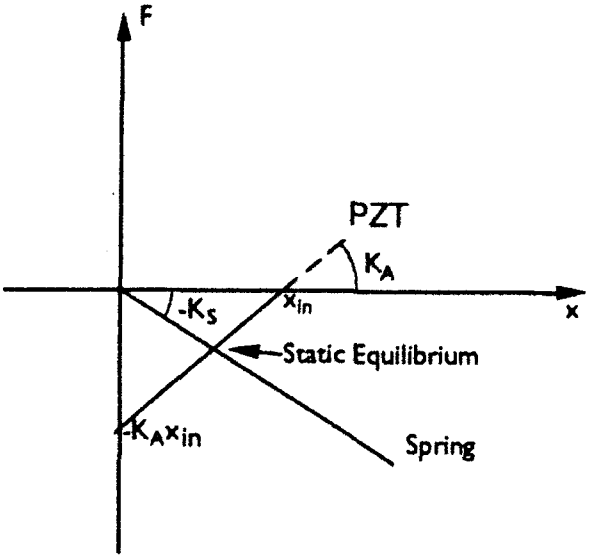

Figure 2. Determination of the static equilibrium.

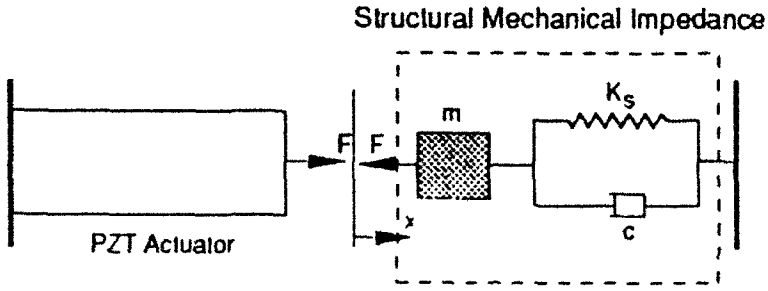

Figure 3. A schematic representation of the dynamic interaction between actuator and its host structures illustrated by a PZT actuator driven one-degree-of-freedom spring-mass-damper system.

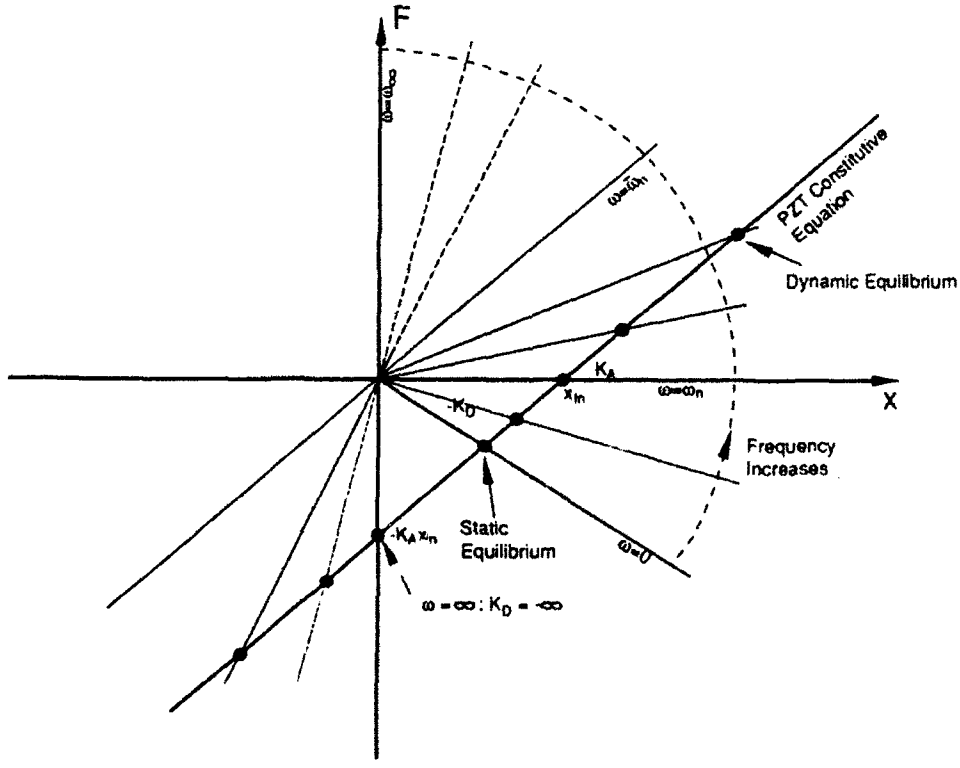

Figure 4. The dynamic actuator and structure interaction chart (DASIC)

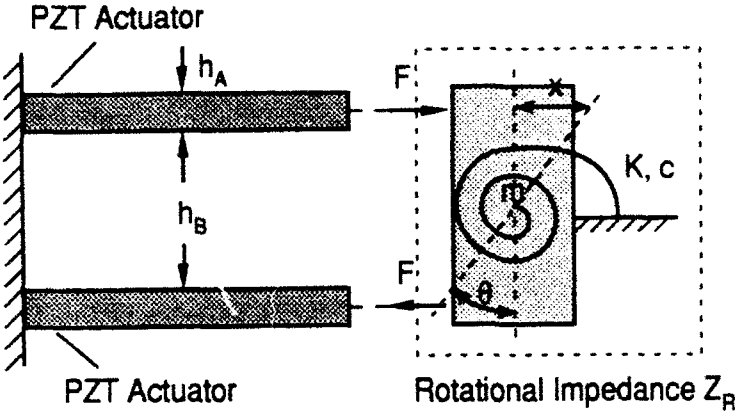

Figure 5. A simplified model for PZT actuators bonded on beam structures

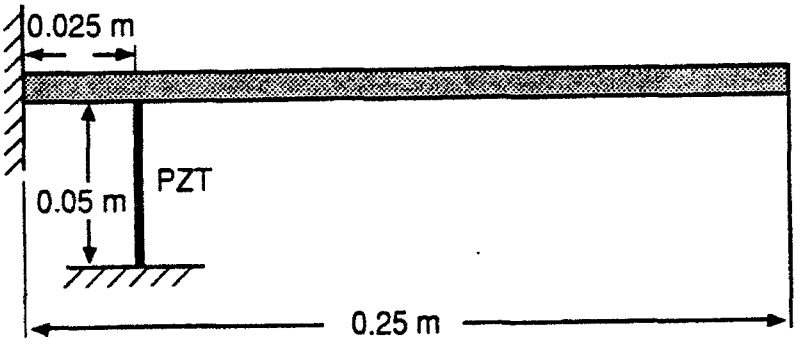

Figure 6. A cantilever beam excited vertically by a PZT actuator with one end fixed

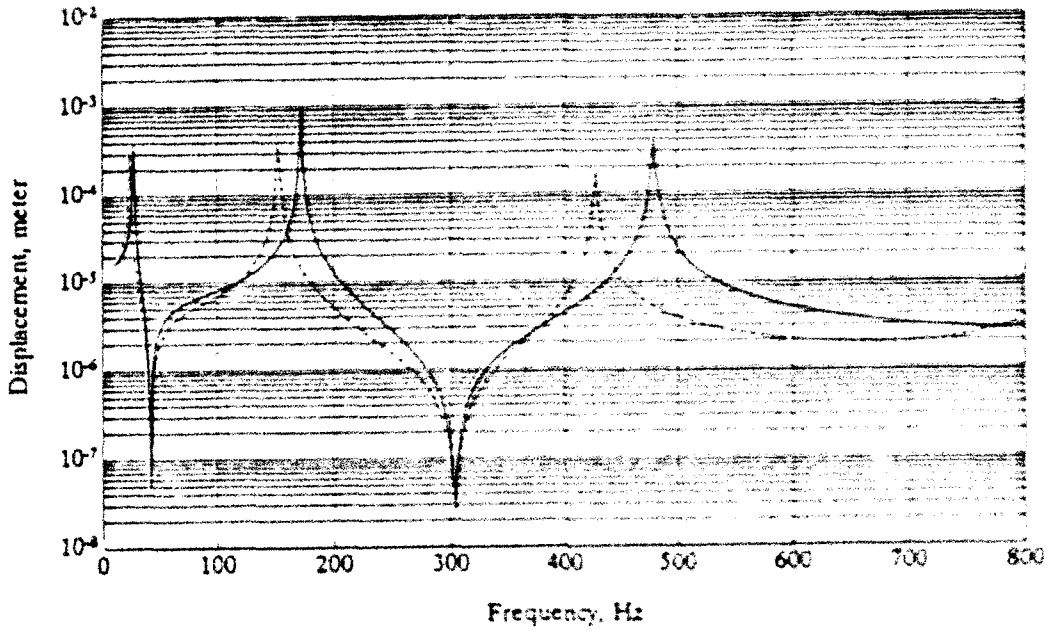

Figure 7. The dynamic response of the cantilever beam at 0.1 m from its root. Solid line is predicted by the impedance approach. The dashed line, which is completely coincident with the solid line, is predicted by the equivalent thermal expansion approach. The dash-dotted line is from the static approach.

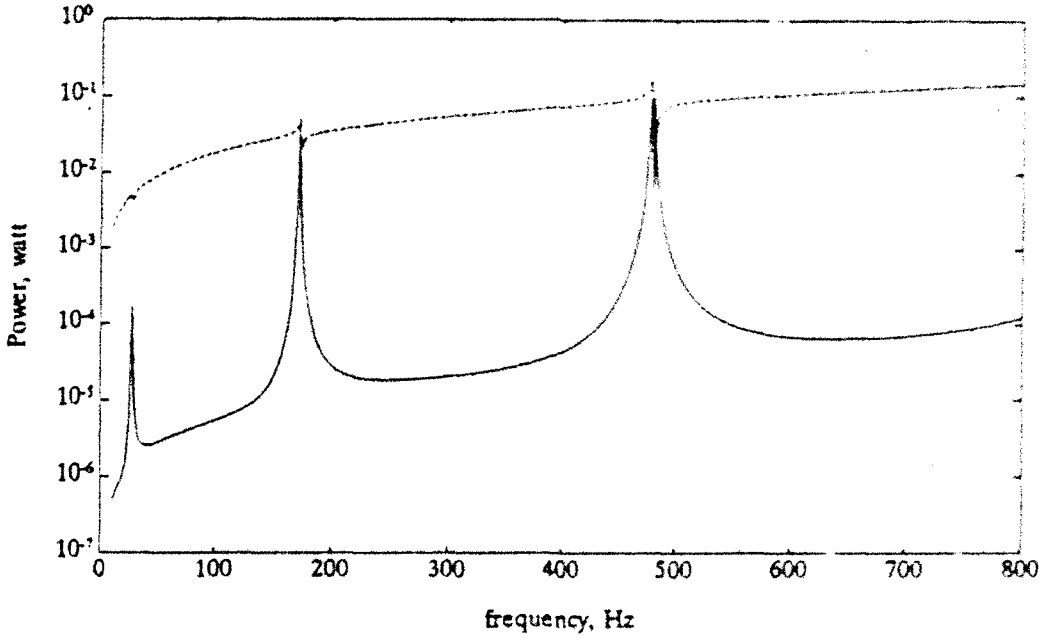

Figure 8. Resistive and reactive power supplied to the PZT actuator. Solid line is the resistive power. Dashed line is the reactive power.

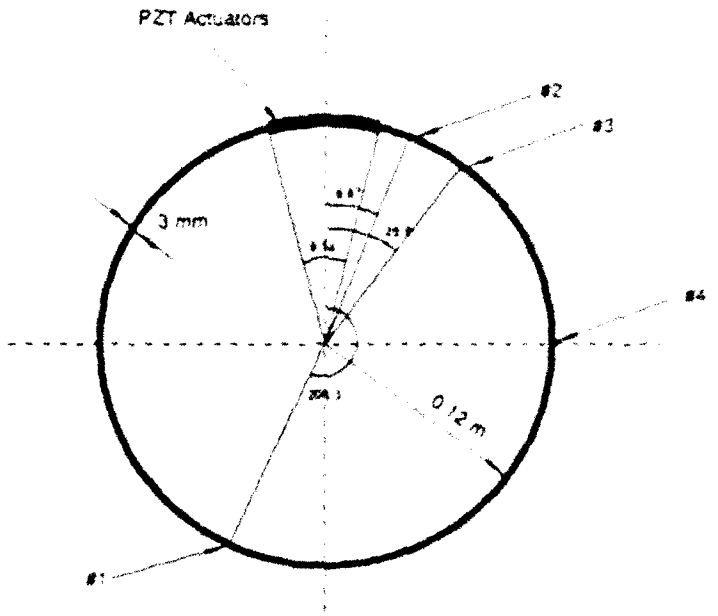

Figure 9. An aluminum ring excited by two PZT actuators. The velocity response of the ring is measured at point #1, #2, #3. and #4. (Rossi et al., 1993)

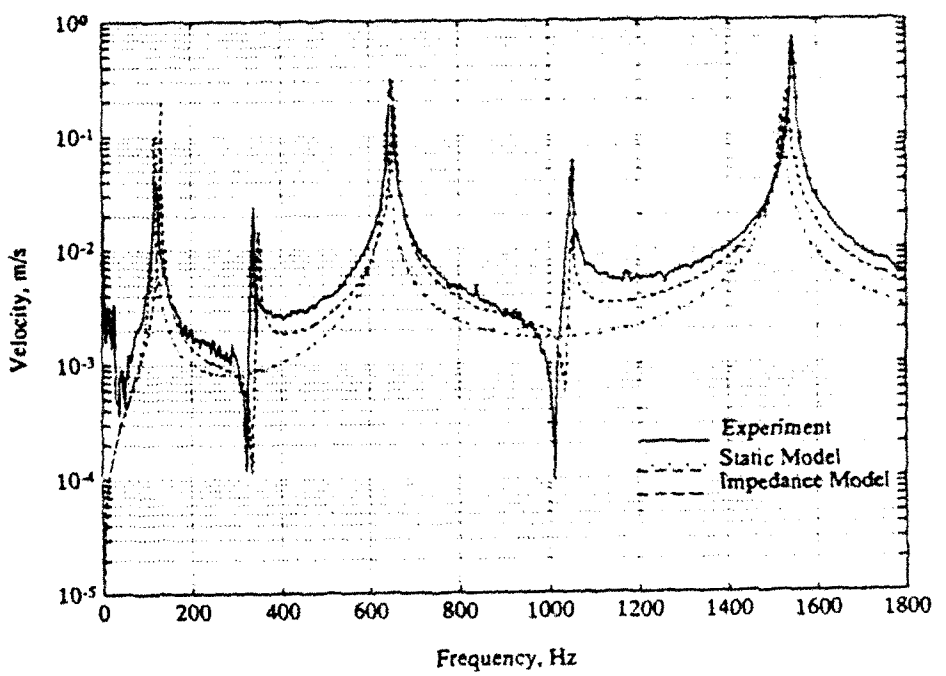

Figure 10. Experimental Measurement and theoretical prediction of the velocity response of the aluminum ring at point #4 (Rossi et al., 1993)

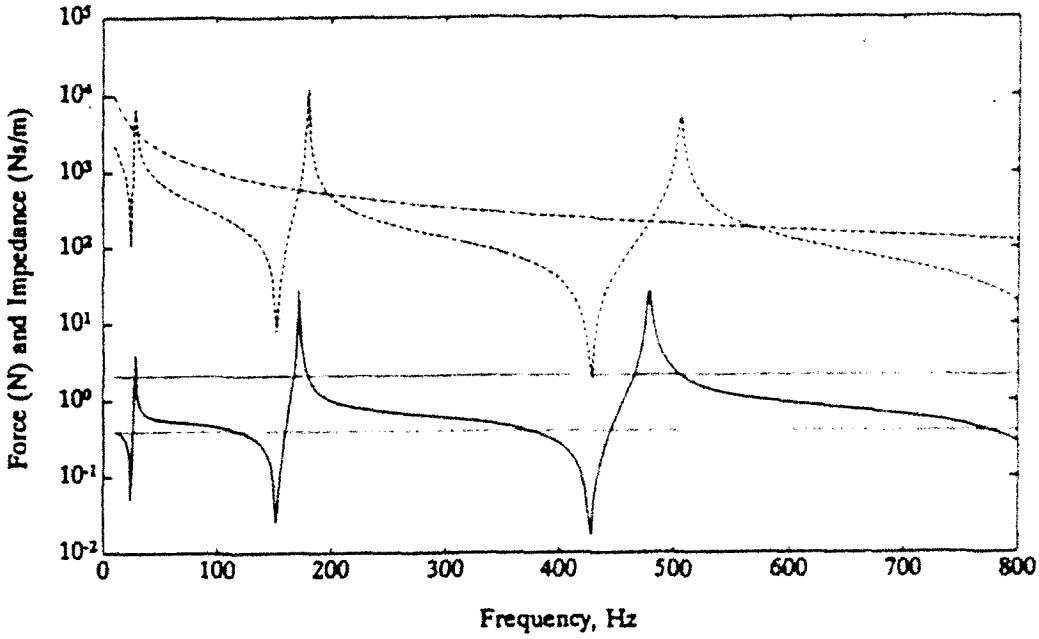

Figure 11. Mechanical impedance of the beam at 0.1 m from the root (dash-dotted line), mechanical impedance of the PZT actuator (dashed line), force output from the PZT actuator (solid line), equivalent force used by the static approach (lower dotted line), and the excitation force used by the equivalent thermal expansion approach (upper dotted line).

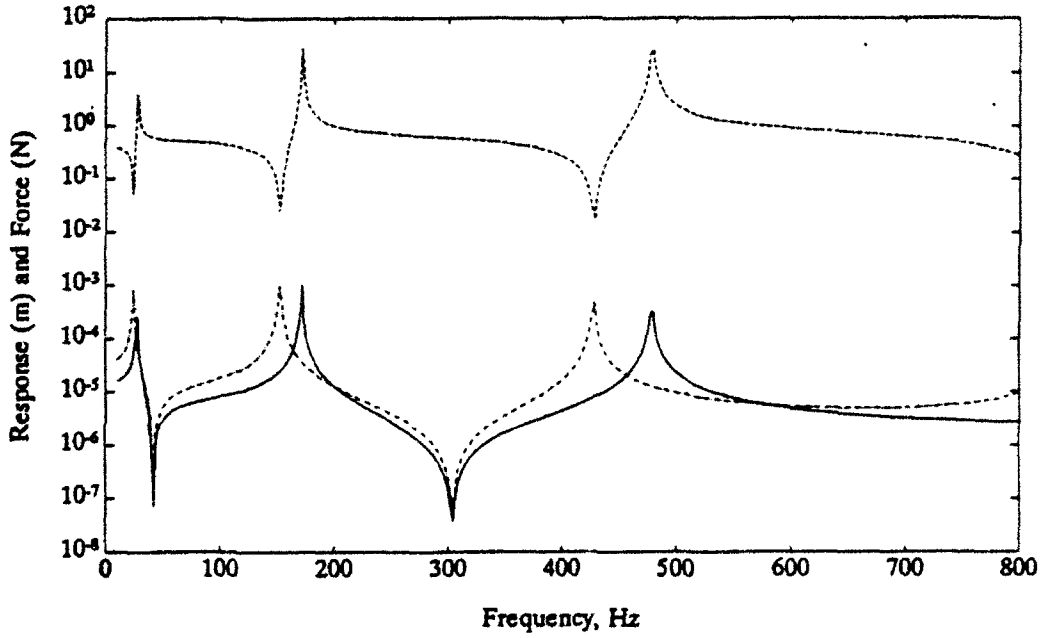

Figure 12. Determination of dynamic response based on frequency response function and actuator force output. Dashed line is the actuator force output, dash-dotted line is the frequency response function, and the solid line is the true dynamic response predicted by the impedance approach (actuator force output times the frequency response function).